Single Molecule Analysis of Biomembrane Heterogeneity

By

Brittany N. Dewitt

Submitted to the graduate degree program in Department of Chemistry and the Graduate Facility of the University of Kansas in partial fulfillment of the requirements for the degree of Doctor of Philosophy.

Chairperson: Dr. Robert Dunn

Dr. Cindy Barrie

Dr. Minae Mure

Dr. Mario Rivera

Dr. Jennifer Roberts

Date Defended: 05/11/2017

The Dissertation Committee for Brittany N. DeWitt

certifies that this is the approved version of the following dissertation:

Single Molecule Analysis of Biomembrane Heterogeneity

Chairperson: Dr. Robert Dunn

Date Approved: 06/12/2017

Single Molecule Analysis of Biomembrane Heterogeneity

By

Brittany N. Dewitt

Abstract –

The biological membrane is a complex and dynamic structure that participates in many important cellular functions. As such, model membranes are frequently employed to study membrane structure and its relationship to function. In this dissertation, a defocused single molecule analysis technique will be presented and applied to explore several questions of biomembranes structure. First, the role of cholesterol in inducing domain separation in Langmuir-Blodgett films will be investigated as cholesterol is an important lipid raft component. Next, the role of the hybrid lipid POPC will be evaluated in forming and stabilizing small domains to aid in explaining how lipid rafts, which are 10 – 200 nm in diameter, are stable in the complex biological membrane. Two alternative models for membrane structure, spin-coated supported lipid bilayers and droplet interface bilayers, will be presented and evaluated for their unique properties. Finally, a preliminary study for using droplet interface bilayers to investigate important biological problems will be suggested. Through these studies, we will demonstrate the utility of model membranes and defocused single molecule analysis for investigating biomembranes structure.

Dissertation Outline

Chapter 1: Introduction

Chapter 2: Techniques for Membrane Interrogation

Chapter 1—Introduction

1.1 Biological Membranes

The biological membrane is the physical boundary between the inside and outside of a cell or organelle. In addition to serving a structural role, the membrane also participates in complex functions including communicating with the surrounding environment, transporting molecules across the membrane, and assisting in certain metabolic functions, to name a few examples [1, 2]. Due to this diversity of function, the cellular membrane has a complex structure and is dynamic in nature. However, the earliest models of the cell membrane proposed a less involved role, suggesting that membrane merely provided a physical barrier and matrix for membrane associated proteins.

Amphiphilic phospholipid molecules are the main component of the membrane and consist of a polar headgroup and nonpolar tail group. In an aqueous environment, these amphiphilic molecules spontaneously form a bilayer where the hydrophobic tails face each other in the core of the structure and the hydrophilic headgroups interact with the surrounding water. This arrangement of molecules maximizes hydrophobic and hydrophilic interactions, creating a thermodynamically stable structure [3]. Early models proposed that the membrane was a homogenous bilayer; however, more recent models have been published that build upon that model while explaining that the membrane has a complex, heterogeneous structure with specific roles for certain types of lipids, sterols, and membrane proteins.

The view of the biological membrane has fundamentally changed in the last several decades with the publication of hypotheses relating membrane organization and structure to the various functions of the membrane. However, as the biological membrane is dynamic and complex, there are still many questions to be answered. New tools, including single molecule analysis and high resolution imaging techniques, are being utilized to provide an updated view

of membrane structure and its relationship to function. These tools are frequently paired with model membranes to elucidate the role that specific membrane components play in membrane function.

1.1.1 Models of Membrane Structure

The view that cell membranes are composed of a lipid bilayer was first demonstrated by Gorter and Grendel in 1925 [4]. They extracted lipids from a sample of erythrocyte cells, which were chosen because they were known to lack internal membranes. Gorter and Grendel assumed that since the cells lacked internal membranes, all of the lipids in the extract must come from the cell membrane. The lipid extract was spread onto a water surface, and the surface coverage was measured. The total surface area of the cells in the extract was estimated, and Gorter and Grendel found that the lipids in the extract covered an area twice as large as the estimated surface area of the cells. This observation was used to support the conclusion that cells are surrounded by a layer of lipids that are two molecules thick—a bilayer.

Gorter and Grendel's work significantly advanced the field's understanding of the membrane; however, there was still interest in a more detailed model. This came in the form of the "Fluid Mosaic Model", illustrated in **Figure 1.1**, which was proposed by Singer and Nicolson in 1972 [5]. The model expands on the idea that the biological membranes are composed of a double layer of lipids, which are the main structural element of the membrane. Additionally, it says that membrane proteins are associated throughout the lipid matrix, and that molecules within the bilayer all have the ability to laterally diffuse along the plan of the membrane in a fluid manner. The model suggests that membrane proteins are associated with either the lipid's polar headgroups or are embedded directly within the bilayer, thus separating membrane

proteins into peripheral (headgroup associated) or integral (hydrophobic-matrix associated) proteins based on their position in the membrane.

The fluid mosaic model addressed a number of questions about membrane structure, but still had limitations. First, it suggested that the lipid bilayer acts as a passive solvent for proteins, which implies that the lipid matrix itself does not take part in cellular processes. It is now commonly accepted that the membrane participates in many important cellular functions. Additionally, the fluid mosaic model states that all of the components in the membrane are freely diffusing, creating a homogeneous structure. However, short and long range lateral organization have been observed in cellular membranes, demonstrating that they have a greater range of heterogeneity than previously thought.

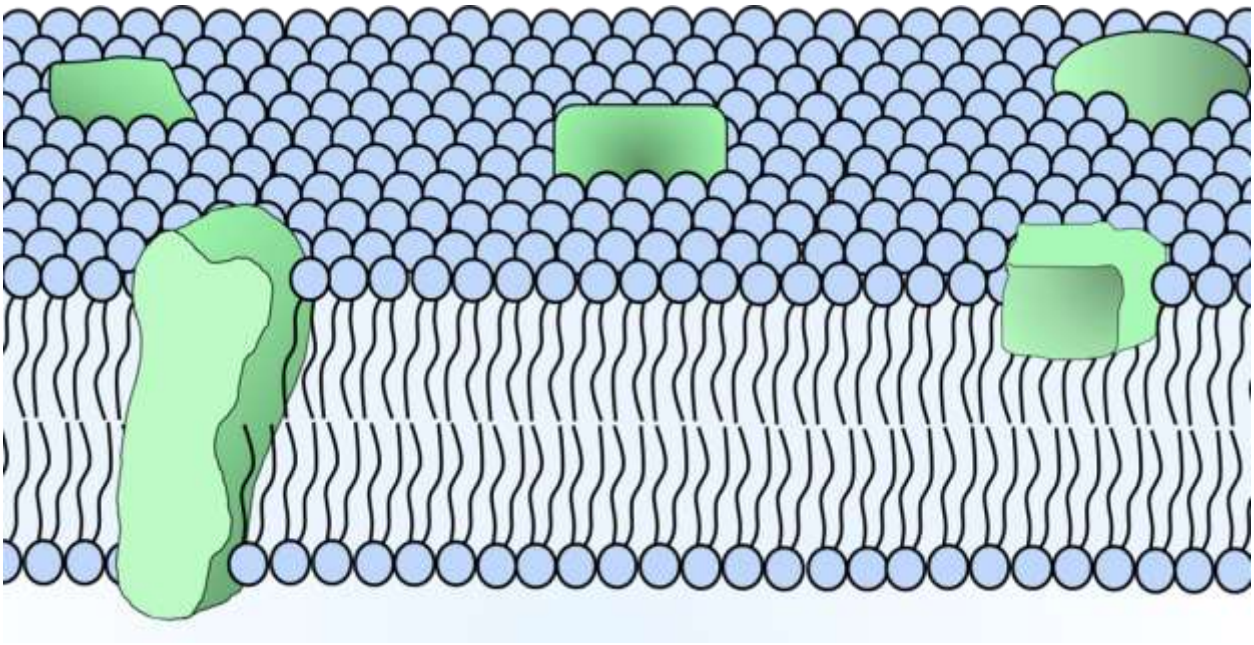

Figure 1.1 shows a representative image of the fluid mosaic model, as proposed by Singer and Nicholson in 1972. In this figure, the phospholipid bilayer is shown with the polar headgroups in blue and the nonpolar tail groups in black. Proteins, shown in green, are located throughout phospholipid bilayer.

1.1.2 The Heterogeneous Nature of Biological Membranes

The heterogeneous nature of membranes is a phenomenon that has been experimentally observed and cannot be explained using the fluid mosaic model. Considering the complex mixture of lipids, proteins, and sterols that make up biological membranes, it is not altogether surprising that they have been shown to exhibit a range of structure including the ability to organize into domains [6]. Domains have been observed on a macroscopic level in, for example, epithelial cells which have significant compositional differences between the basolateral and apical regions. On a nanoscopic level, functional domains have been observed that partition certain lipids and proteins to participate in cellular processes. However, the formation of domains is highly dependent on the chemical composition of the membrane.

Lipidomics studies have shown that the plasma membrane contains hundreds of types of lipids from several major categories including fatty acids, glycerolipids, phospholipids, sphingolipids, and sterols [7]. **Table 1.1** shows the relative distribution of lipid categories within the human plasma membrane. The number of individual species that were identified within each category is also shown and totals to 580 unique lipid species in the plasma membrane, demonstrating the extent of lipid diversity in just one type of biological membrane. In addition to containing many different lipid and sterol molecules, the plasma membrane also contains approximately 1 protein molecule for every 50 to 100 lipid molecules.

***Table 1.1* – Lipid Diversity in the Human Plasma Membrane**

Lipid Category	Number of Individual Species	Percentage (%)
Fatty Acids	107	2.7
Glycerolipids	73	13.8
Phospholipids	160	32.4
Sphingolipids	204	4.0
Sterols	36	47.1

The diverse array of molecules present in biological membranes has led to interest in why cells expend energy generating such a complex molecular composition. A complex and robust pattern of lipid sorting was first observed in epithelial cells [8]. To explain this sorting, the authors proposed that clusters of lipids are formed within the Golgi membrane and used to transport lipids and proteins to their target location in the membrane. The lipid clusters have been termed functional rafts or lipid rafts, and in addition to playing a role in lipid sorting, rafts are thought to incorporate certain lipids and proteins to create sites for the membrane to participate in functions like cell signaling and membrane transport [9].

To further investigate this hypothesis, Brown and Rose subjected epithelial cells to cold detergent extraction using Triton-X, a non-ionic detergent, at 4 °C and observed that membranes rich in GPI-anchored proteins, cholesterol, and glycosphingolipids selectively float to the top of the preparation, into the low-density, detergent-insoluble fraction [10]. They hypothesized that these components separate because of the tight packing between fatty acyl chains and cholesterol, and suggested a definition for lipid rafts as domains that are specifically enriched in cholesterol and sphingolipids, and resist extraction from cell membranes using nonionic detergents [11]. Based upon this work, detergent extraction was used to identify other receptor proteins that were thought to be associated with rafts. These studies were considered further evidence that rafts were specialized membrane domains that play a role in cellular processes including apoptosis, cell adhesion, cell migration, cytoskeletal organization, and cell recognition.

Detergent extraction methods were widely used in early lipid raft studies, and some skepticism emerged about the existence of rafts, as researchers were concerned that detergent extraction could be inducing the formation of domains. Additionally, the direct imaging of domains in biological membranes was challenging due to the small size (10 – 200 nm) and dynamic nature of the domains [12-16]. Since the introduction of the lipid raft hypothesis in

1997, however, advances in optical techniques have strengthened evidence for the existence of lipid rafts. Fluorescence correlation spectroscopy, fluorescence resonant energy transfer, fluorescence recovery after photobleaching, near=field scanning optical microscopy and photoactivated localization microscopy have all be used to provide data supporting the lipid raft hypothesis [17-21].

1.1.3 The Vital Role of Cholesterol

Cholesterol is the single most prevalent component of the plasma membrane, and is present in concentrations up to ten-fold higher than any other membrane component. It plays several key structural roles and can have a dramatic influence on membrane properties. Cholesterol helps to regulate membrane permeability, provide mechanical stability, and participates in lipid organization [22]. In the absence of cholesterol, many plasma membrane components, namely saturated phospholipids and sphingomyelin, are solid in their pure, hydrated form at physiological temperatures suggesting that cholesterol aids in the membrane's ability to remain fluid at a range of physiologically relevant temperatures. When cholesterol is added to bilayers of pure, saturated phospholipids or sphingomyelin, the area per lipid decreases and the lipids enter into a liquid phase that is maintained at a range of temperatures [23-25]. It is vital that the membrane remains fluid under a variety of cellular conditions, and cholesterol seems to play a key role in that process.

Additionally, cholesterol is necessary for lipid raft formation. Studies using cholesterol-depleting agents show that raft domains do not form in the absence of cholesterol. However, the structural role that cholesterol plays in raft domains is less clearly understood [26-29]. One important characteristic of lipid rafts is their tight acyl chain packing, which is thought to be assisted by a unique interaction between saturated lipids and cholesterol where the flat, rigid

sterol structure helps to order the saturated acyl chains in raft-like domains. Hydrogen-bonding between the hydroxyl-headgroup of cholesterol and charged headgroup of sphingomyelin may help to further stabilize domains [30, 31].

Considering the complex structure, dynamic nature, and diverse array of molecule types in native membranes, it is difficult to elucidate the role of a single membrane component, like cholesterol, from within such a complex matrix. Thus, our current understanding of the role of cholesterol and other components in biological membranes was achieved in part using simplified models of membranes. A variety of model membranes have been optimized and utilized to study biological membranes because these models provide a simple platform for investigating the structural and functional roles of various membrane components.

1.2 Experimental Model Membranes

Given the complexity of natural membranes and the challenges of performing membrane research on live cells, models of biological membranes are frequently employed instead. Model membranes mimic the basic structure of the biological membrane, either a monolayer or bilayer of lipid molecules, but also offer several advantages over naturally occurring membranes for research. There are a variety of well-established techniques for preparing model membranes including Langmuir-Blodgett (LB) monolayers, Langmuir-Blodgett/Langmuir-Schaefer (LB/LS) bilayer deposition, and vesicle formation and fusion techniques.

Model membranes can be prepared using commercially available, synthetic lipids which facilitate the study of specific components of the membrane. Additionally, model membranes contain far fewer variables than natural membranes, enabling clearer data analysis and interpretation. However, each model has certain advantages and limitations. For example, the composition of LB monolayers can be controlled precisely, along with their thermodynamic

properties using temperature and surface pressure. However, only monolayers can be prepared using this technique, which somewhat limits their comparison to biological systems.

1.2.1 Langmuir-Blodgett Monolayers

One of the earliest model membrane systems developed was the Langmuir monolayer. This technique, named for Irvine Langmuir, is used to prepare a monolayer at a liquid-air interface. Irvine Langmuir designed an apparatus that could be used to prepare and study monolayer films [32, 33]. A modern version of this apparatus, later named the Langmuir-Blodgett (LB) trough, is shown in **Figure 1.2**. The general design of the LB trough includes an aqueous subphase held in a container made of polytetrafluoroethylene (PTFE), a movable barrier, and Wilhelmy plate pressure sensor. Using this design, a monolayer's area is controlled by adjusting the movable barrier and the surface pressure is monitored using the Wilhelmy plate sensor. Another feature of the modern LB trough is a dipping mechanism to transfer films onto a solid surface.

Commonly, a hydrophilic substrate like glass or mica is used as a support for LB monolayers, and results in a monolayer arrangement with the lipid headgroups against the substrate and the tail group pointing away from the substrate. Alternatively, a hydrophobic substrate can be used to prepare a monolayer with tail groups against the substrate and headgroups facing out. After selecting a substrate, it is lowered into the aqueous subphase. Lipid molecules are dissolved into a volatile solvent, like chloroform, and dispersed onto the subphase where they become trapped at the air-water interface, spontaneously forming a

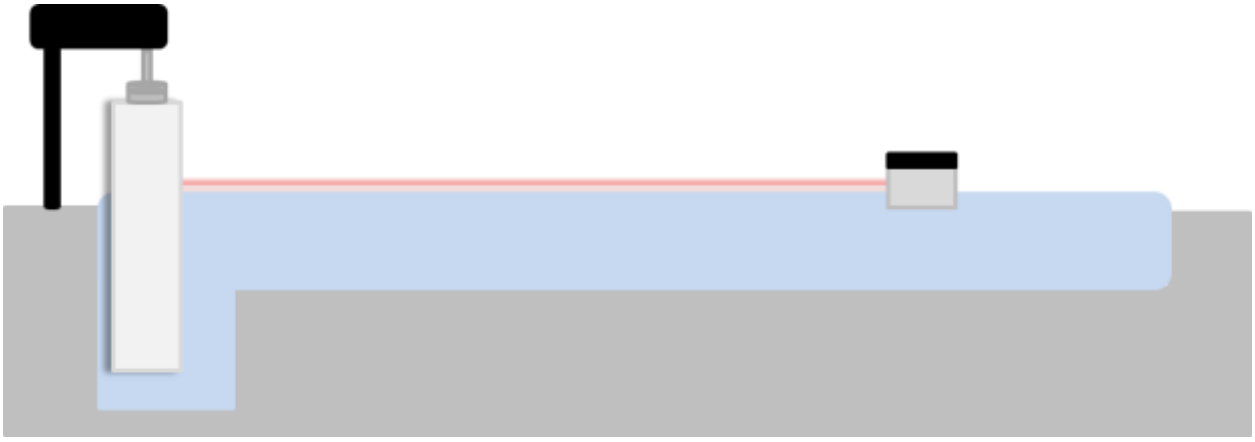

Figure 1.2 shows a Langmuir-Blodgett trough. In this image, the PTFE trough is shown in grey. The trough is filled with an aqueous subphase, and lipids are dispersed onto the subphase in the area shown in red. The area that the lipids may occupy is controlled by a barrier, shown on the right-hand side of the image. Lipids can be transferred onto a solid substrate, for example a glass slide, using the dipping mechanism shown on the left-hand side of the image.

monolayer. The monolayer can then be compressed to the desired surface pressure and transferred onto the solid substrate by drawing the substrate up slowly through the interface between the subphase and air. The surface pressure (π) is defined by:

$$\pi = \gamma_0 - \gamma \qquad \textbf{Eqn. 1.1}$$

where surface pressure (π) is equal to the surface tension due to the monolayer (γ) subtracted from the surface tension of water (γ_0) which is 72.8 mN/m [34].

The measured surface pressure can be plotted versus surface area to create pressure – area isotherms that show the phase behavior of the lipid studied. A representative isotherm for the lipid DPPC is shown in **Figure 1.3**. When the lipid solution is initially disbursed at a low concentration onto the subphase, the lipids are loosely packed. This state is called the liquid expanded (LE) phase, and each molecule is allowed a high degree of orientational freedom [35, 36]. As the film is compressed and the surface pressure increases, the area per lipid molecule

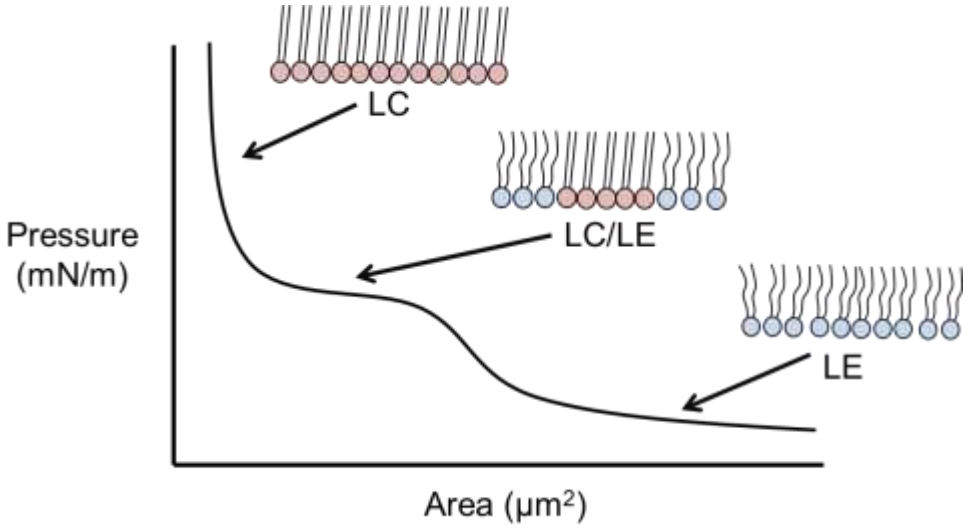

A representative pressure—area isotherm of the lipid DPPC is shown in **Figure 1.3**. When the area occupied by the monolayer film is small, the DPPC molecules each have a small area per molecule and are in the liquid condensed (LC) phase, shown in red. When the film's area is large, each lipid molecule occupies a larger area and is allowed a greater motional freedom. This state is the liquid expanded (LE) phase, shown in blue. At intermediate pressures, both LE and LC phases coexist.

is reduced and certain areas in the film adopt a more ordered, compact structure called the phase liquid condensed (LC) phase. Phase coexistence, where both the LE and LC phases are present in the monolayer, can be seen on the pressure – area isotherm where the surface pressure is constant as the film area changes. This area of very shallow slope is indicative of a transition. As the area is reduced further, all of the lipids transition into the LC phase, which is shown on the pressure – area isotherm as having a steep slope where small changes in area result in large changes in pressure. Another membrane phase called the solid phase is possible at very high surface pressures and not indicated on the pressure-area isotherm shown. Finally, at high enough surface pressures, the monolayer will collapse into a multilayer when the area is reduced to a point that the lipid molecules can no longer form monolayer [37]. The film can be

transferred onto a solid substrate at any of the surface pressures discussed for interrogation using analytical techniques.

LB monolayers can be prepared quickly and inexpensively, with a great deal of control over experimental parameters. The composition of the monolayer is determined by the lipid mixture that is used to prepare the monolayer, so monolayers with many different compositions can be created. The temperature and surface pressure of the monolayer can be controlled to explore thermodynamic processes. And as monolayers are planar, they are an ideal design for imaging studies. However, monolayers are inadequate to study certain biological problems where bilayers are more biologically comparable.

1.2.2. Langmuir-Blodgett Langmuir Schaefer (LB/LS) Deposition

Other model membranes have been developed to create bilayers, which offer more realistic models of naturally occurring biological membranes. One popular technique is Langmuir Blodgett Langmuir-Schaefer (LB/LS) deposition, where an LB monolayer is further modified to create a solid-supported bilayer using the LB trough [38, 39]. An LB monolayer is first created on a hydrophilic substrate. Once transferred onto the substrate, the lipid's headgroups are in contact with the hydrophilic substrate, and the hydrophobic tail groups oriented away from the substrate. If this monolayer is brought into contact with a second monolayer on the surface of the LB trough, the hydrophobic tail groups interact with one another and are stabilized via hydrophobic interactions. The substrate is then lifted away from the water interface, creating a bilayer.

LB/LS bilayers, like LB monolayers, are simple to fabricate. Additionally, variables including the membrane composition, surface pressure, and temperature can all be controlled. Asymmetric bilayers, bilayers with different lipid compositions in their top and bottom leaflet, can

also be prepared using this technique. However, as the two leaflets are formed separately and the bottom leaflet is in contact with the substrate, studying the interactions between the two leaflets is difficult. Given these qualities, LB monolayers and LB/LS bilayers are widely used models for membrane investigation.

1.2.3 Unilamellar Vesicles

Unilamellar lipid vesicles are another useful model for membrane investigations. A unilamellar lipid vesicle has an aqueous core surrounded by a single spherical bilayer. When multiple bilayers surround an aqueous core it is called a multilamellar vesicle. In both model systems, the lipids are arranged so that the polar headgroups oriented toward the interior and exterior aqueous phases. Vesicles can be prepared in a variety of sizes, depending on the preparation technique chosen. For example, small unilamellar vesicles (SUVs) can be as large as 100 nm in diameter and are prepared using sonication [40]. First, a lipid is dissolved into a volatile solvent and disbursed onto a solid substrate, usually inside a glass vial. The solvent is allowed to completely evaporate before warm buffer solution is added. The lipids naturally rehydrate into multilamellar vesicles over the course of several hours. After rehydrating, the multilamellar vesicles can be sonicated to form unilamellar vesicles. Once formed, SUVs can be incubated with a hydrophilic solid substrate at high temperature, where they will form a supported lipid bilayer on the substrate surface.

1.3 Fundamentals of Model Membranes

Early studies of model membranes relied heavily on fluorescence microscopy, where a small concentration of amphiphilic fluorescent probe was used within a model membrane to

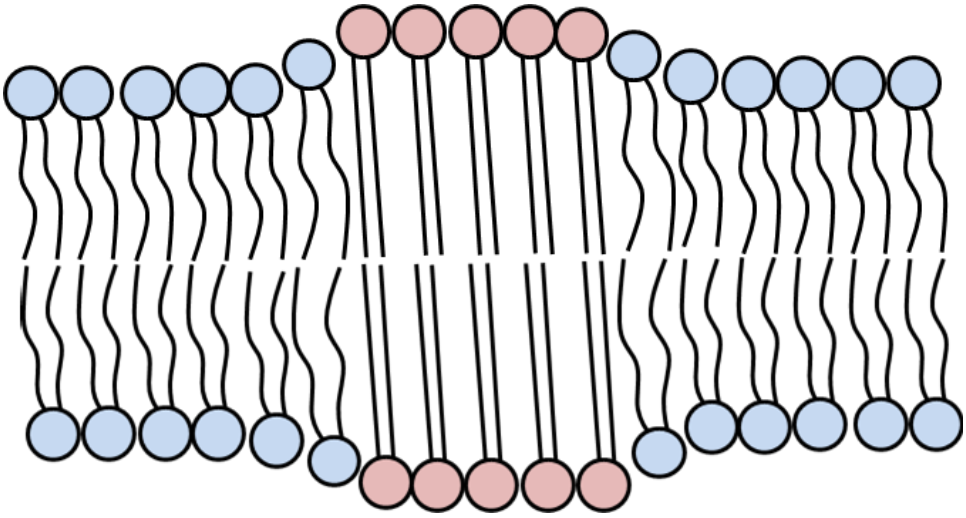

Figure 1.4 shows a representative lipid bilayer. In blue, lipids with unsaturated tail groups are shown. Lipids with saturated tail groups are shown in red. The area of the bilayer rich in saturated lipids is thicker than the domain rich in unsaturated lipids. This creates a small mismatch in size that leads to an excess free energy, called line tension, between the two domains.

reveal a diversity of coexisting phases at the air-water interface. Several phases are possible in membranes, including fluid and solid phases, that are characterized by the spatial arrangement and degree of motional freedom the lipids exhibit in relation to their neighboring molecules [41, 42]. Fluorescent probes generally partition into one phase preferentially, and can be used to reveal lipid phase separation. Domains can exhibit a variety of sizes and shapes that are dependent on chemical composition, surface pressures, and temperature [36]. These observations led to interest in how the size and shape of domains in membranes are controlled. It is now understood that two fundamental parameters, line tension and dipole moment density, are responsible for the formation of coexisting domains.

Line tension is a measure of the free energy per unit length at the boundary between two coexisting phases [43]. This force is conceptually similar to surface tension in a three-dimensional system. A major cause of line tension in membranes is the thickness mismatch

between coexisting domains [44]. Commonly, lipids in model systems separate into domains that are rich in unsaturated lipids and domains that are rich in saturated lipids. The saturated lipid domains are usually thicker than the domains rich in unsaturated lipids, as shown in **Figure 1.4**. At the interface between the two, an area of mismatch is created where the acyl-tail groups of the saturated lipids are exposed to water, creating line tension.

Another significant force that influences the size and shape of lipid domains is dipole moment density. This force arises from the dipole moment that exists across the headgroup of most lipids. When domains have different chemical compositions or packing densities, the density of the dipole moments becomes variable, creating repulsive forces between domains. In model membranes, this repulsion is further amplified by the structure of the membrane, where lipid molecules are all contained within a plane and oriented in roughly the same direction. Water molecules are present within the bilayer, and help to reduce dipole moment density but are not able to completely screen the dipole-dipole interactions; thus long range electrostatic interactions are present within the membrane.

The competing effects of these two fundamental parameters ultimately determine the final size and shape of coexisting domains. Theoretical and experimental work has shown that the minimum radius of a domain can be expressed mathematically:

$$R_o = \frac{\delta e^3}{4} \cdot e^{\frac{4\pi E E_0 \lambda}{\Delta m}} \qquad \textbf{Eqn 1.2}$$

In this equation, R_o is the minimum domain radius, δ is a molecular cut-off distance, ~0.5 nm, E is the dielectric constant of water, E_o is the permittivity of free space, λ is the line tension, and Δm is the dipole density [45]. This equation demonstrates the interplay between domain dipole moment density differences and line tension. Increasing line tension will increase the domain radius, and increasing dipole moment density will decrease the domain radius. The two parameters cannot be separated and expressed independently. Further work has shown that

high dipole moment density differences lead to domains with branched, irregular shapes, shown in **Figure 1.5** (A), and high line tension leads to domains with round shape, shown in **Figure 1.5** (B) to minimize the perimeter of the domain.

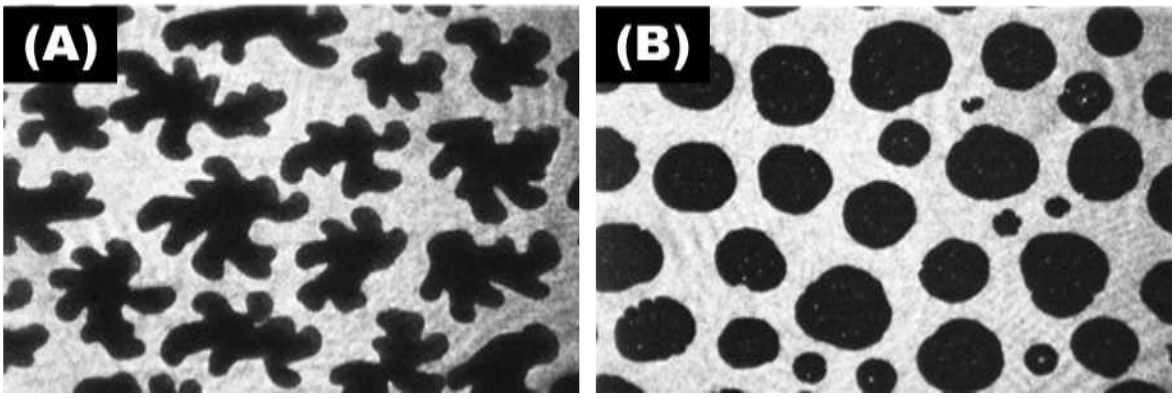

Figure 1.5 illustrates the different domain sizes and shapes that may appear in LB monolayers as a function of varying line tension and dipole moment differences. Image (A) shows a monolayer composed of DPPC/DOPC (1:1) with 1.0 mol % cholesterol and has a branched, irregular shape suggesting high dipole moment density. SM/DOPC (1:1) with 1.0 mol % cholesterol included is shown in image (B). These domains are round to minimize domain perimeter, suggesting high line tension between domains.

Research is currently being performed to understand how line tension and dipole moment density differences affect the behaviors of lipid rafts within biological membranes. One important hypothesis proposes that line tension is a key parameter that must be minimized to stabilize lipid rafts within a complex biological lipid matrix. As raft domains are very small, 10 – 200 nm in diameter, the line tension between the raft domain and surrounding matrix must be small in order for stable domains to form [46-50]. The line tension between domains may also play an important role in lipid-protein interactions. The interfacial area along a raft domain is thought to be a weak point in the cell membrane that serves as an entry and exit site for microbial pathogens and toxins like influenza virus, cholera toxin, and HIV-1 [51]. Thus, a greater understanding of line tension and dipole moment density differences in membranes could help clarify these and other questions.

1.4 Motivation and Dissertation Overview

Understanding the structural and functional role of various constituents in the biological membrane has been a longstanding challenge. Biological membranes have complex structure and dynamic nature, making direct membrane studies challenging. Due to this challenge, model membranes have been invaluable in helping to understand the role of various components of the membrane. Specific membrane components, including cholesterol and sphingomyelin, have been implicated in raft formation, but their exact role remains unclear. Additionally, the mechanisms that stabilize small lipid raft domains are still debated. In this dissertation, model membrane studies utilizing LB monolayers will be paired with a single molecule fluorescence technique to provide a new molecular level view of how certain membrane components, specifically cholesterol and POPC, influence membrane structure and heterogeneity.

In addition to structural studies of raft-like monolayers, this dissertation will investigate several alternative model membrane types that have unique properties for investigating membrane structure. Spin-coated bilayers and droplet interface bilayers will all discussed in terms of their utility in membrane research. Spin-coating can be used to prepare dry, air-stable bilayer and this technique will be used to prepare a variety of bilayer for bulk fluorescence and single molecule analysis. Droplet interface bilayers will be presented as a model for investigating surfactant—emulsion interactions using imaging techniques. Lastly, a future study utilizing droplet interface bilayers will be presented to investigate a new hypothesis on the cause of drug resistance.

1.5 References

1. Field, K.A., D. Holowka, and B. Baird, *FcεRI-mediated recruitment of p53/56lyn to detergent-resistant membrane domains accompanies cellular signaling.* Proc. Natl. Acad. Sci. U. S. A., 1995. **92**(20): p. 9201-5.

2. van Meer, G., D.R. Voelker, and G.W. Feigenson, *Membrane lipids: where they are and how they behave.* Nat. Rev. Mol. Cell Biol., 2008. **9**(2): p. 112-124.

3. Almeida, P.F.F., *Thermodynamics of lipid interactions in complex bilayers.* Biochim. Biophys. Acta, Biomembr., 2009. **1788**(1): p. 72-85.

4. Lombard, J., *Once upon a time the cell membranes: 175 years of cell boundary research.* Biol Direct, 2014. **9**: p. 32.

5. Singer, S.J. and G.L. Nicolson, *The fluid mosaic model of the structure of cell membranes.* Science, 1972. **175**(4023): p. 720-31.

6. Joergensen, K., J.H. Ipsen, and O.G. Mouritsen. *Lipid-bilayer heterogeneity*. 1997. JAI Press.

7. Levental, I. and S.L. Veatch, *The continuing mystery of lipid rafts.* J. Mol. Biol., 2016. **428**(24_Part_A): p. 4749-4764.

8. Simons, K. and G. Van Meer, *Lipid sorting in epithelial cells.* Biochemistry, 1988. **27**(17): p. 6197-202.

9. Simons, K. and E. Ikonen, *Functional rafts in cell membranes.* Nature (London), 1997. **387**(6633): p. 569-572.

10. Brown, D.A. and J.K. Rose, *Sorting of GPI-anchored proteins to glycolipid-enriched membrane subdomains during transport to the apical cell surface.* Cell (Cambridge, Mass.), 1992. **68**(3): p. 533-44.

11. Nickels, J.D., J.C. Smith, and X. Cheng, *Lateral organization, bilayer asymmetry, and inter-leaflet coupling of biological membranes.* Chem Phys Lipids, 2015. **192**: p. 87-99.

12. Munro, S., *Lipid rafts: Elusive or illusive?* Cell (Cambridge, MA, U. S.), 2003. **115**(4): p. 377-388.

13. Hsia, C.-Y., M.J. Richards, and S. Daniel, *A review of traditional and emerging methods to characterize lipid-protein interactions in biological membranes.* Anal. Methods, 2015. **7**(17): p. 7076-7094.

14. Nyholm, T.K.M., *Lipid-protein interplay and lateral organization in biomembranes.* Chem. Phys. Lipids, 2015. **189**: p. 48-55.

15. Sonnino, S., et al. *Lipid membrane domains in glycobiology*. 2007. Elsevier Ltd.

16. Wustner, D. and K. Solanko, *How cholesterol interacts with proteins and lipids during its intracellular transport.* Biochim. Biophys. Acta, Biomembr., 2015. **1848**(9): p. 1908-1926.

17. Castro, B.M., et al., *Biochemical and imaging methods to study receptor membrane organization and association with lipid rafts.* Methods Cell Biol., 2013. **117**(Receptor-Receptor Interactions): p. 105-122,, 1 plate.

18. Bader, A.N., et al., *Homo-FRET Imaging as a Tool to Quantify Protein and Lipid Clustering.* ChemPhysChem, 2011. **12**(3): p. 475-483.

19. Bader, A.N., et al., *Homo-FRET imaging enables quantification of protein cluster sizes with subcellular resolution.* Biophys. J., 2009. **97**(9): p. 2613-2622.

20. Manzo, C., T.S. van Zanten, and M.F. Garcia-Parajo, *Nanoscale Fluorescence Correlation Spectroscopy on Intact Living Cell Membranes with NSOM Probes.* Biophys. J., 2011. **100**(2): p. L8-L10.

21. Sengupta, P., et al., *Probing protein heterogeneity in the plasma membrane using PALM and pair correlation analysis.* Nat. Methods, 2011. **8**(11): p. 969-975.

22. Gumi-Audenis, B., et al., *Structure and Nanomechanics of Model Membranes by Atomic Force Microscopy and Spectroscopy: Insights into the Role of Cholesterol and Sphingolipids.* Membranes (Basel), 2016. **6**(4).

23. Huang, J. and G.W. Feigenson, *A microscopic interaction model of maximum solubility of cholesterol in lipid bilayers.* Biophys. J., 1999. **76**(4): p. 2142-2157.

24. Radhakrishnan, A. and H. McConnell, *Condensed complexes in vesicles containing cholesterol and phospholipids.* Proc. Natl. Acad. Sci. U. S. A., 2005. **102**(36): p. 12662-12666.

25. Hung, W.-C., et al., *The condensing effect of cholesterol in lipid bilayers.* Biophys. J., 2007. **92**(11): p. 3960-3967.

26. Krause, M.R. and S.L. Regen, *The structural role of cholesterol in cell membranes: From condensed bilayers to lipid rafts.* Acc. Chem. Res., 2014. **47**(12): p. 3512-3521.

27. Arita, Y., et al., *Targeting Cholesterol in a Liquid-Disordered Environment by Theonellamides Modulates Cell Membrane Order and Cell Shape.* Chem. Biol. (Oxford, U. K.), 2015. **22**(5): p. 604-610.

28. Ercole, F., et al., *Cholesterol Modified Self-Assemblies and Their Application to Nanomedicine.* Biomacromolecules, 2015. **16**(7): p. 1886-1914.

29. Wustner, D., et al., *Imaging approaches for analysis of cholesterol distribution and dynamics in the plasma membrane.* Chem. Phys. Lipids, 2016. **199**: p. 106-135.

30. Kessel, A., N. Ben-Tal, and S. May, *Interactions of cholesterol with lipid bilayers: the preferred configuration and fluctuations.* Biophys. J., 2001. **81**(2): p. 643-658.

31. Khelashvili, G.A. and H.L. Scott, *Combined Monte Carlo and molecular dynamics simulation of hydrated 18:0 sphingomyelin-cholesterol lipid bilayers.* J. Chem. Phys., 2004. **120**(20): p. 9841-9847.

32. Blodgett, K.B. and I. Langmuir, *Built-up films of barium stearate and their optical properties.* Phys. Rev., 1937. **51**: p. 964-82.

33. Langmuir, I., *Constitution and fundamental properties of solids and liquids. II. Liquids.* J. Am. Chem. Soc., 1917. **39**: p. 1848-1906.

34. Schofield, R.K. and E.K. Rideal, *The kinetic theory of surface films. II. Gaseous, expanded and condensed films.* Proc. R. Soc. London, Ser. A, 1926. **110**: p. 167-77.

35. Kaganer, V.M., H. Mohwald, and P. Dutta, *Structure and phase transitions in Langmuir monolayers.* Rev. Mod. Phys., 1999. **71**(3): p. 779-819.

36. McConnell, H.M., *Structures and transitions in lipid monolayers at the air-water interface.* Annu. Rev. Phys. Chem., 1991. **42**: p. 171-95.

37. Smith, R.D. and J.C. Berg, *The collapse of surfactant monolayers at the air-water interface.* J. Colloid Interface Sci., 1980. **74**(1): p. 273-86.

38. Neurath, H., *Built-up films of proteins and their properties.* Science (Washington, DC, U. S.), 1937. **85**: p. 289-90.

39. Langmuir, I., V.J. Schaefer, and H. Sobotka, *Multilayers of sterols and the adsorption of digitonin by deposited monolayers.* J. Am. Chem. Soc., 1937. **59**: p. 1751-9.

40. Maguire, L.A., H. Zhang, and P.A. Shamlou, *Preparation of small unilamellar vesicles (SUV) and biophysical characterization of their complexes with poly-L-lysine-condensed plasmid DNA.* Biotechnol. Appl. Biochem., 2003. **37**(1): p. 73-81.

41. Sonnino, S. and A. Prinetti, *Membrane domains and the "lipid raft" concept.* Curr. Med. Chem., 2013. **20**(1): p. 4-21.

42. Ziblat, R., L. Leiserowitz, and L. Addadi, *Crystalline Lipid Domains: Characterization by X-Ray Diffraction and their Relation to Biology.* Angew. Chem., Int. Ed., 2011. **50**(16): p. 3620-3629.

43. Wurlitzer, S., P. Steffen, and T.M. Fischer, *Line tension of Langmuir monolayer phase boundaries determined with optical tweezers.* J. Chem. Phys., 2000. **112**(13): p. 5915-5918.

44. Heberle, F.A., et al., *Bilayer thickness mismatch controls domain size in model membranes.* J. Am. Chem. Soc., 2013. **135**(18): p. 6853-6859.

45. Lee, D.W., et al., *Relating domain size distribution to line tension and molecular dipole density in model cytoplasmic myelin lipid monolayers.* Proc. Natl. Acad. Sci. U. S. A., 2011. **108**(23): p. 9425-9430, S9425/1-S9425/4.

46. Garcia-Saez, A.J., S. Chiantia, and P. Schwille, *Effect of Line Tension on the Lateral Organization of Lipid Membranes.* J. Biol. Chem., 2007. **282**(46): p. 33537-33544.

47. Hassan-Zadeh, E., et al., *Complex Roles of Hybrid Lipids in the Composition, Order, and Size of Lipid Membrane Domains.* Langmuir, 2014. **30**(5): p. 1361-1369.

48. Idema, T., J.M.J. van Leeuwen, and C. Storm, *Phase coexistence and line tension in ternary lipid systems.* Phys. Rev. E: Stat., Nonlinear, Soft Matter Phys., 2009. **80**(4-1): p. 041924/1-041924/9.

49. Kim, K.H., et al., *Effect of cholesterol nanodomains on monolayer morphology and dynamics.* Proc. Natl. Acad. Sci. U. S. A., 2013. **110**(33): p. E3054-E3060,SE3054/1-SE3054/6.

50. Dhingra, S., et al., *Dynamic morphological changes induced by GM1 and protein interactions on the surface of cell-sized liposomes.* Materials, 2013. **6**: p. 2522-2533.

51. Yang, S.-T., V. Kiessling, and L.K. Tamm, *Line tension at lipid phase boundaries as driving force for HIV fusion peptide-mediated fusion.* Nat. Commun., 2016. **7**: p. 11401.

Chapter 2—Techniques for Membrane Interrogation

2.1 Introduction

In the previous chapter, several experimental methods for preparing model membranes were introduced. A variety of analytical techniques are available to evaluate the properties of model membranes. In this chapter, relevant techniques will be reviewed with a focus on fluorescence microscopy, beginning with fundamental studies using bulk fluorescence and ending with a review of fluorescence techniques to probe membrane structure at and below the optical resolution limit of traditional spectroscopy. Finally, a single molecule analysis technique will be introduced that is utilized in subsequent chapters.

2.2 A Review of Fluorescence Microscopy in Model Membranes

2.2.1 Fundamentals of Optical Microscopy

Many of the earliest model membrane studies utilized fluorescence microscopy, which revealed the diversity of phase behavior that even simple model membranes can exhibit. Fluorescence microscopy studies often make use of amphiphilic fluorescent probes that are doped into membrane films at low concentrations and emit a signal that is bright enough to be readily distinguished from the background. This technique can be used to image the location or activity of a fluorophore within a model membrane, and is employed in the following chapters to investigate membrane heterogeneity and structure. Optical microscopy is a powerful and versatile technique; however its application can be limited by resolution.

Optical resolution is the ability to distinguish two adjacent objects, like two individual fluorophores within a membrane, rather than seeing them as one single object. Resolution is measured using the emission from a point source, for example a fluorophore, that has been

diffracted through the microscope and imaged. The image that is collected has an Airy disk pattern, shown in **Figure 2.1**, which is formed when the light waves emitted from the point source converge at the imaging plane. The Airy disk appears as a spherical bright spot surrounded by diffraction rings that are created by interference of light waves near the plane of the image. The resolution, which is dependent upon a number of experimental parameters, can be determined by measuring the full width at half of the maximum (FWHM) value of the light intensity.

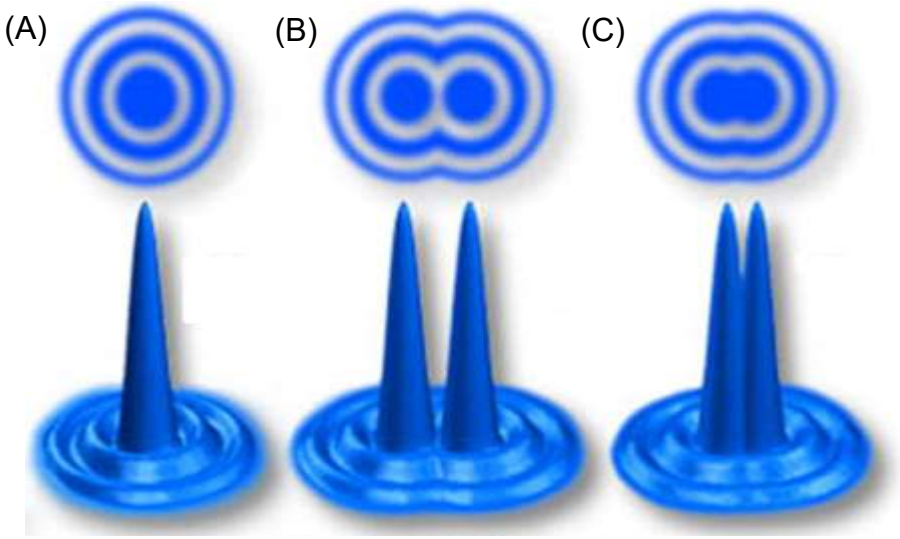

Figure 2.1 on the left (A) shows the diffraction pattern, called an Airy disk pattern that is caused by light from a point source being focused onto an imaging plane. The image in the middle (B) shows two point sources that are separated and resolved, and the image on the right (C) shows a situation where the two point sources cannot be optically resolved. This figure was adapted from [1].

A mathematical relationship for resolution was published by German physicist Ernst Abbe in 1873 as follows:

$$d = \frac{\lambda}{2n \cdot sin\theta} \qquad \textbf{Eqn. 2.1}$$

where d is the smallest distance apart that two point sources can be resolved, λ is the wavelength of light emitted, n is the refractive index of the imaging medium, and sinθ, also called numerical aperture (NA) is the aperture angle. Generally speaking, a higher NA value denotes an objective that has the ability to collect higher spatial frequencies of light than an objective with a lower NA value, and most modern objectives have a NA of around 1. Visible light microscopy generally occurs in a wavelength range of 400 to 800 nm. For 500 nm light and an NA of 1, the theoretical resolution limit is 250 nm.

In 1896, Lord Rayleigh defined that two point sources observed through a microscope objective are considered resolved when the two spots are equal to or farther apart than the diameter of one individual point source, which is approximately λ/2. This is seen on **Figure 2.1** where the two point sources are separated by enough distance to be resolved in image (B) but cannot be resolved in image (C). Limited optical resolution poses a challenge when studying lipid rafts because the average size of a lipid raft ranges from 10 nm – 200 nm, meaning that raft domains can be seen but not be resolved in native membranes using traditional techniques. However, a number of advanced optical techniques have been developed that aid in investigating small structures like lipid rafts.

2.2.2 Advanced Optical Techniques

Fluorescence correlation spectroscopy (FCS) is one such fluorescence technique that is used to interrogate biomembranes for structures below the visible light resolution limit [2, 3]. FCS provides high temporal resolution and can be used to track an individual fluorophore within a system. Using this technique, a fluorescence signal is collected over time, with special interest paid to the minute intensity fluctuations of the fluorophore that occur as a response to the changing physical parameters of its local environment [4]. Fluctuations in signal are

quantified in terms of their strength and duration using a mathematical procedure to create an autocorrelation curve, which can be used to derive the lateral diffusion coefficient of the object.

FCS studies on model membranes have shown that the translational diffusion coefficient of a fluorophore can vary by as much as two orders of magnitude, depending on the local lipid composition. For example, in a study using a model membrane composed of DLPC/DPPC/cholesterol, which spontaneously phase separates into areas of high and low order at room temperature, the lateral diffusion coefficient was measured to be approximately 3×10^{-8} cm^2/s in the less ordered, fluid phase and about 2×10^{-10} cm^2/s in the more ordered areas of the membrane [5]. FCS has been used in live plasma membrane cells to probe for lipids rafts. Raft domains, which are smaller than the resolution limit for traditional imaging, were shown to act as obstacles to molecules diffusing throughout the membrane. The shape of FCS curves in native membranes thus exhibit small areas of decay where the fluorophore has encountered such an obstacle [6]. While these studies cannot be used to determine the diameter of lipid rafts, they do provide supporting evidence for their existence in live cells, as FCS curve decay is not present in model membranes. Additionally, FCS is non-destructive to the sample, can be used to track an individual molecule or up to hundreds of molecules, and provides immediate data with a reasonably high statistical confidence. Disadvantages of this technique include that it provides a limited insight into the diversity of single molecule behavior.

A similar technique that can be employed to measure diffusion coefficients is fluorescence recovery after photobleaching (FRAP). To determine diffusion coefficients with FRAP, a high-intensity laser beam is used to photobleach an area of sample and the sample is monitored using fluorescence microscopy to observe the return of signal to the photobleached region. This technique is performed on model membranes by incorporating a low concentration of fluorescently labeled lipid into the sample and monitoring the fluorophore's diffusion. FRAP is frequently used to measure lateral diffusion coefficients for various membrane components and

characterize the phases present in a sample. It can also be used to track diffusion of other molecules of interest like proteins in membranes [7]. FRAP is versatile, as it can be used to determine the diffusion coefficient of slowly and rapidly diffusing molecules by adjusting the area of the photobleached region. However, unlike FCS, FRAP limited to making bulk measurements and is insensitive to measurements of a mixed population where some molecules are diffusing and others restricted in their mobility [8].

Fluorescence resonance energy transfer (FRET) is a useful technique for detecting molecular interactions, like lipid-lipid or protein-protein interactions, that occur at distances of 1 – 10 nm separation [9]. FRET occurs when a donor fluorophore in an excited state transfers energy to an acceptor fluorophore via intermolecular dipole-dipole coupling. As this nonradiative transfer can only occur at short distances, FRET is useful for measuring molecular proximity. For example, this technique has been used to show that about 40% of GPI-proteins in the membrane are localized into small clusters of 3 to 4 proteins, providing support for the hypothesis that lipid rafts bring proteins into close proximity to carry out signaling events [10].

FRET is also frequently used to image coexisting lipid domains in membrane systems. This can be accomplished by selecting a donor fluorophore that preferentially partitions into one lipid domain and an acceptor fluorophore that prefers the other domain [11]. At the interfacial region between the domains, FRET occurs. Alternatively, FRET imaging can be used to show if two components prefer the same domain. This experimental design has been used to show that within the plasma membrane GM1 and GPI-anchored protein compounds cluster together in sub-micro sized domains [12-14]. Raft domains are thought to be preferentially enriched in GPI-anchored proteins and ganglioside molecules, most predominantly the ganglioside GM1, supporting the idea that these cluster together in raft domains.

FCS, FRAP, and FRET all provide data that indirectly supports the existence of small (<200 nm) structures in biomembranes, but these structures have also been imaged using high-resolution optical techniques. Near-field scanning optical microscopy (NSOM), for example, is a useful technique for exploring the size and structure of lipid raft domains. When a sample is interrogated using light, the sample's emission takes two separate forms. There is a far-field component, which consists of propagating light, and a near-field component which is non-propagating. The near-field component exists near the surface of the sample, contains high-frequency spatial information, and exponentially decays in intensity. NSOM is the measurement of the near-field component, and its resolution is not limited by the wavelength of the excitation light source but by its aperture size. The excitation source is placed very near the sample, typically only a few nanometers away. Due to the experimental configuration, this technique is ideal for investigating surfaces and has been used to explore the size of raft domains. Raft domains are usually estimated to be 10 – 200 nm in diameter, but studies using NSOM have shown that average domain radius depends largely on the lipid composition of the raft, and the composition can vary depending on the host cell type [15-17].

Photoactivated localization microscopy (PALM) and stochastic optical reconstruction microscopy (STORM) are both techniques that are used to overcome the diffraction barrier and thus images with a resolution of tens of nanometers [18, 19]. These techniques utilize fluorescent molecules that are initially in an inactivated state and are stochastically activating to a fluorescent state, imaged, and deactivated [20]. Activation, imaging, and deactivation are continued cyclically so that only a small number of molecules are imaged at once, and molecules that would otherwise be indistinguishable are temporally resolved. The images are then analyzed to determine and map the centroid positions of individual molecules, which are used to create a single high-resolution image. Since the introduction of these techniques, images showing raft-associated protein clustering in native plasma membranes have been

published. However, quantitative analysis of this data is limited by the concern that one single molecule could be assigned multiple locations in the final image or a single molecule could remain photoactivated longer than expected, causing it to appear as a molecular cluster in the final image. Additionally, this technique and others discussed in this section can be used to investigate biomembranes structure but frequently average data over large populations, which could mask certain trends.

2.2.3 Motivation for Single Molecule Analysis

This limitation provides the motivation for developing single molecule fluorescence techniques that probe structure on a molecular level, illuminating trends that can be hidden in ensemble measurements. For example, fluorescence recovery after photobleaching (FRAP) can be used to determine the diffusion coefficient of a membrane component, but diffusion rates for a large population of fluorescently modified probes is averaged in the process [21]. Single particle tracking (SPT) studies, on the other hand, can also be used to determine diffusion coefficients at the single species level. A single molecule study using SPT on live cells has shown that a G-protein coupled receptor in the plasma membrane diffuses from raft domain to raft domain, and is confined to a domain compartment for a short time period before diffusing to another compartment [22]. If this data were analyzed on a bulk scale, the protein confinement event would be lost. This and other single molecule techniques have shown the utility of single molecule analysis in elucidating protein dynamics, oligomerization processes, and molecular structure in membranes [23-25].

2.3 Defocused Fluorescence Imaging to Determine Single Molecule Orientations

Advances in single molecule fluorescence detection have provided novel ways to investigate membrane structure. For example, polarized total internal reflection fluorescence microscopy (PTIRF-M) is especially useful for investigating complex biological problems, as it provides a method to probe the three-dimensional orientations of fluorescent molecules doped into biological systems. This technique has been used to investigate the orientation and rotational behavior of the motor protein myosin V, to determine the rigidity and orientation of macromolecules on actin filaments, and to investigate the structure of lipid membranes [26-28]. Membrane structural changes caused by surface pressure and hydration have been investigated, as well as the effect of additives like ganglioside molecules and sterols [29-34].

2.3.1 Emission at an Interface

In order to track single molecule orientations, fluorophores are doped into model lipid membranes at a concentration of 10^{-8} mol %. One fluorescent molecule used in this work is BODIPY-PC, a lipid with a phosphocholine headgroup lipid and two saturated acyl tailgroups. A boron-dipyrromethene (BODIPY) fluorophore is conjugated onto one of the tailgroups, as shown in **Figure 2.2**. In that image, native lipid molecules are shown on the right and left hand sides and fluorescent BODIPY-PC is shown in the center of the figure, with the emission dipole of the BODIPY fluorophore indicated in red. The emission dipole lies along the long axis of the conjugated bond system with a 13° difference between the absorption and emission dipoles. [35, 36].

In free space, the emission of an individual dipole takes the shape of a $\sin^2$ pattern around the emission dipole. This pattern becomes distorted if it is brought to an interface of changing refractive index, as shown in **Figure 2.3**. Therefore, when the emission is collected

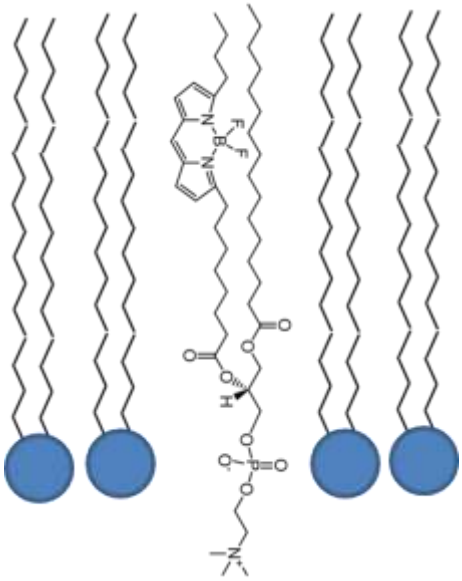

Figure 2.2 shows an illustrated view of the monolayer sample used for single molecule analysis. In this sample, BODIPY-PC, shown in the center of the figure, is included in the monolayer at concentrations of approximately 10^{-8} mol %. Other lipids, shown on the sides of the figure, are not fluorescent and make up the remainder of the sample. The fluorescent lipid inserts into the monolayer similarly to natural lipids, with the BODIPY moiety located in the tail

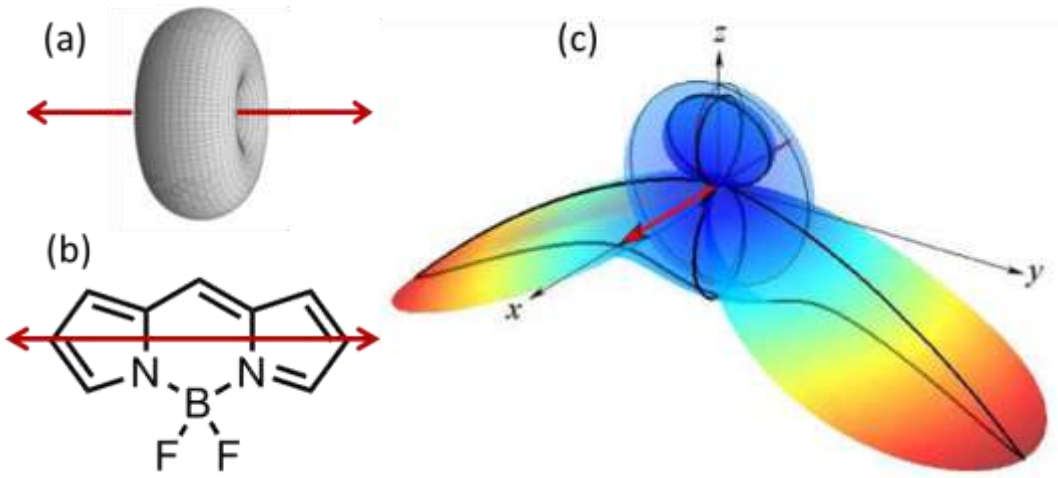

Figure 2.3 – Image (a) shows the fluorescence intensity of an emission dipole, which takes the shape of a $\sin^2$ function around the emission dipole. The emission dipole of the BODIPY fluorophore is parallel to the long axis of the conjugated ring system (b). When the emission dipole is located at an interface of differing refractive index, the fluorescent emission becomes distorted in the medium of higher refractive index. One such distortion pattern is shown in (c), where the emission dipole is parallel to the interface.

and imaged using a microscope, the signal intensity is angle dependent based upon the orientation of the emission dipole at the interface. Modern objectives correct for this angle dependence, created by spherical aberrations, so that the light emitted from a single point on the sample surface appears as a single bright spot in the image. However, by defocusing the optics by approximately 500 nm, spherical aberrations can be reintroduced as illustrated in **Figure 2.4**, causing the signal from each dipole to appear as a distinctive emission pattern. Emission patterns, like those shown in **Figure 2.5**, are unique for the orientation of the fluorophore and can be extracted from the image.

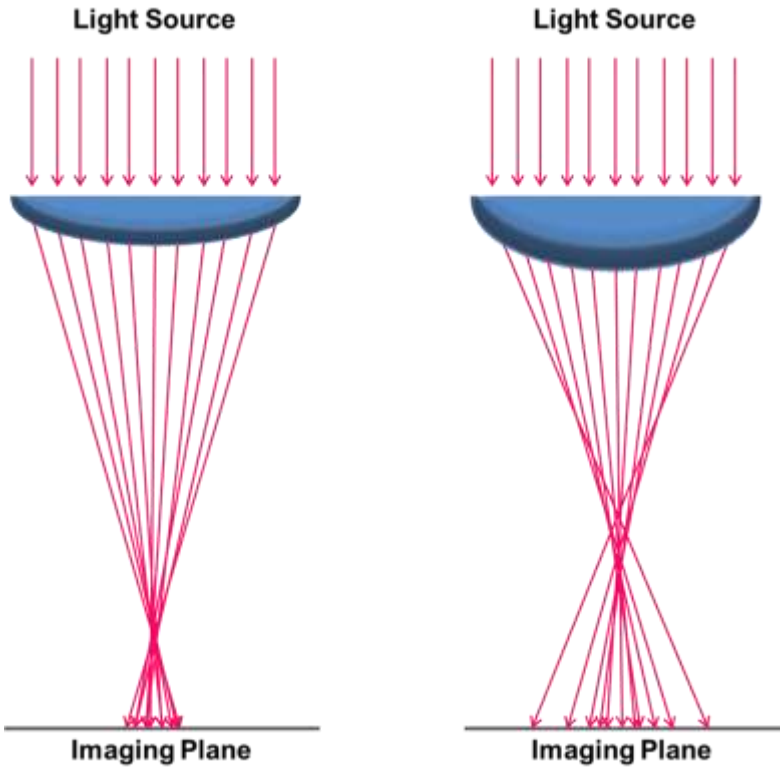

Figure 2.4 shows a lens that is used to collect light from a sample and focus it onto an imaging plane. Two imaging configurations are shown here. On the left side of the image, light is collected and focused onto the imaging plane in a traditional manner to create an in-focus image. On the right side of the figure, spherical aberrations have been introduced into the sample by defocusing the optics.

The emission patterns generated by defocused imaging can be modeled using a MATLAB simulation to show the expected emission patterns based on emission dipole orientation. The simulation is based on an equation that describes the diffraction of light through a lens in the presence of spherical aberrations. An example equation is shown in Equation 2.3.

$$l(l,y,z) = \frac{l_o(\theta,\varphi)}{z^2}\left|\int_0^1 J_o\left(ka\rho\frac{\sqrt{x^2+y^2}}{z}\right)exp(-ik\cdot opd(\rho))\cdot\rho\cdot dp\right|^2 \qquad \textbf{Eqn. 2.3}$$

Here, the intensity pattern of the emission dipole can be described in Cartesian coordinates using the intensity pattern created by the emission dipole in spherical coordinates $l(\theta,\varphi)$, where

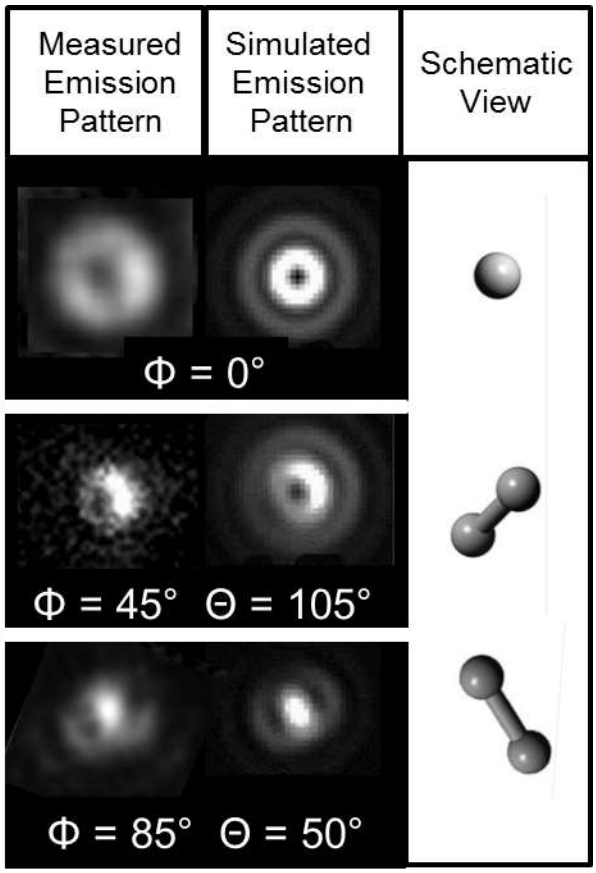

Figure 2.5 shows the measured and simulated emission patterns for three different fluorophores in lipid monolayers. The measured emission patterns are compared to simulations of emission patterns generated using MATLAB.

theta (θ) is the polar coordinate, phi (φ) is the azimuthal coordinate of the emission dipole in relation to the sample surface, and z is the tube length of the microscope [37]. The integral utilizes the zero-order Bessel function (J_o), the wave vector magnitude (k), and the limiting aperture of the imaging system (a). The non-ideality of the optics is described within the term (ρ), and opd(ρ) is the optical path difference of the light traveling through the center and outer edge of the objective as a function of ρ. A MATLAB simulation based upon this equation has been used to create a library of possible dipole emission patterns. Within the simulation, experimental parameters including the numerical aperture and magnification of the objective are entered and held constant. Variable parameters like the defocusing distance and emission dipole orientation are adjusted to fit the measured emission patterns.

Using this technique, a fluorescent lipid analog can be included within a monolayer at a

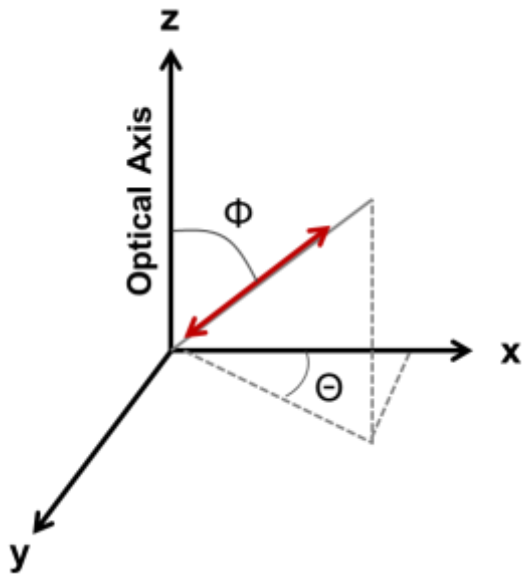

Figure 2.6 – The three-dimensional orientation of each emission dipole is defined in relation to the Cartesian coordinate system shown above. The tilt angle (Φ) describes the orientation of the emission dipole between the z and x axis. The azimuthal angle (Θ) describes the position of the emission dipole between the y and z axis.

concentration of 10^{-8} mol %, where individual fluorophores can be imaged and resolved. The fluorescent lipid analogs are contained within a lipid monolayer, which causes the emission dipoles to lie within a single z-plane. A piezoelectric focusing collar can be attached to the objective and used to defocus the optics by 500 nm, eliminating defocusing distance as a variable parameter. Thus, the polar (Φ) and azimuthal (Θ) angles of the emission dipole orientation are the only variable parameters that are used to create a library of potential dipole emission patterns. **Figure 2.6** shows the polar and azimuthal angles in a three-dimensional plot, in order to illustrate how these two angles can be used to describe the positioning of a fluorophore within a monolayer.

Experimental data is collected and the resulting emission patterns are compared to the library of potential emission patterns to determine the three-dimensional orientation of each fluorophore within the monolayer. After the fluorophore orientations have been extracted from the monolayer, a tilt angle histogram is created plotting the range of potential orientations versus the total number of fluorophores at each orientation. This histogram can be used to evaluate the structure of the monolayer.

2.3.2 Total Internal Reflection for Excitation of the Sample

One important consideration in the experimental design is the method of excitation. It is critical that the excitation configuration has the ability to excite all of the fluorophores within the sample, instead of preferentially exciting fluorophores at certain orientations. Epifluorescence is a common configuration for fluorescence imaging; however, it is inadequate for this purpose because it only excites molecules with their absorption dipoles oriented parallel to the direction of electric oscillation of the propagating light waves [38]. Instead, a total internal reflection (TIR) configuration using p-polarized light is chosen because the electrical component of the p-

polarized light is parallel to the optical axis and has the ability to excite all molecular orientations [37, 39].

As light travels from a medium of higher refractive index, through an interface, and into a medium of lower refractive index, the light beam undergoes reflection and refraction. The refracted beam bends away from the normal at the interface into the medium of lower refractive index, while a portion of the light is reflected at the interface into the medium of higher refractive

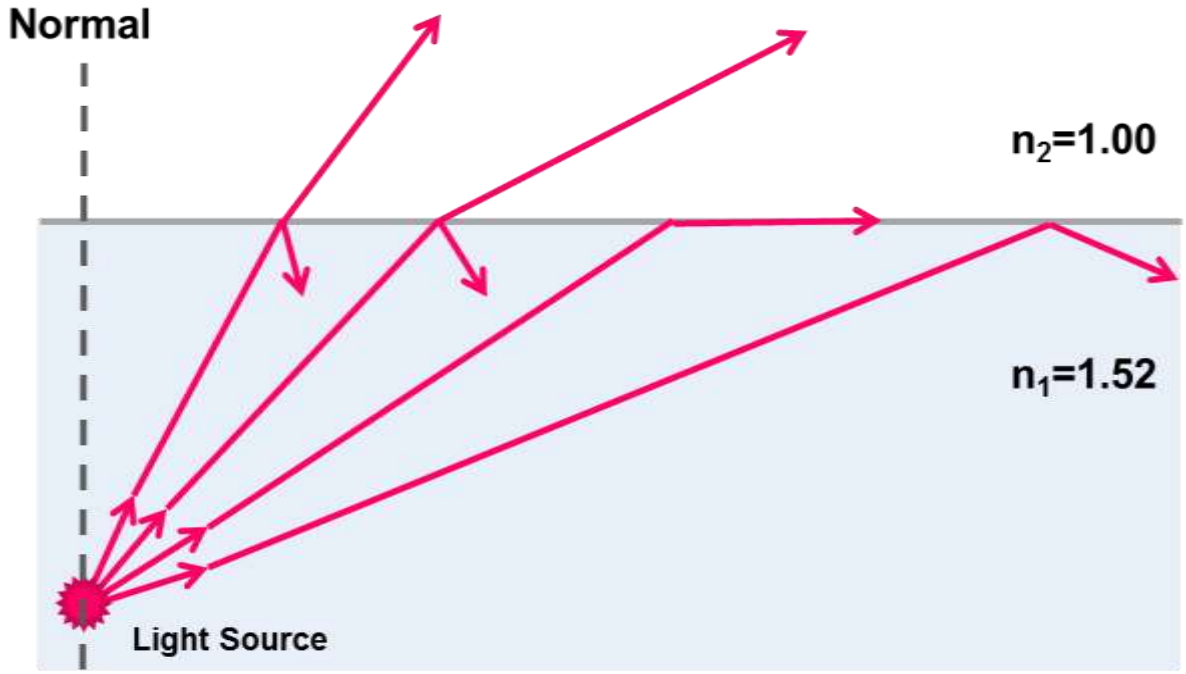

Figure 2.7 – The process of total internal reflection is illustrated. Total internal reflection occurs when the beam of light reaches an interface of changing refractive index at a larger angle than the critical angle. At this condition, the beam of light is completely reflected back into the medium of higher refractive index. When the angle between the normal and the beam is smaller than the critical angle, the beam is reflected into the higher refractive index medium and refracted into the lower refractive index medium, as shown on the right side of the figure.

index. The optical phenomenon of refraction is described by Snell's Law:

$$\frac{Sin\theta_1}{\sin\theta_2} = \frac{n_2}{n_1} \qquad \textbf{Eqn. 2.4}$$

where n is the refractive index of each medium and θ is the angle of the light from normal in each medium. At any larger angle than the critical angle the beam will be completely reflected into the higher refractive index material instead of passing into the second medium, as shown on the far right of **Figure 2.7**, and this process is called total internal reflection (TIR). The critical angle can be calculated using Snell's Law:

$$\theta_{critical} = arcsin\frac{n_2}{n_1} \qquad \textbf{Eqn. 2.5}$$

where n_2 is greater than n_1. For light at the interface of glass (n = 1.52) and a vacuum (n = 1.00), the critical angle is 41.2°.

When TIR occurs, an evanescent wave is created at the interface that penetrates into the medium of lower refractive index. The evanescent wave is a non-propagating, exponentially decaying field at the interface that can be used to excite fluorophores. When p-polarized light is used to create an evanescent field, the electric field component of the electromagnetic wave is oriented parallel to the optical axis and arcs along the interface, allowing molecules with components of their absorption dipole in the x – z and y – z plane to be excited equally. In this experiment, the evanescent wave is created at the interface between the glass substrate and the lipid monolayer on top of the substrate.

The technique described above can be used to perform single molecule analysis for structural studies. Model lipid monolayers are prepared with a small concentration of fluorescent lipid analog using a Langmuir-Blodgett (LB) trough. The monolayer is transferred onto a glass substrate, which is placed onto an inverted microscope. Index-matched immersion oil is added between the objective and the slide, and the sample is excited using TIR of p-

polarized light from a 514 nm argon-ion laser. TIR excites all fluorophores in the membrane plane, providing a view of structure. The collection optics are defocused by 500 nm, allowing the three-dimensional orientations of the fluorophores to be extracted from the images. Finally, images of the sample are collected using a CCD camera and analyzed to create tilt angle histograms of the molecular orientations. This technique has been used to investigate structure in many different sample types.

2.4 Review of Single Molecule Orientation Analysis for Structural Investigation

PTIRF-M was originally theorized using calculations to show that single molecule orientations could be extracted from a dipole-moment located at in interface between materials of differing refractive index [40]. Specifically, Hellen and Alexrod used a fixed-power dipole model to calculate the angle emission distortion of a fluorophore at the interface between air and a bare dielectric substrate or a dielectric substrate with a thin metal coating. They modeled the angle dependence of the emission as a function of dipole-moment orientation and the distance of the dipole moment from the interface. Next, the theory was applied to an experimental system where a glass substrate was coated with a thin polymer coating that included a small concentration of fluorescent molecules. In this study, the authors demonstrated that the experimentally observed emission patterns matched the theoretically predicted patterns and noted that molecular rotation and diffusion could be observed in real time using this method [39].

Subsequently, the dynamic motion of the motor protein myosin V was studied as it traveled along actin with temporal resolution as high as 20 milliseconds, and the data was used to determine the step size and range of rotational motion for the biomolecule [41]. This study was later expanded to demonstrate that myosin has both large and small step sizes, which can be

distinguished using defocused imaging [26]. The degree of rigidity of actin and the role of actin motion in myosin motility has also been investigated using PTIRF-M [27]. These studies together illustrate the utility of this method for investigating complex biological processes with high spatial and temporal resolution.

Single molecule orientations have also been used to investigate the structural and biophysical properties of model biological membranes. PTIRF-M measurements can be made of Langmuir monolayres located directly on the aqueous subphase of an LB trough by lowering a prism onto the lipid tailgroups to excite dipole moments [26]. While this configuration is interesting from a biological prospective, the measurements are influenced by the presence of the hydrophilic glass prism that has been introduced to the hydrophobic tail group area. Alternatively, model membranes can be transferred onto a solid substrate for measurements, creating a true glass-air interface for structural measurements. This configuration has been used recently to investigate the role of surface pressure, hydration, and additives on monolayer structure [29-31, 33].

Surface pressure in LB films is a measure of lipid packing density, with higher surface pressure specifying greater lipid packing density. Surface pressure can be easily controlled in LB films by changing the area that the monolayer occupies. As an initial concept experiment, monolayers were prepared with a small concentration of fluorescently labeled lipid at a variety of surface pressures, and single molecule orientations were measured to track structural changes in the film. This study was used to demonstrate that monolayers with higher surface pressure have greater structural ordering and that single molecule orientation measurements can track that change in order [30]. In fact, the order parameter, or percentage of fluorophores with a tilt angle smaller than 10° increased linearly with increasing surface pressure. In this work, headgroup labeled lipids and acyl tail group labeled lipids were both used as probes, and it was demonstrated that tail group labeled lipids have a greater utility for structural investigation. The

orientations of headgroup labeled lipids were insensitive to lipid packing density, presumably because of their location within the membrane. Acyl-labeled lipids with the fluorophore in the hydrophobic tail group, conversely, responded to changes in packing density as described above.

One challenge that arises when comparing monolayer and bilayer data is that the equivalent surface pressure of bilayers cannot be measured directly because bilayers exist in a tension free state. To address this challenge, PTIRF-M was used to compare lipid packing in LB films and supported lipid bilayers prepared using vesicle fusion. Monolayers were prepared at a range of surface pressures, single molecule orientations measured, and the order parameter calculated. Next, a bilayer was prepared and analyzed for order parameter. The two systems were compared to determine which monolayer surface pressure had the same order parameter as the bilayer data, and by comparing the degree of ordering in both models the equivalent surface pressure of bilayers was estimated to be 23 mN/m [29].

Subsequent studies explored the role of humidity on membrane structure as well as changes due to additives like cholesterol and GM1 [29, 31, 33]. These studies have demonstrated that this technique can be applied to investigate the complex interactions that determine membrane structure in a controlled manner. Using LB films as a model membrane system for investigation allows for precise control of lipid composition and packing density. Analysis using PTIRF-M is simplified because the molecules are transferred onto a glass subphase, thus are all located within a single z-plane, allowing a consistent defocus distance for each fluorophore. Because of these advantages, this technique will be used in the following chapters to investigate complex mixed monolayers to elucidate the role that specific membrane components play in the formation and stabilization of membrane domains.

2.5 – Conclusion

Several of the studies discussed in the following chapters build upon the work described above, applying this technique to investigate relevant biological problems. In chapter 3, this approach will be applied in order to investigate the role that cholesterol plays in the formation of lipid domains using ternary lipid monolayers that mimic lipid raft structure. This data will be discussed in terms of the important role that cholesterol plays in lipid rafts. In chapter 4, POPC, a lipid of mixed acyl-tail group saturation, will be used to investigate the role of hybrid lipids in forming and stabilizing small domains in order to understand how 10 – 200 nm lipid rafts are stable in biological membranes. These two studies were possible in part because this technique had been previously characterized. The advantages of the technique, including the ability to control model membrane composition, were critical for investigating the role that specific components play in membrane domain formation and structure.

2.6 References

1. Abramowitz, M. and M. Davidson. *Numerical Apeture and Resolution*.

2. Schwille, P., J. Korlach, and W.W. Webb, *Fluorescence correlation spectroscopy with single-molecule sensitivity on cell and model membranes.* Cytometry, 1999. **36**(3): p. 176-182.

3. Kahya, N., et al., *Probing lipid mobility of raft-exhibiting model membranes by fluorescence correlation spectroscopy.* J. Biol. Chem., 2003. **278**(30): p. 28109-28115.

4. Thompson, N.L., *Fluorescence correlation spectroscopy.* Top. Fluoresc. Spectrosc., 1991. **1**: p. 337-78.

5. Korlach, J., et al., *Characterization of lipid bilayer phases by confocal microscopy and fluorescence correlation spectroscopy.* Proc. Natl. Acad. Sci. U. S. A., 1999. **96**(15): p. 8461-8466.

6. Bacia, K., et al., *Fluorescence correlation spectroscopy relates rafts in model and native membranes.* Biophys. J., 2004. **87**(2): p. 1034-1043.

7. Crane, J.M. and L.K. Tamm, *Role of cholesterol in the formation and nature of lipid rafts in planar and spherical model membranes.* Biophys. J., 2004. **86**(5): p. 2965-2979.

8. van den Wildenberg, S.M.J.L., Y.J.M. Bollen, and E.J.G. Peterman, *How to quantify protein diffusion in the bacterial membrane.* Biopolymers, 2011. **95**(5): p. 312-321.

9. Parton, R.G., *Ultrastructural localization of gangliosides; GM1 is concentrated in caveolae.* J. Histochem. Cytochem., 1994. **42**(2): p. 155-66.

10. Shaw, A.S., *Lipid rafts: now you see them, now you don't.* Nat. Immunol., 2006. **7**(11): p. 1139-1142.

11. Sekar, R.B. and A. Periasamy, *Fluorescence resonance energy transfer (FRET) microscopy imaging of live cell protein localizations.* The Journal of Cell Biology, 2003. **160**(5): p. 629-633.

12. Kenworthy, A.K. and M. Edidin, *Distribution of a glycosylphosphatidylinositol-anchored protein at the apical surface of MDCK cells examined at a resolution of <100 Å using imaging fluorescence resonance energy transfer.* J. Cell Biol., 1998. **142**(1): p. 69-84.

13. Kenworthy, A.K., N. Petranova, and M. Edidin, *High-resolution FRET microscopy of cholera toxin B-subunit and GPI-anchored proteins in cell plasma membranes.* Mol. Biol. Cell, 2000. **11**(5): p. 1645-1655.

14. Varma, R. and S. Mayor, *GPI-anchored proteins are organized in submicron domains at the cell surface.* Nature (London), 1998. **394**(6695): p. 798-801.

15. Dickenson, N.E., et al., *Near-field scanning optical microscopy: a tool for nanometric exploration of biological membranes.* Anal. Bioanal. Chem., 2010. **396**(1): p. 31-43.

16. Ianoul, A. and L.J. Johnston, *Near-field scanning optical micorscopy to identify membrane microdomains.* Methods Mol. Biol. (Totowa, NJ, U. S.), 2007. **400**(Methods in Membrane Lipids): p. 469-480.

17. Chen, Y., J. Qin, and Z.W. Chen, *Fluorescence-topographic NSOM directly visualizes peak-valley polarities of GM1/GM3 rafts in cell membrane fluctuations.* J. Lipid Res., 2008. **49**(10): p. 2268-2275.

18. Castro, B.M., et al., *Biochemical and imaging methods to study receptor membrane organization and association with lipid rafts.* Methods Cell Biol, 2013. **117**: p. 105-22.

19. Dedecker, P., et al., *Widely accessible method for superresolution fluorescence imaging of living systems.* Proc. Natl. Acad. Sci. U. S. A., 2012. **109**(27): p. 10909-10914, S10909/1-S10909/20.

20. Gunewardene, M.S., et al., *Superresolution Imaging of Multiple Fluorescent Proteins with Highly Overlapping Emission Spectra in Living Cells.* Biophys. J., 2011. **101**(6): p. 1522-1528.

21. Kang, M., et al., *Simplified equation to extract diffusion coefficients from confocal FRAP data.* Traffic (Oxford, U. K.), 2012. **13**(12): p. 1589-1600.

22. Suzuki, K., et al., *Rapid hop diffusion of a G-protein-coupled receptor in the plasma membrane as revealed by single-molecule techniques.* Biophys J, 2005. **88**(5): p. 3659-80.

23. Abe, K., et al., *Correlation between the activities and the oligomeric forms of pig gastric H/K-ATPase.* Biochemistry, 2003. **42**(51): p. 15132-8.

24. Li, N., et al., *Single-Molecule Imaging Reveals the Activation Dynamics of Intracellular Protein Smad3 on Cell Membrane.* Sci. Rep., 2016. **6**: p. 33469.

25. Wang, X., et al., *Single-molecule fluorescence imaging to quantify membrane protein dynamics and oligomerization in living plant cells.* Nat. Protoc., 2015. **10**(12): p. 2054-2063.

26. Toprak, E., et al., *Defocused orientation and position imaging (DOPI) of myosin V.* Proc. Natl. Acad. Sci. U. S. A., 2006. **103**(17): p. 6495-6499.

27. Forkey, J.N., M.E. Quinlan, and Y.E. Goldman, *Measurement of single macromolecule orientation by total internal reflection fluorescence polarization microscopy.* Biophys. J., 2005. **89**(2): p. 1261-1271.

28. Tronin, A., T. Xu, and J.K. Blasie, *In Situ Determination of Orientational Distributions in Langmuir Monolayers by Total Internal Reflection Fluorescence.* Langmuir, 2005. **21**(17): p. 7760-7767.

29. Livanec, P.W., H.A. Huckabay, and R.C. Dunn, *Exploring the Effects of Sterols in Model Lipid Membranes Using Single-Molecule Orientations.* J. Phys. Chem. B, 2009. **113**(30): p. 10240-10248.

30. Livanec, P.W. and R.C. Dunn, *Single-Molecule Probes of Lipid Membrane Structure.* Langmuir, 2008. **24**(24): p. 14066-14073.

31. Huckabay, H.A. and R.C. Dunn, *Hydration Effects on Membrane Structure Probed by Single Molecule Orientations.* Langmuir, 2011. **27**(6): p. 2658-2666.

32. Armendariz, K.P., et al., *Single molecule probes of membrane structure: Orientation of BODIPY probes in DPPC as a function of probe structure.* Analyst (Cambridge, U. K.), 2012. **137**(6): p. 1402-1408.

33. Armendariz, K.P. and R.C. Dunn, *Ganglioside Influence on Phospholipid Films Investigated with Single Molecule Fluorescence Measurements.* J. Phys. Chem. B, 2013. **117**(26): p. 7959-7966.

34. DeWitt, B.N. and R.C. Dunn, *Interaction of Cholesterol in Ternary Lipid Mixtures Investigated Using Single-Molecule Fluorescence.* Langmuir, 2015. **31**(3): p. 995-1004.

35. Karolin, J., et al., *Fluorescence and Absorption Spectroscopic Properties of Dipyrrometheneboron Difluoride (BODIPY) Derivatives in Liquids, Lipid Membranes, and Proteins.* J. Am. Chem. Soc., 1994. **116**(17): p. 7801-6.

36. Chung, P.-H., C. Tregidgo, and K. Suhling, *Determining a fluorophore's transition dipole moment from fluorescence lifetime measurements in solvents of varying refractive index.* Methods Appl Fluoresc, 2016. **4**(4): p. 045001.

37. Bartko, A.P. and R.M. Dickson, *Imaging Three-Dimensional Single Molecule Orientations.* J. Phys. Chem. B, 1999. **103**(51): p. 11237-11241.

38. Kohen, E., et al., *Microspectrofluorometric study of cell structure and function.* Microbeam Anal., 1987. **22nd**: p. 192-6.

39. Bartko, A.P. and R.M. Dickson, . J. Phys. Chem. B, 1999. **103**(16): p. 3053-3056.

40. Hellen, E.H. and D. Axelrod, *Fluorescence emission at dielectric and metal-film interfaces.* J. Opt. Soc. Am. B: Opt. Phys., 1987. **4**(3): p. 337-50.

41. Forkey, J.N., et al., *Three-dimensional structural dynamics of myosin V by single-molecule fluorescence polarization.* Nature (London, U. K.), 2003. **422**(6930): p. 399-404.

Chapter 3 – Interaction of Cholesterol in Ternary Lipid Mixtures Investigated using Single Molecule Fluorescence

3.1 Introduction

Mammalian membranes are highly complex structures that occupy central roles in many cellular processes. Approximately 20-30 mol % of the plasma membrane in higher eukaryotes is cholesterol, making it the single most abundant component in the plasma membrane and illustrating its importance in proper cellular function [1]. Besides its established links with cardiovascular disease [2], cholesterol has also been associated with cancer, diabetes, and dementia [3]. Cholesterol sits at the junction of several important metabolic pathways and a variety of genetic diseases are associated with changes in cholesterol metabolism, illustrating the importance of cholesterol homeostasis in human health [4].

Approximately 90% of the free cholesterol in animal cells is found in the plasma membrane, with the remaining distributed to varying degrees in the organelles [5, 6]. The incorporation of cholesterol into lipid membranes can lead to significant, functionally relevant physical changes in membrane properties. For example, cholesterol can order fluid membranes, leading to lower passive permeability, and increase the mechanical strength of membranes while maintaining favorable diffusive properties, as mentioned in Chapter 1. These effects are driven by the structure of cholesterol, which leads to a condensing effect when added to fluid membranes [7-13] .

The structure of cholesterol is shown in **Figure 3.1** along with other species important in this study. Cholesterol inserts into membranes with its hydroxyl headgroup oriented towards the membrane interface where it can form favorable electrostatic or hydrogen bonding interactions with neighboring headgroups [14] . The hydrophobic body of cholesterol inserts into the bilayer

interior where favorable van der Waals interactions with the surrounding acyl tail groups stabilize its insertion [15]. The small hydroxyl headgroup of cholesterol, however, cannot adequately screen the bulky hydrophobic ring system from water at the membrane interface. In the umbrella model, neighboring lipids are recruited to help screen cholesterol from these unfavorable interactions. Large headgroup lipids such as phosphatidylcholine (PC) and sphingomyelin (SM) pack near cholesterol, which offsets towards the interior of the membrane. Under this headgroup 'umbrella', the rigid steroid structure of cholesterol aligns along and helps order the acyl chains of the neighboring lipids [11] . This favors interactions with saturated

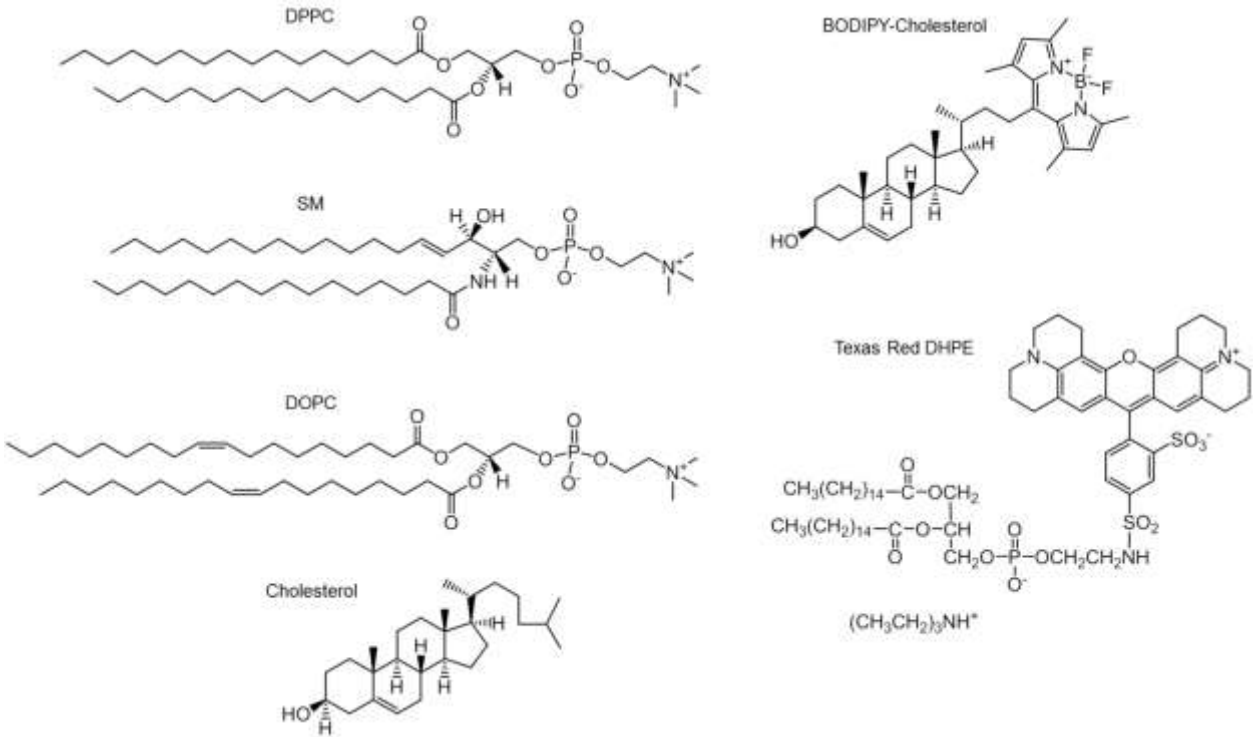

Figure 3.1- Structures of 1,2-Dipalmitoyl-*sn*-glycero-3-phosphatidylcholine (DPPC), 1,2-dioleoyl-sn-glycero-3-phosphocholine (DOPC), chicken egg sphingomyelin (SM), cholesterol, 23-(dipyrromethene boron difluoride)-24-norcholesterol (BODIPY-cholesterol), and Texas Red 1,2-dihexadecanoyl-*sn*-glycero-3-phosphoethanolamine triethylammonium salt (Texas Red DHPE) are shown. Chicken egg sphingomyelin is a mixture of sphingomyelins of different tail group lengths. The most predominant species is shown in this figure.

hydrocarbon chains that can align along the rigid cholesterol ring and contributes to the well-known condensing effect of cholesterol.

The favorable interactions of cholesterol with saturated lipids also contribute to the formation of heterogeneities within the membrane. To study these heterogeneities, fluorescence microscopy is often used where small amounts of a fluorescent cholesterol analog are doped into the system to track the behavior of natural cholesterol. Often, however, the behavior of modified cholesterols deviates significantly from that of natural cholesterol thus complicating these measurements.

Studies have shown that the intrinsically fluorescent sterols, cholestatrienol (CTL) and dehydroergosterol (DHE), most closely mimic natural cholesterol. These sterols fluoresce due to conjugation in the steroid ring system, which minimally perturbs the overall structure when compared with natural cholesterol. Studies have shown that they stabilize the liquid-ordered (Lo) phase like cholesterol and partition similarly in cellular systems. Molecular dynamics simulations and experimental observations show that both compounds order membranes to a similar degree as cholesterol, with CTL slightly better than DHE owing to its structural similarity to cholesterol [16]. Simulations also suggest that both occupy similar transverse locations within the membrane and orient like cholesterol [17]. The poor optical properties of these analogs, however, limit their use. They both absorb weakly in the ultraviolet, have low quantum yields, and photobleach rapidly [18, 19].

Recently, several new BODIPY-cholesterol analogs such as the one shown in **Figure 3.1** have been introduced which show great promise for studying cholesterol in model and natural systems [20]. The particular analog shown in **Figure 3.1** has a BODIPY fluorophore linked at carbon-24 of cholesterol (TopFluor Cholesterol, Avanti Polar Lipids, Alabaster, AL). Boron dipyrromethene difluoride (BODIPY) is an exceptionally good fluorescent probe with an

extinction coefficient of ~90,000 M^{-1} cm^{-1}, a quantum yield of ~0.8, and excellent photostability properties [21]. Unlike previous fluorescent analogs, which fail to adequately mimic key cholesterol metrics, analogs such as that shown in **Figure 3.1** capture many cholesterol properties [22, 23]. With the BODIPY fluorophore linked at carbon-24 of cholesterol, this analog partitions into Lo domains of model membranes and also distributes and traffics in living cells similarly to cholesterol [20, 24]. MD simulations comparing BODIPY-cholesterol and cholesterol in bilayers of 1,2-dipalmitoyl-*sn*-glycero-3-phosphocholine (DPPC) and SM find similar characteristics. Parameters such as average lipid area, membrane thickness, and position of the sterol in the bilayer show close agreement between BODIPY-cholesterol and cholesterol.

Insight into why this particular BODIPY analog seems to mimic natural cholesterol comes from simulations that reveal two preferred orientations within lipid bilayers: an elongated structure with the BODIPY group near the bilayer interior and a conformation in which the BODIPY group tilts towards the headgroups [24]. The latter is expected to be more perturbative to the surrounding lipid matrix and less cholesterol-like. Simulations of NBD-cholesterol derivatives, for example, show the propensity of the tail bound NBD groups in these analogs to wrap back towards the membrane interface [25]. This disrupts the condensing effect observed for natural cholesterol and experimentally leads to much different behavior for these derivatives than natural cholesterol. For BODIPY-cholesterol, calculations suggest that the preferred orientation has an elongated structure in the membrane that maintains the favorable, cholesterol-like interactions between the sterol ring system and neighboring acyl chains. This insertion geometry also places the BODIPY fluorophore near the membrane interior, where its interactions with the surrounding acyl chains are minimized. Moreover, these interactions decrease further as the order in the membrane increases, thus enhancing the ability of BODIPY-cholesterol to mimic natural cholesterol.

These results clearly illustrate the importance of characterizing probe orientation and insertion geometry when developing fluorescent cholesterol analogs that mimic natural cholesterol. As others have shown, molecular orientations can be extracted from single molecule fluorescence measurements using p-polarized total internal reflection excitation, as discussed in Chapter 2 [26-31]. Spherical aberrations introduced through defocusing of the optics lead to single molecule fluorescence patterns that reflect the orientation of the emission dipole. In previous studies, we have shown that defocused single-molecule fluorescence images can be used to quantify the orientation of individual fluorescent lipid probes doped into lipid matrices. This approach enables quantitative analysis of fluorophore orientations which we have used to characterize changes due to surface pressure [32-34], presence of additives [35, 36], and ambient conditions [37].

Here we use fluorescence microscopy and single molecule fluorescence measurements of 23-(dipyrromethene boron difluoride)-24-norcholesterol (BODIPY-cholesterol) to probe its interactions with lipid monolayers formed using the Langmuir-Blodgett (LB) technique. BODIPY-cholesterol is studied in ternary mixed monolayers of DPPC/1,2-dioleoyl-*sn*-glycero-3-phosphocholine (DOPC)/Chol and SM/DOPC/Chol, which are often used models to study cholesterol mixing [38-40]. The two model mixtures are studied at low (8 mN/m) and high (30 mN/m) surface pressures as a function of cholesterol added to explore their phase partitioning and the influence of cholesterol on their properties.

Fluorescence microscopy on films doped with 0.10 mol % BODIPY-cholesterol reveal similar trends in phase partitioning with surface pressure and cholesterol for both mixed monolayers. In agreement with previous studies, these measurements suggest that BODIPY-cholesterol tracks native cholesterol in both ternary lipid mixtures and is a promising fluorescent analog for studying cholesterol [20]. Single molecule fluorescence measurements of BODIPY-cholesterol doped into films at ~10^{-8} mol % are used to characterize the orientation of the dye in both

monolayers. Tilt angle histograms of the BODIPY-cholesterol emission dipole angle away from the membrane normal are measured at each film condition. These measurements reveal approximately four distinct insertion angles for BODIPY-cholesterol with emission dipole tilt angles centered near 0, 24, 78 and 90 degrees.

In all membranes studied, the addition of cholesterol leads to negligible changes in the BODIPY-cholesterol orientation or population distribution. For SM/DOPC/Chol monolayers, this distribution is also insensitive to surface pressure. For DPPC/DOPC/Chol monolayers, however, distinct changes in the BODIPY-cholesterol tilt angle histograms are observed as the surface pressure is increased from 8 mN/m to 30 mN/m. At the elevated surface pressure, the population of BODIPY-cholesterol oriented near 78° significantly decreases with an accompanying increase in populations tilted near 0° and 24°. The data are discussed in terms of a squeeze-out mechanism for BODIPY-cholesterol in monolayers of DPPC/DOPC/Chol at elevated surface pressures. The significant differences observed between SM/DOPC/Chol and DPPC/DOPC/Chol at 30 mN/m suggest that BODIPY-cholesterol is more strongly anchored in monolayers of SM/DOPC/Chol. This is interesting in light of the known propensity of natural cholesterol to interact more strongly with SM in model membranes.

3.2 Materials and Methods

DPPC, DOPC, chicken egg SM (fatty acid distribution 86% 16:0, 6% 18:0, 3% 22:0, 3% 24:1, 2% unknown), BODIPY-cholesterol (Avanti Polar Lipids, Alabaster, AL), and cholesterol (Sigma Aldrich, St. Louis, MO) were obtained at >99% purity. Texas Red 1,2-dihexadecanoyl-*sn*-glycero-3-phosphoethanolamine triethylammonium salt (Texas Red DHPE) (Life Technologies, Carlsbad, CA) was obtained at >98% purity. All lipids were used without further purification. Lipid stock solutions of DPPC, DOPC, SM and cholesterol were prepared at 1

mg/mL in chloroform. BODIPY-cholesterol and Texas Red DHPE solutions were prepared and diluted in methanol to obtain appropriate working concentrations. The chemical structures for the lipids employed in this study are shown in **Figure 3.1**.

Lipid monolayers were prepared from DPPC/DOPC/Chol and SM/DOPC/Chol with the appropriate amount of cholesterol added. Lipid monolayers for bulk fluorescence images were doped with 0.10 mol % BODIPY-cholesterol, and monolayers for single molecule measurements were doped with ~10^{-8} mol % of the dye. Approximately 50 µL of the appropriate lipid solutions were dispersed onto a subphase of ultrapure (18 MΩ) water in a Langmuir-Blodgett trough (Type 611, Nima Technology, Coventry, England). The chloroform from the lipid stock solutions was allowed to evaporate for 15 minutes after dispersion onto the subphase. Monolayers were compressed at a speed of 100 cm^2/min and expanded at a speed of 80 cm^2/min. The compression and expansion cycles were repeated twice to anneal the monolayer. Each monolayer was then compressed to the target pressure at a rate of 100 cm^2/min and held at that pressure for 10 minutes before transferring onto Piranha-cleaned glass slides. The monolayers were transferred at a dipping velocity of 5 mm/min and all experiments were done in air at a temperature of 22° C and a relative humidity between 40 and 45%. Example pressure – area isotherms of DPPC/DOPC/Chol and SM/DOPC/Chol are shown in **Figure 3.2**.

Monolayers were imaged using a total internal reflection microscope (TIRF-M) (Olympus IX71, Olympus, Center Valley, PA) equipped with a 60x, 1.45 NA objective (Achromat, Olympus) for bulk fluorescence imaging and a 100x, 1.45 NA objective for single molecule measurements. Excitation light from the 514 nm line of an argon ion laser (Coherent Innova 90, Coherent, Inc., Santa Clara, CA) was P-polarized using half and quarter wave plates. Emission was collected through a ZT514rdc dichroic mirror and HQ522/40m band pass filter (Chroma, Rockingham, VT). All images were collected using a cooled CCD camera (CoolSnap HQ2, Photometrics, Tucson, AZ). Image collection was controlled using Micromanager software

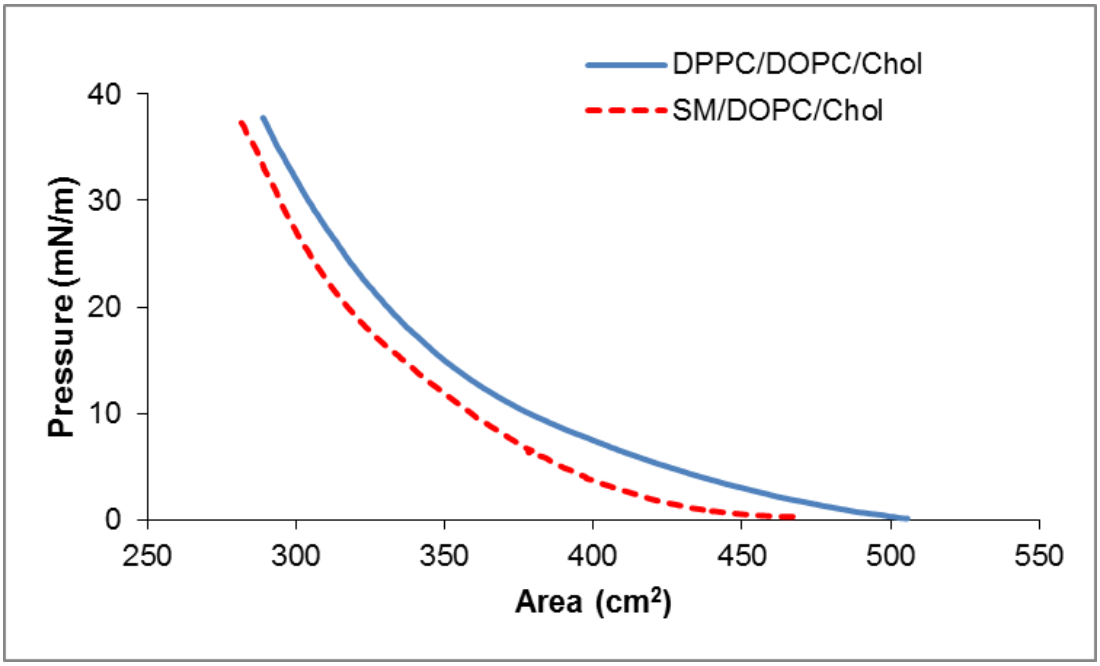

Figure 3.2 – representative pressure – area isotherms are shown for DPPC/DOPC/Chol and SM/DOPC/Chol monolayers prepared using equimolar mixtures of DPPC/DOPC and SM/DOPC with 30 mol % cholesterol.

(version 1.4.14) with 500 ms integration times and no binning [41]. For single molecule measurements, excitation light was defocused by ~500 nm using a piezo-electric focusing collar (Mad City Laboratories, Inc., Madison, WI). All images were analyzed using ImageJ (U.S. National Institutes of Health, Bethesda, MD) and MATLAB (Mathworks, Natick, MA).

3.3 – Results and Discussion

To probe the insertion geometry and behavior of BODIPY-cholesterol, monolayers of DPPC/DOPC/Chol are compared with monolayers of SM/DOPC/Chol. These are commonly studied ternary lipid mixtures for probing cholesterol induced domain formation and provide a well characterized system for understanding the partitioning and insertion geometry of BODIPY-

cholesterol [38-40]. The structures of the lipids and fluorescent probes used throughout this study are shown in **Figure 3.1**.

3.3.1 – DPPC/DOPC/Chol Monolayers

Figure 3.3 shows a series of fluorescence images of DPPC/DOPC/Chol monolayers doped with 0.10 mol % BODIPY-cholesterol that illustrates the evolution in structure observed as cholesterol is increased in the mixed monolayers. All monolayers are composed of an equimolar ratio of DPPC and DOPC and transferred onto a cleaned glass substrate at a surface pressure of 30 mN/m using the LB method. The surface pressure was selected to mimic the effective surface pressure of natural bilayers [42]. DPPC/DOPC/Chol monolayers doped with 0.0 mol %, 0.2 mol %, 1.0 mol %, 1.5 mol %, 2.0 mol %, 3.0 mol %, 6.0 mol %, 8.0 mol %, 20.0 mol %, and 40.0 mol % cholesterol are compared.

The images in **Figure 3.3** reveal significant changes in the DPPC/DOPC/Chol monolayers as cholesterol levels increase, as previously reported [43]. At 0.0 mol % cholesterol, the structure revealed by the fluorescent probe BODIPY-cholesterol is consistent with the known immiscibility of DPPC and DOPC. Dark, semi-circular domains that exclude the fluorescent BODIPY-cholesterol probe reflect condensed domains enriched in DPPC while the surrounding bright areas incorporating the probe are expanded regions enriched in DOPC. With the addition of 0.2 mol % cholesterol, the DPPC rich domains transition to a branched shape as the added cholesterol lowers the line tension between domains [44]. The condensed domains grow in size up to approximately 1.0 mol % added cholesterol, above which they transition back to a semi-circular geometry and reduce in size as new, cholesterol rich domains begin to emerge.

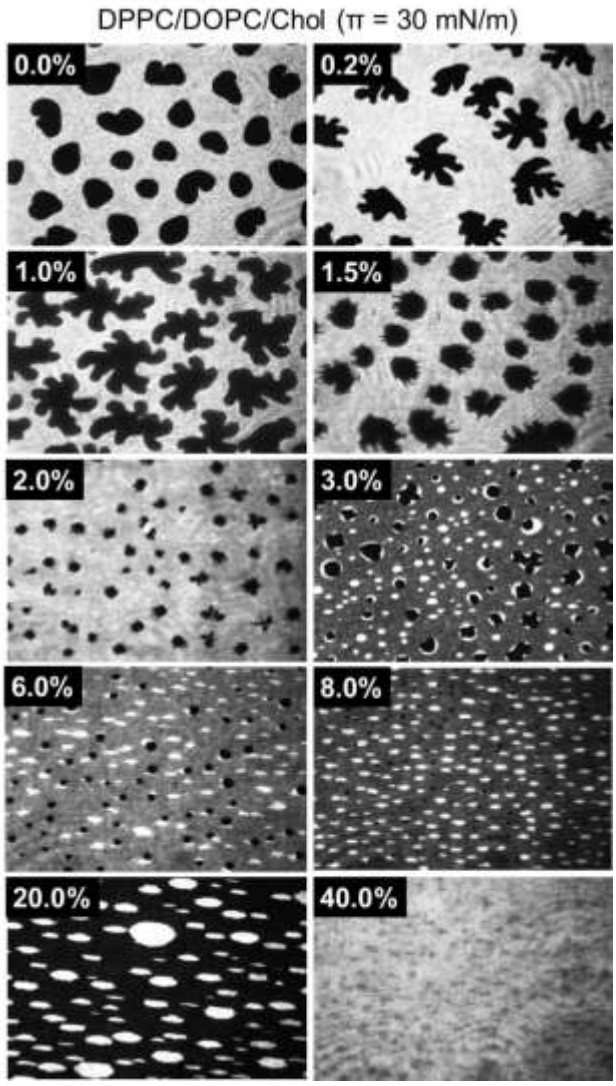

Figure 3.3 - Fluorescence images of DPPC/DOPC/Chol monolayers with indicated mol % of cholesterol added. The monolayers were doped with 0.10 mol % of the fluorescent cholesterol analog BODIPY-cholesterol and transferred at a surface pressure of π = 30 mN/m. Each image is 64 μm x 85 μm.

Between approximately 1.5 – 2.0 mol % added cholesterol, a new phase is apparent in the films which is consistent with the known propensity of cholesterol to induce an Lo state enriched in cholesterol [45, 46]. This is most apparent at 3.0 mol % cholesterol, where three fluorescence intensity levels are clearly observed in the film. Both bright and dark round domains are seen in the film with surrounding areas of intermediate intensity. As observed with some of the dark domains, high fluorescence intensity nucleates around their borders and eventually grows into the round fluorescent domains. As cholesterol is increased above 3.0 mol %, the films adopt two intensity levels as bright domains become larger and more elliptical. At 40.0 mol % cholesterol, much of the definition is lost and the films appear diffuse.

3.3.2 – SM/DOPC/Chol Monolayers

For comparison, similar measurements were carried out on monolayers of SM/DOPC/Chol doped with 0.10 mol % BODIPY-cholesterol and transferred at 30 mN/m. This ternary mixture is also used to study cholesterol induced domain formation, and the series of fluorescence images in **Figure 3.4** shows remarkably similar behavior to the DPPC/DOPC/Chol monolayers. With no added cholesterol, the SM/DOPC/Chol monolayer shown in **Figure 3.4** appears mostly expanded with small dark domains enriched in SM. The dark domains are smaller than in the DPPC/DOPC/Chol mixed monolayers, consistent with previous studies [47, 48]. The addition of small amounts of cholesterol increases the size of the semi-circular dark domains up to approximately 1.5 mol % added cholesterol. As in the DPPC/DOPC/Chol mixtures, a new phase appears in **Figure 3.4** between 1.5 and 2.0 mol % added cholesterol. Again this is most readily seen at 3.0 mol % cholesterol where the film contains three fluorescence intensity levels. A mixture of bright and dark round domains are observed with many of the dark domains

exhibiting bright fluorescent regions near the domain boundaries. As before, the surrounding lipid areas have fluorescence intensity intermediate between the bright and dark domains,

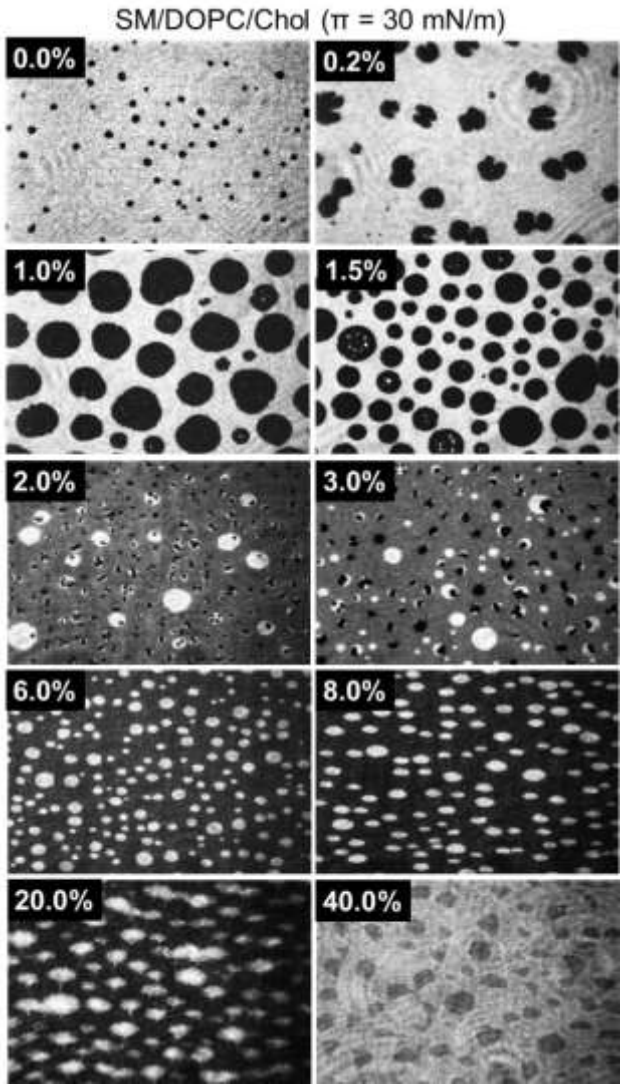

Figure 3.4 - Fluorescence images of SM/DOPC/Chol monolayers with indicated mol % of cholesterol added. The monolayers were doped with 0.10 mol % of the fluorescent cholesterol analog BODIPY-cholesterol and transferred at a surface pressure of π = 30 mN/m. Each image is 64 μm by 85 μm.

suggesting some fraction of the BODIPY-cholesterol also partitions in these areas. As cholesterol is increased above 6.0 mol %, bright elliptical domains are observed surrounded by areas excluding the fluorescent probe. At 40.0 mol % cholesterol, the structure in the SM/DOPC/Chol film loses definition and becomes diffuse much like the DPPC/DOPC/Chol monolayer.

The series of images in **Figures 3.3 and 3.4** show that BODIPY-cholesterol partitioning is complex and cholesterol dependent. In both mixed monolayers, BODIPY-cholesterol appears to partition into expanded regions at low cholesterol levels and transition into newly formed Lo phase as cholesterol levels increase. BODIPY-cholesterol has previously been reported to partition into the Lo phase of multilamellar vesicles formed from cholesterol and sphingomyelin [20]. To support the phase assignments in **Figures 3.3 and 3.4**, complementary measurements were carried out using the fluorescent lipid probe Texas Red DHPE. Texas Red DHPE is well-known to partition into expanded lipid phases, thus providing a good marker of these regions in both mixed monolayers [49].

3.3.3 – BODIPY-Cholesterol versus Texas Red DHPE Partitioning

Figure 3.5 compares the fluorescence structure observed in the mixed monolayers when doped with 0.10 mol % BODIPY-cholesterol versus 0.10 mol % Texas Red DHPE, a well-known marker of the expanded phase. Each film was studied at three representative cholesterol levels and each fluorescent probe was studied separately in equivalently prepared monolayers to avoid complications from crosstalk between the fluorescence channels. As before, all films were transferred onto a glass substrate using the LB method at a surface pressure of 30 mN/m.

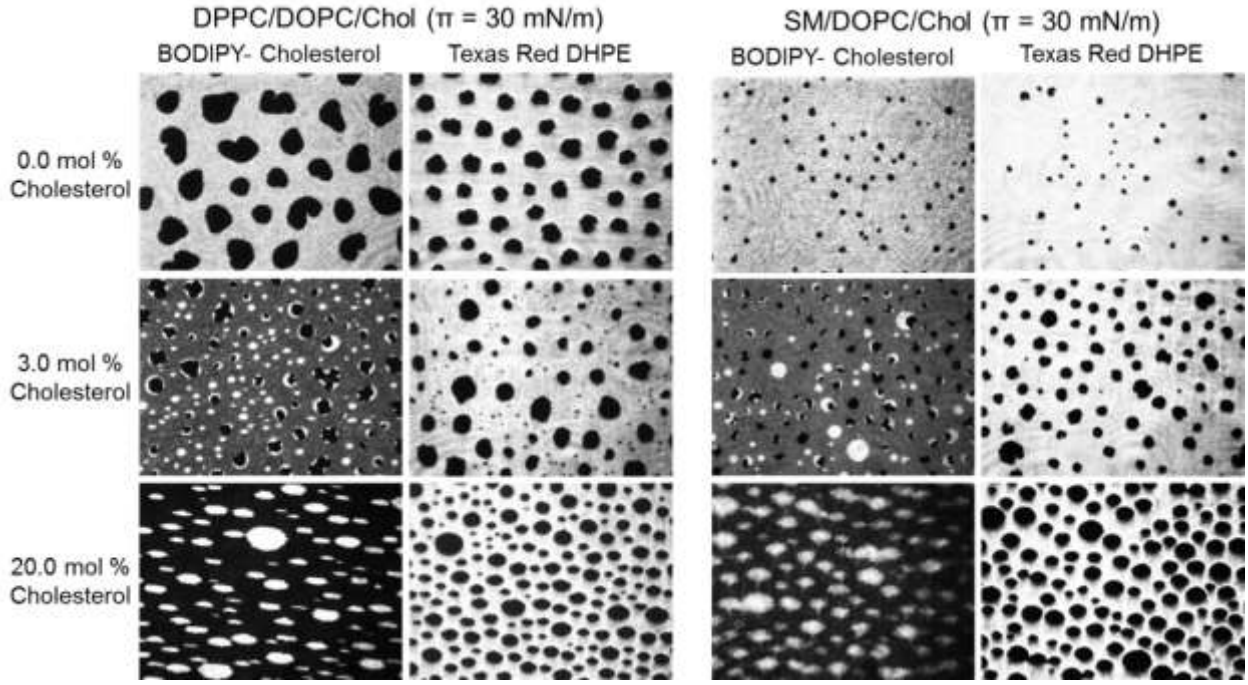

Figure 3.5 - Fluorescence images of DPPC/DOPC/Chol (left) and SM/DOPC/Chol (right) monolayers containing the indicated concentrations of cholesterol and transferred at π = 30 mN/m. At each condition, separate monolayers were doped individually with 0.10 mol % BODIPY-cholesterol or 0.10 mol % Texas Red DHPE as indicated above the appropriate series of images. Texas Red DHPE is well known to partition into expanded phases, providing a reliable marker of DOPC rich regions in the films. For each lipid mixture, comparison of the fluorescence images at low cholesterol levels show that BODIPY-cholesterol co-locates with Texas Red DHPE in the DOPC rich phase. At 3.0 mol % cholesterol, comparisons of the fluorescence images show that BODIPY-cholesterol partitions into domains that exclude Texas Red DHPE. The BODIPY-cholesterol rich domains are also well defined from regions excluding both dyes that reflect DPPC or SM-rich condensed domains. These images, therefore, are consistent with BODIPY-cholesterol partitioning into cholesterol rich domains of each film. Each image is 64 μm by 85 μm.

At 0 mol % added cholesterol, the mixed monolayers reveal colocalization of the BODIPY-cholesterol and Texas Red DHPE probes. In both mixed monolayers, the fluorescent probes partition into the DOPC rich expanded phase of the films that surround the semi-circular dark domains of condensed lipid. At 3.0 mol % cholesterol, however, both mixed monolayers show

that the Texas Red DHPE is totally excluded from the round dark domains while the BODIPY-cholesterol probe partially partitions into these regions. This signals the presence of the Lo phase in both monolayer systems and supports the results of previous studies showing BODIPY-cholesterol partitions into cholesterol rich domains. This also illustrates the utility of BODIPY-cholesterol over other fluorescent cholesterol analogs, which often behave much differently than native cholesterol. Finally, at 20.0 mol % added cholesterol, complementary staining is observed where BODIPY-cholesterol partitions into the elliptical cholesterol-rich domains while Texas Red DHPE is observed exclusively in the surrounding expanded DOPC rich matrix.

The trends measured in **Figures 3.3 – 3.5** show a similarity in the phase partitioning with cholesterol for both DPPC/DOPC/Chol and SM/DOPC/Chol monolayers. Analysis of the percent area occupied by each phase as a function of cholesterol, shown in **Figure 3.6,** are comparable for both mixtures and each mixture exhibits the onset of a new cholesterol rich Lo phase when cholesterol levels increase above approximately 1.5 mol %. These measurements, therefore, suggest that BODIPY-cholesterol tracks the partitioning of native cholesterol in both ternary lipid mixtures. The partitioning of BODIPY-cholesterol into Lo domains, as discussed in previous reports, makes it a particularly attractive fluorescent probe for studying cholesterol partitioning given the limitations of other fluorescent cholesterol analogs. To further understand how BODIPY-cholesterol interacts with these lipid mixtures fluorescence measurements at the single molecule level were carried out.

3.3.4 – Single Molecule Orientation Measurements of BODIPY-Cholesterol Insertion

Given the similarity in bulk BODIPY-cholesterol partitioning in DPPC/DOPC/Chol and SM/DOPC/Chol monolayers (**Figures 3.3 and 3.4**), single molecule fluorescence

measurements of BODIPY-cholesterol were used to compare film properties. Single molecule fluorescence measurements carried out using defocused polarized total internal reflection fluorescence microscopy (PTIRF) lead to distinct shapes in the single molecule emission images that reflect the three-dimensional orientation of each fluorophore in the image. We have previously used single molecule orientation measurements to characterize the evolution in lipid

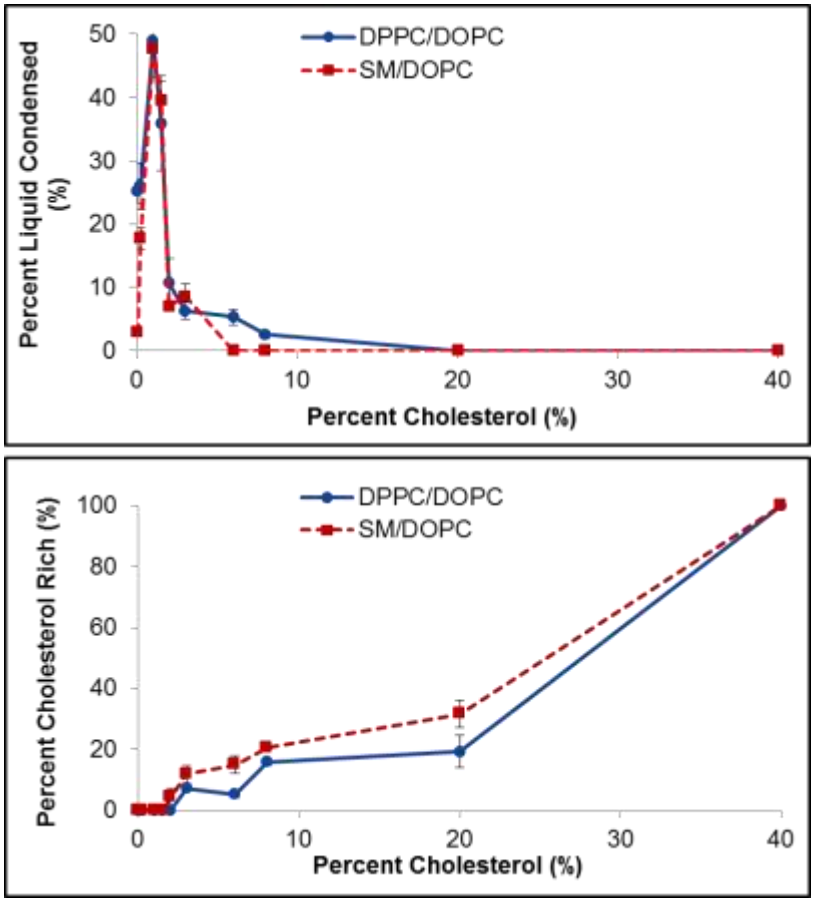

Figure 3.6 – Shows analysis of the images shown in Figures 3.2 – 3.3. Initially, both films increase in percent liquid condensed area. By about 8 mol % cholesterol, that phase is lost in the films and replaced by a cholesterol rich Lo phase, shown on the right. The DPPC/DOPC films are shown in blue with a solid line in this figure, and SM/DOPC films are shown in red with a dashed line.

monolayers with surface pressure [32-34], relative humidity [37], and the presence of additives such as GM1 and cholesterol [35, 36]. Here we extend those studies to compare the tilt angle of BODIPY-cholesterol doped into DPPC/DOPC/Chol and SM/DOPC/Chol monolayers as a function of cholesterol.

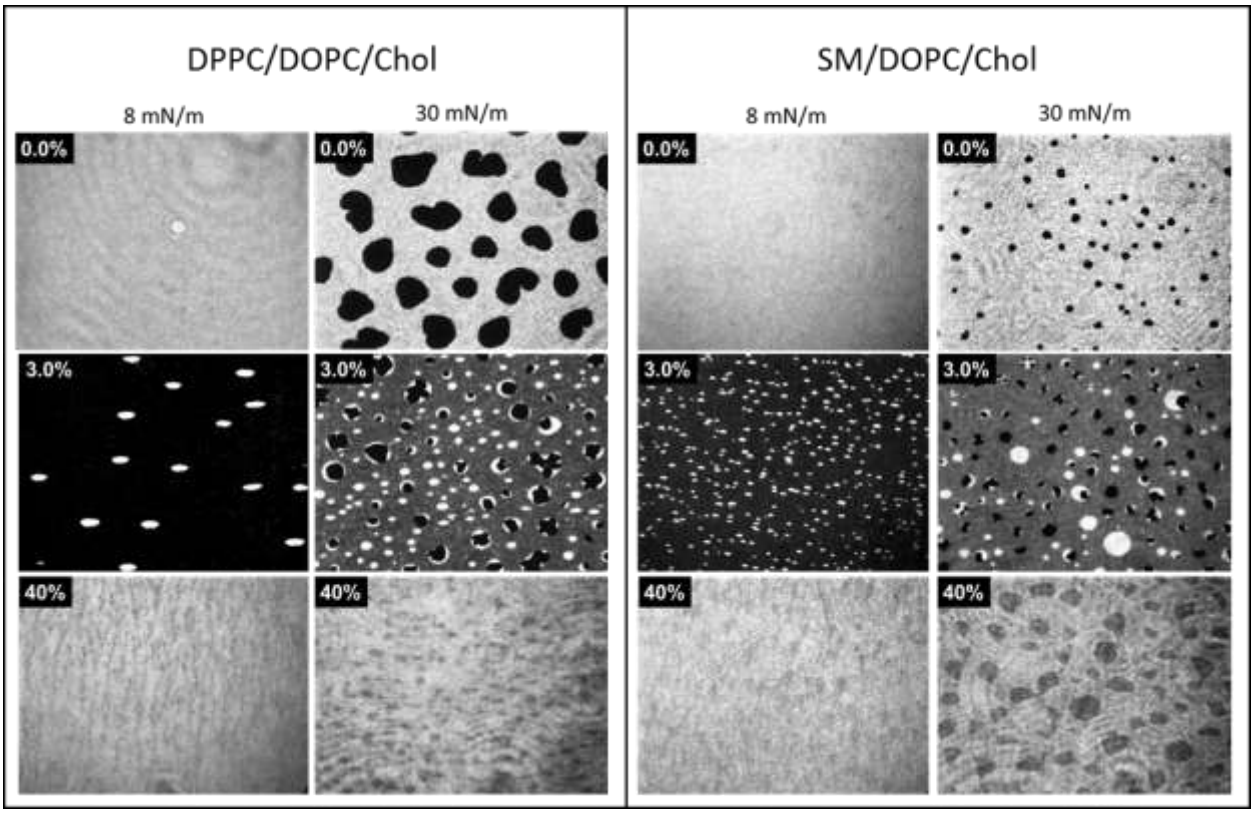

Figure 3.7 shows representative high dye images of the monolayers analyzed using single molecule analysis. DPPC/DOPC/Chol monolayers are shown on the left and SM/DOPC/Chol monolayers are shown on the right. Both sets of monolayers were prepared at low (π = 8 mN/m) and biologically comparable (π = 30 mN/m) surface pressure. Each image is 64 µm by 85 µm.

Single molecule analysis was performed on DPPC/DOPC/Chol and SM/DOPC/Chol monolayers at two different equivalent surface pressures. First, monolayers were prepared at 8 mN/m. At this surface pressure, lipids are less densely packed than in biological membranes, and **Figure 3.7** shows that at 0.0 % and 40 % cholesterol, these films do not exhibit obvious phases. At 3.0 mol % cholesterol phase structure is present in both monolayers, where coexisting phases are seen. At 30 mN/m, a biological equivalent packing density, coexisting

phases are readily apparent at 0.0 mol % and 3.0 mol % cholesterol. At 40 mol % cholesterol, both the DPPC/DOPC/Chol and SM/DOPC/Chol monolayers appear almost homogeneous. These images are useful for interpreting single molecule results, as they reveal which phase the fluorescent analog occupies at each condition.

Figure 3.8 shows a representative defocused single molecule fluorescence image of BODIPY-cholesterol doped into a DPPC/DOPC monolayer at ~10^{-8} mol %. This particular monolayer was deposited on glass at 30 mN/m using the LB technique. Each bright feature in the image represents the emission from a single BODIPY-cholesterol immobilized in the DPPC/DOPC monolayer. Samples are imaged dry in air to reduce reorientation dynamics and

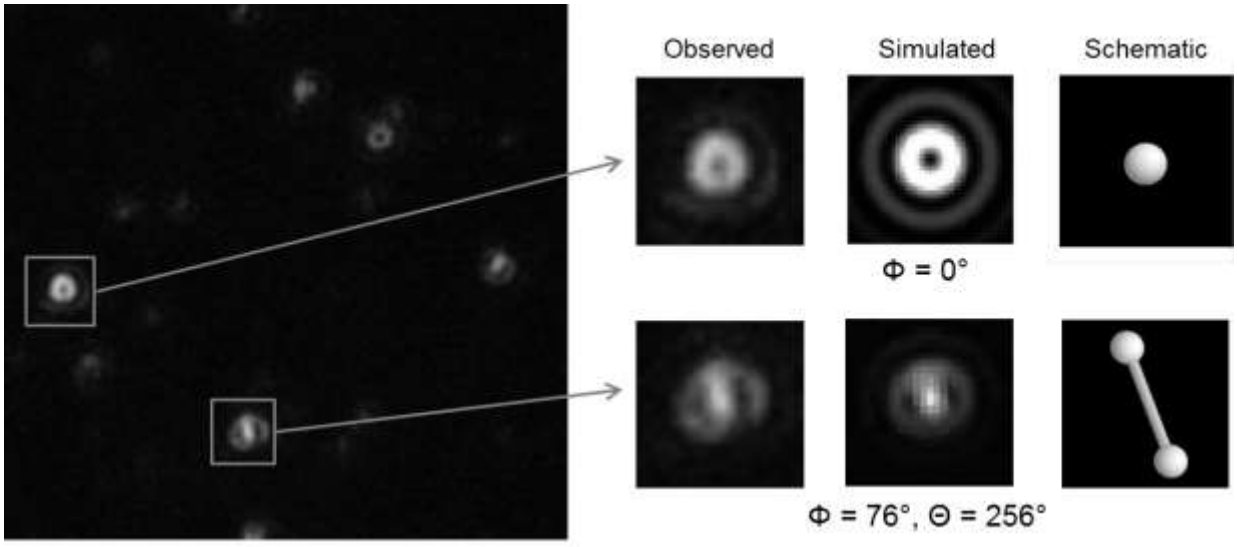

Figure 3.8 - An 11 µm by 11 µm single molecule fluorescence image taken using defocused P-TIRF microscopy of ~10^{-8} mol % BODIPY-cholesterol doped into a DPPC/DOPC monolayer. As shown by others, the observed emission patterns reflect the three-dimensional orientation of the emission dipole in the sample matrix [26-31]. Two representative emission patterns from the image are shown along with simulated emission patterns used to extract the polar (Φ) and azimuthal (Θ) angles. As shown schematically, this enables the orientation of the emission dipole of each BODIPY-cholesterol in the image to be extracted. As we have shown previously, population histograms of the tilt angle away from the membrane normal (Φ) can be used to track changes in membrane structure [32-37].

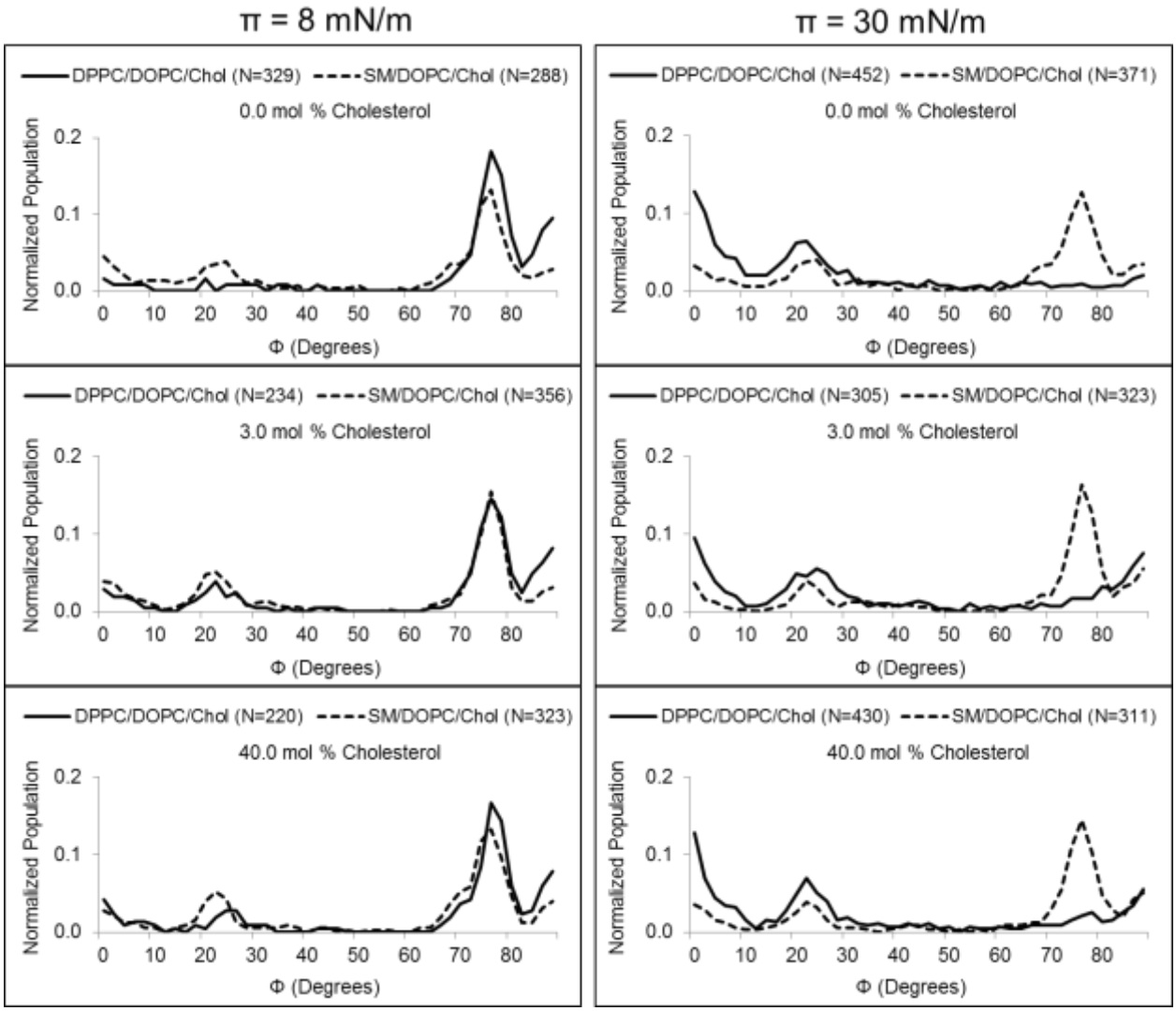

Figure 3.9 - Tilt angle histograms for BODIPY-cholesterol in mixed monolayers of DPPC/DOPC/Chol and SM/DOPC/Chol as a function of added cholesterol and surface pressure. Population histograms are plotted as lines to help guide the eye and the number of molecules analyzed at each condition is indicated by N. At low surface pressure (π = 8 mN/m, left panels), the tilt angle histograms reveal four preferred angles with the most probable populated near 78°. At high surface pressure (π = 30 mN/m, right panels), significant differences are observed in the tilt angle histograms for BODIPY-cholesterol in the two mixed monolayers. While the BODIPY-cholesterol orientations in SM/DOPC/Chol monolayers remain similar to that observed at low pressure, the population near 78° is significantly reduced in DPPC/DOPC/Chol monolayers. This decrease is accompanied by increases in populations at smaller tilt angles suggesting a change in BODIPY-cholesterol insertion at the elevated surface pressure.

diffusion of the incorporated dye. Distinct emission patterns are observed that reflect the orientation of the emission dipole of the BODIPY-cholesterol probe, which lies approximately along the long axis of the BODIPY ring system [50]. As shown in **Figure 3.8**, donut-like features arise from emission dipoles oriented normal to the membrane plane while emission dipoles oriented in-plane lead to central bright spots that are surrounded by a halo of fluorescence. While both the azimuthal (Θ) and polar angles (Φ) for each molecule can be extracted from these images, the polar angle or tilt angle away from the membrane normal is most reflective of changes in membrane structure. Here we analyze large populations of single molecule emission features at each membrane condition to create tilt angle population histograms such as that shown in **Figure 3.9**.

Figure 3.9 compares the tilt angle histograms for BODIPY-cholesterol doped into the ternary mixtures of DPPC/DOPC/Chol and SM/DOPC/Chol as a function of cholesterol and surface pressure. Films were transferred at surface pressures of 8 and 30 mN/m, and BODIPY-cholesterol was doped into the films at a concentration of ~10^{-8} mol % to ensure that single molecules are measured. In **Figure 3.9**, cholesterol levels are compared at 0.0, 3.0, and 40.0 mol % and the population histograms are plotted as lines to help guide the eye.

The tilt angle histograms for BODIPY-cholesterol at 8 mN/m reveal a preferred orientation centered near 78**°**, which reflects the tilt angle between the BODIPY emission dipole and the membrane normal. Smaller populations are observed at tilt angles centered near 0°, 24°, and 90°, where the latter represents emission dipoles lying in the plane of the film. The insensitivity of these distributions to changes in cholesterol content at low surface pressure likely reflects an insertion geometry that places the BODIPY chromophore outside of the monolayer near the end of the tailgroups, where it is less sensitive to surrounding structural changes [24]. Previous experimental and simulation work have suggested that BODIPY-cholesterol inserts into membranes with its hydroxyl group oriented towards the headgroups. The BODIPY fluorophore,

in the hydrophobic region of bilayers, extends beyond the end of the surrounding acyl chains [24]. This insertion geometry is consistent with the insensitivity of the BODIPY-cholesterol chromophore to orientation changes in the surrounding lipid matrix. Structural changes taking place within the membrane due to the addition of cholesterol would be expected to have little impact on BODIPY orientation, in agreement with the single molecule data summarized in **Figure 3.9**.

Interestingly, as the surface pressure is increased to 30 mN/m, significant differences are observed in the tilt angle histograms of BODIPY-cholesterol measured in the two ternary lipid mixtures. While the tilt angle histograms in SM/DOPC/Chol monolayers remain consistent with those previously measured at low pressure, the histograms for DPPC/DOPC/Chol reflect a loss of the population oriented near 78°. This is a striking loss of population at the orientation found most prevalent at other conditions. The histograms in **Figure 3.9** show that the decrease in molecules oriented near 78° leads to increases in the populations oriented near 0° and 24°**.** These changes are only observed at the higher surface pressure and are insensitive to cholesterol added into the membrane. This data is further emphasized in **Figure 3.10**, where representative DPPC/DOPC/Chol and SM/DOPC/Chol single molecule images at 40 mol % cholesterol are shown to highlight the differences observed in each monolayer. The single molecule measurements summarized in **Figure 3.9** and shown again in **Figure 3.10**, therefore, reveal significant differences in the way BODIPY-cholesterol inserts into the two ternary lipid mixtures when surface pressures are increased to biologically relevant levels. Additionally, these trends were not readily apparent in high dye images, where differences in the size and shape of domains can be observed but changes in molecular level structure remain hidden.

Figure 3.11 plots the average integrated populations of the four predominant BODIPY-cholesterol orientations at low and high surface pressure for each lipid mixture. Given the insensitivity of the orientations to cholesterol in **Figure 3.9**, the cholesterol data have been

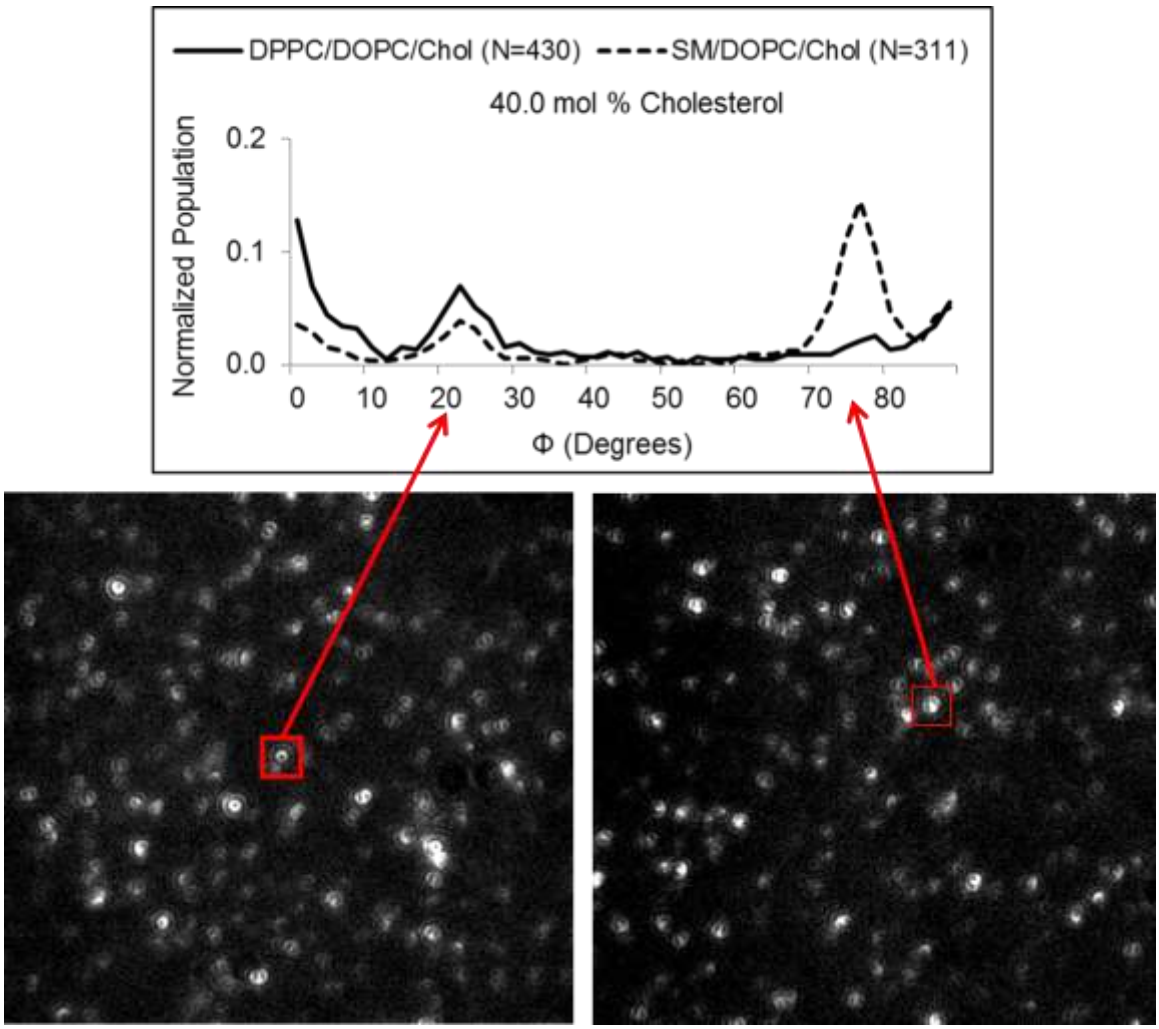

Figure 3.10 shows representative single molecule data. On the left, an image of DPPC/DOPC/Chol at 30 mN/m is shown, and an emission dipole that is tilted at 24° from normal is indicated in red. On the right, an image of SM/DOPC/Chol is shown and an emission dipole that is tilted 78° from normal is indicated in red.

combined in constructing the histograms shown in **Figure 3.11**. At low surface pressure, the population histograms in **Figure 3.11** further illustrate the similar insertion geometries observed for BODIPY-cholesterol in DPPC/DOPC/Chol and SM/DOPC/Chol monolayers. This pattern is also seen at high surface pressure for monolayers of SM/DOPC/Chol. For DPPC/DOPC/Chol monolayers, however, **Figure 3.11** reveals significant changes in BODIPY-cholesterol insertion at high surface pressure. The histograms show the large loss in the population centered near

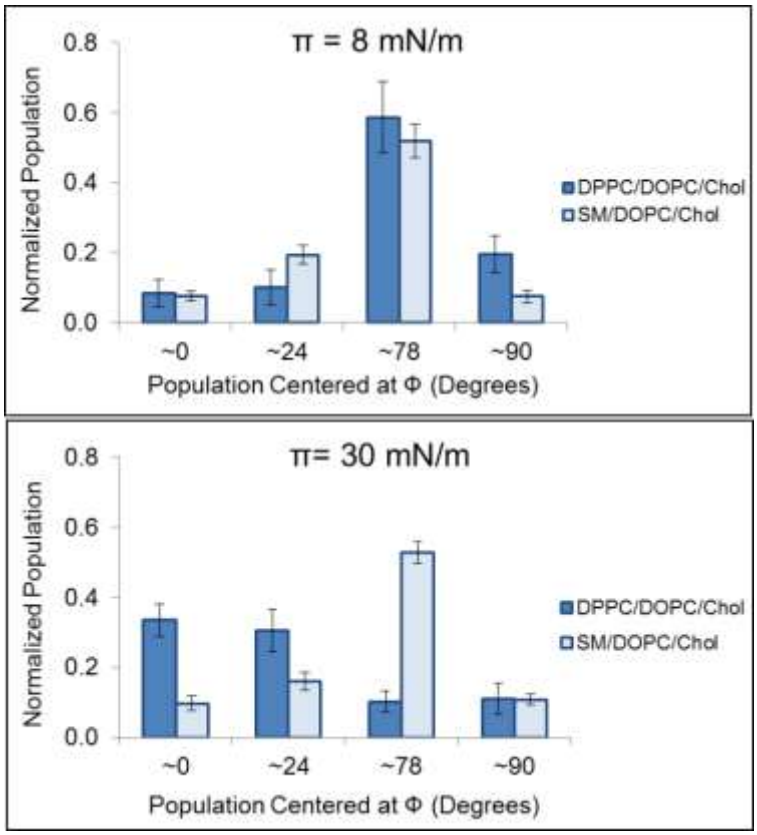

Figure 3.11 - Comparison of the integrated populations from the four predominant tilt angles (centered near 0°, 24°, 78° and 90°) of BODIPY-cholesterol measured in monolayers of SM/DOPC/Chol and DPPC/DOPC/Chol. Given the insensitivity to cholesterol, each point represents the averaged populations for all cholesterol levels at the specified tilt angle and monolayer composition for low and high surface pressures. At low surface pressure the normalized populations for the four preferred orientations closely track each other in the two ternary lipid mixtures. At high surface pressure, however, significant deviations are observed. While the orientations of BODIPY-cholesterol in SM/DOPC/Chol are consistent with the other films studied, the DPPC/DOPC/Chol monolayers experience a loss of population near 78**°** accompanied by increases near 0° and 24°.

78° accompanied by increases in populations found near 0° and 24**°.** These differences reflect changes in the way BODIPY-cholesterol interacts with the two ternary lipid mixtures that are not readily apparent when comparing results from bulk fluorescence measurements, such as those shown in **Figures 3.3 and 3.4**.

The data shown in **Figure 3.9** suggest BODIPY-cholesterol interacts differently with SM and DPPC in the mixed monolayers. Studies have shown that native cholesterol has a condensing effect on both SM and DPPC, but SM tends to occupy less area than DPPC in ordered domains with cholesterol [51]. This suggests there are stronger cohesive interactions between SM and cholesterol which is supported by recent NMR and calorimetry studies comparing DPPC/DOPC/Chol and SM/DOPC/Chol mixtures [38]. This and other studies have found evidence for specific interactions between SM and cholesterol that are missing in domains enriched in DPPC [38, 52-54]. Several studies have suggested that cholesterol packs between sphingolipids using a network of hydrogen bonding and van der Waal's interactions that leads to a preferential association with SM over other saturated lipids such as DPPC [55-57].

The single molecule data shown in **Figure 3.9** are consistent with the view that BODIPY-cholesterol is more strongly anchored via intermolecular forces in mixed monolayers containing SM over those incorporating DPPC. As the surface pressure of a Langmuir monolayer increases, the surface density of lipids increases and the film begins to experience a stressing force that can be relieved by collapsing or selectively squeezing out molecules from the interface. Previous studies utilizing headgroup modified cholesterol analogs, including thiocholesterol and cholesteryl acetate, have shown that these modified cholesterols are squeezed out of monolayers of cholesterol at surface pressures lower than the total monolayer collapse pressure [58, 59]. The single molecule results summarized in **Figures 3.9 and 3.11** are consistent with a model in which BODIPY-cholesterol is selectively squeezed-out of DPPC/DOPC/Chol membranes at elevated surface pressure while remaining anchored in SM/DOPC/Chol monolayers.

Given the initial recessed location of BODIPY-cholesterol in the monolayer, the small hydroxyl headgroup, and placement of the bulky BODIPY fluorophore near the tail group plane, it seems reasonable that squeeze-out, if occurring, will leave BODIPY-cholesterol on the

hydrophobic side of the monolayer. In bulk fluorescence images, the fluorophore likely remains associated with the domain that the fluorophore is squeezed-out of due to restricted mobility. As shown in **Figures 3.9 and 3.11**, this process is accompanied by a loss of population oriented near 78° and growth of populations oriented more normal to the membrane plane. This may reflect BODIPY-cholesterol lying along the membrane plane with the BODIPY group inserted into the surrounding acyl chains, such that its long axis is oriented approximately normal to the membrane plane. Molecular dynamics simulations are currently being carried out to further probe these processes. It should be noted, however, that we see no evidence for squeeze-out in the pressure isotherms even when the dye concentration is elevated, which may suggest that other mechanisms lead to the differences observed in **Figures 3.9 and 3.11**. Regardless, the results presented here clearly establish a difference in the way that BOIDPY-cholesterol interacts with various lipid matrices and help define the partitioning of BODIPY-cholesterol for future membrane studies.

The single molecule data presented is specifically of interest if BODIPY-cholesterol is used in a FRET pair. It is well known that during resonant energy transfer, the orientation of the emission dipole can have a significant impact on the quantum yield of the energy transfer. The results presented show that BOIDPY-cholesterol is relatively unaffected by changes in cholesterol and surface pressure, which is a desirable characteristic for a FRET experiment. Additionally, the discovery that the probe is susceptible to squeeze out at higher surface pressure in a DPPC/DOPC/Chol lipid matrix should be useful for these studies.

3.4 – Conclusion

The fluorescent cholesterol analog BODIPY-cholesterol is studied in model membranes composed of DPPC/DOPC/Chol and SM/DOPC/Chol. Fluorescence microscopy measurements

of LB films transferred at 8 mN/m and 30 mN/m are used to track the partitioning of BODIPY-cholesterol as a function of membrane cholesterol levels. In agreement with previous studies, these measurements suggest that BODIPY-cholesterol localizes with cholesterol in the lipid mixtures studied, illustrating its utility as a probe of native cholesterol distribution. In the ternary lipid mixtures, DPPC/DOPC/Chol and SM/DOPC/Chol, these measurements reveal similar trends in BODIPY-cholesterol partitioning with changes in surface pressure and cholesterol. At low cholesterol levels, BODIPY-cholesterol partitions into the DOPC rich expanded regions of the films. As cholesterol increases, structure in the fluorescence images reflects the emergence of a cholesterol rich phase with similar behavior observed for both DPPC/DOPC/Chol and SM/DOPC/Chol monolayers.

To provide a more molecular view of BODIPY-cholesterol interactions in the ternary lipid mixtures, single molecule fluorescence measurements were conducted as described in Chapter 2. Defocused P-TIRF microscopy measurements at the single molecule level lead to distinctive emission patterns that are used to extract the three-dimensional orientations of BODIPY-cholesterol. These measurements are used to create population histograms of the BODIPY-cholesterol emission dipole tilt angle away from the membrane normal as a function of membranes constituents and surface pressure. Four distinct orientations are observed for BODIPY-cholesterol doped at ~10^{-8} mol % into LB monolayers of SM/DOPC/Chol. The most probable orientation is centered near 78° and the distributions are relatively insensitive to surface pressure and cholesterol content. Similar orientation histograms are also observed for BODIPY-cholesterol in DPPC/DOPC/Chol monolayers transferred at 8 mN/m. At this surface pressure, the angles and relative populations observed are similar to those observed for BODIPY-cholesterol in SM/DOPC/Chol monolayers and, like the results for SM/DOPC/Chol films, the orientations are insensitive to added cholesterol.

For DPPC/DOPC/Chol films transferred at 30 mN/m, however, significant deviations in the single molecule orientations of BODIPY-cholesterol are observed. For these films, the most probable orientation at 78° is significantly reduced with increasing populations observed at 0° and 24°. This may reflect a “squeeze-out” mechanism in which BODIPY-cholesterol in DPPC/DOPC/Chol transitions out of the membrane and associates with the tailgroups at elevated surface pressures. Therefore, even though the bulk fluorescence data for DPPC/DOPC/Chol and SM/DOPC/Chol are similar, the deviation in single molecule results at high surface pressure suggest that BODIPY-cholesterol is anchored more strongly in SM/DOPC/Chol films.

3.5 References

1. Van Meer, G., *Lipid traffic in animal cells.* Annu. Rev. Cell Biol., 1989. **5**: p. 247-75.

2. Anonymous, et al., *Blood cholesterol and vascular mortality by age, sex, and blood pressure: a meta-analysis of individual data from 61 prospective studies with 55,000 vascular deaths.* Lancet, 2007. **370**(9602): p. 1829-39.

3. Maxfield, F.R. and I. Tabas, *Role of cholesterol and lipid organization in disease.* Nature, 2005. **438**(7068): p. 612-621.

4. Yeganeh, B., et al., *Targeting the mevalonate cascade as a new therapeutic approach in heart disease, cancer and pulmonary disease.* Pharmacology & Therapeutics, 2014. **143**(1): p. 87-110.

5. Lange, Y., et al., *Plasma membranes contain half the phospholipid and 90% of the cholesterol and sphingomyelin in cultured human fibroblasts.* J Biol Chem, 1989. **264**(7): p. 3786-93.

6. Bloch, K., *Cholesterol: evolution of structure and function.* New Compr. Biochem., 1991. **20**(Biochem. Lipids, Lipoproteins Membr.): p. 363-81.

7. Demel, R.A., L.L.M. Van Deenen, and B.A. Pethica, *Monolayer interactions of phospholipids and cholesterol.* Biochim. Biophys. Acta, Biomembr., 1967. **135**(1): p. 11-19.

8. Stockton, G.W. and I. C.P. Smith, *A deuterium nuclear magnetic resonance study of the condensing effect of cholesterol on egg phosphatidylcholine bilayer membranes. I. Perdeuterated fatty acid probes.* Chemistry and Physics of Lipids, 1976. **17**(2–3): p. 251-263.

9. Lai, M.Z., N. Duzgunes, and F.C. Szoka, *Effects of replacement of the hydroxyl group of cholesterol and tocopherol on the thermotropic behavior of phospholipid membranes.* Biochemistry, 1985. **24**(7): p. 1646-53.

10. Smaby, J.M., H.L. Brockman, and R.E. Brown, *Cholesterol's interfacial interactions with sphingomyelins and-phosphatidylcholines: Hydrocarbon chain structure determines the magnitude of condensation.* Biochemistry, 1994. **33**(31): p. 9135-42.

11. Huang, J. and G.W. Feigenson, *A microscopic interaction model of maximum solubility of cholesterol in lipid bilayers.* Biophys. J., 1999. **76**(4): p. 2142-2157.

12. Radhakrishnan, A. and H. McConnell, *Condensed complexes in vesicles containing cholesterol and phospholipids.* Proc. Natl. Acad. Sci. U. S. A., 2005. **102**(36): p. 12662-12666.

13. de Meyer, F. and B. Smit, *Effect of cholesterol on the structure of a phospholipid bilayer.* Proc. Natl. Acad. Sci. U. S. A., 2009. **106**(10): p. 3654-3658.

14. Kessel, A., N. Ben-Tal, and S. May, *Interactions of cholesterol with lipid bilayers: the preferred configuration and fluctuations.* Biophys. J., 2001. **81**(2): p. 643-658.

15. Khelashvili, G.A. and H.L. Scott, *Combined Monte Carlo and molecular dynamics simulation of hydrated 18:0 sphingomyelin-cholesterol lipid bilayers.* J Chem Phys, 2004. **120**(20): p. 9841-7.

16. Scheidt, H.A., et al., *The potential of fluorescent and spin-labeled steroid analogs to mimic natural cholesterol.* J. Biol. Chem., 2003. **278**(46): p. 45563-45569.

17. Robalo, J.R., et al., *Behavior of fluorescent cholesterol analogues dehydroergosterol and cholestatrienol in lipid bilayers: A molecular dynamics study.* J. Phys. Chem. B, 2013. **117**(19): p. 5806-5819.

18. Schroeder, F., M.E. Dempsey, and R.T. Fischer, *Sterol and squalene carrier protein interactions with fluorescent Δ5,7,9(11)-cholestatrien-3β-ol.* J. Biol. Chem., 1985. **260**(5): p. 2904-11.

19. Smutzer, G., B.F. Crawford, and P.L. Yeagle, *Physical properties of the fluorescent sterol probe dehydroergosterol.* Biochim. Biophys. Acta, Biomembr., 1986. **862**(2): p. 361-71.

20. Li, Z., E. Mintzer, and R. Bittman, *First synthesis of free cholesterol-BODIPY conjugates.* J. Org. Chem., 2006. **71**(4): p. 1718-1721.

21. Ariola, F.S., et al., *Membrane fluidity and lipid order in ternary giant unilamellar vesicles using a new bodipy-cholesterol derivative.* Biophys J, 2009. **96**(7): p. 2696-708.

22. Shaw, J.E., et al., *Correlated fluorescence-atomic force microscopy of membrane domains: structure of fluorescence probes determines lipid localization.* Biophys. J., 2006. **90**(6): p. 2170-2178.

23. Maxfield, F.R. and D. Wustner, *Analysis of cholesterol trafficking with fluorescent probes.* Methods Cell Biol., 2012. **108**(Lipids): p. 367-393.

24. Holtta-Vuori, M., et al., *BODIPY-cholesterol: a new tool to visualize sterol trafficking in living cells and organisms.* Traffic (Oxford, U. K.), 2008. **9**(11): p. 1839-1849.

25. Robalo, J.R., J.P. Prates Ramalho, and L.M.S. Loura, *NBD-labeled cholesterol analogues in phospholipid bilayers: Insights from molecular dynamics.* J. Phys. Chem. B, 2013. **117**(44): p. 13731-13742.

26. Patra, D., I. Gregor, and J. Enderlein, *Image analysis of defocused single-molecule images for three-dimensional molecule orientation studies.* J. Phys. Chem. A, 2004. **108**(33): p. 6836-6841.

27. Toprak, E., et al., *Defocused orientation and position imaging (DOPI) of myosin V.* Proc Natl Acad Sci U S A, 2006. **103**(17): p. 6495-9.

28. Bartko, A.P. and R.M. Dickson, *Imaging three-dimensional single molecule orientations.* J. Phys. Chem. B, 1999. **103**(51): p. 11237-11241.

29. Bartko, A.P. and R.M. Dickson, *Three-dimensional orientations of polymer-bound single molecules.* J. Phys. Chem. B, 1999. **103**(16): p. 3053-3056.

30. Bohmer, M. and J. Enderlein, *Orientation imaging of single molecules by wide-field epifluorescence microscopy.* J. Opt. Soc. Am. B, 2003. **20**(3): p. 554-559.

31. Forkey, J.N., M.E. Quinlan, and Y.E. Goldman, *Measurement of single macromolecule orientation by total internal reflection fluorescence polarization microscopy.* Biophys. J., 2005. **89**(2): p. 1261-1271.

32. Livanec, P.W. and R.C. Dunn, *Single-Molecule Probes of Lipid Membrane Structure.* Langmuir, 2008. **24**(24): p. 14066-14073.

33. Armendariz, K.P., et al., *Single molecule probes of membrane structure: Orientation of BODIPY probes in DPPC as a function of probe structure.* Analyst (Cambridge, U. K.), 2012. **137**(6): p. 1402-1408.

34. Song, K.C., et al., *Orientation of fluorescent lipid analogue BODIPY-PC to probe lipid membrane properties: Insights from molecular dynamics simulations.* J. Phys. Chem. B, 2011. **115**(19): p. 6157-6165.

35. Livanec, P.W., H.A. Huckabay, and R.C. Dunn, *Exploring the Effects of Sterols in Model Lipid Membranes Using Single-Molecule Orientations.* J. Phys. Chem. B, 2009. **113**(30): p. 10240-10248.

36. Armendariz, K.P. and R.C. Dunn, *Ganglioside Influence on Phospholipid Films Investigated with Single Molecule Fluorescence Measurements.* J. Phys. Chem. B, 2013. **117**(26): p. 7959-7966.

37. Huckabay, H.A. and R.C. Dunn, *Hydration Effects on Membrane Structure Probed by Single Molecule Orientations.* Langmuir, 2011. **27**(6): p. 2658-2666.

38. Fritzsching, K.J., J. Kim, and G.P. Holland, *Probing lipid-cholesterol interactions in DOPC/eSM/Chol and DOPC/DPPC/Chol model lipid rafts with DSC and 13C solid-state NMR.* Biochim. Biophys. Acta, Biomembr., 2013. **1828**(8): p. 1889-1898.

39. Smith, A.K. and J.H. Freed, *Dynamics and ordering of lipid spin-labels along the coexistence curve of two membrane phases: An ESR study.* Chem. Phys. Lipids, 2012. **165**(3): p. 348-361.

40. Davis, J.H., J.J. Clair, and J. Juhasz, *Phase equilibria in DOPC/DPPC-d62/cholesterol mixtures.* Biophys. J., 2009. **96**(2): p. 521-539.

41. Edelstein, A., et al., *Computer control of microscopes using μManager*. Current Protocols in Molecular Biology. 2010: John Wiley & Sons, Inc.

42. Marsh, D., *Lateral pressure in membranes.* Biochim. Biophys. Acta, Rev. Biomembr., 1996. **1286**(3): p. 183-223.

43. Stottrup, B.L., S.L. Veatch, and S.L. Keller, *Nonequilibrium behavior in supported lipid membranes containing cholesterol.* Biophys J, 2004. **86**(5): p. 2942-50.

44. Weis, R.M. and H.M. McConnell, *Cholesterol stabilizes the crystal-liquid interface in phospholipid monolayers.* J. Phys. Chem., 1985. **89**(21): p. 4453-9.

45. Ipsen, J.H., et al., *Phase equilibria in the phosphatidylcholine-cholesterol system.* Biochim. Biophys. Acta, Biomembr., 1987. **905**(1): p. 162-72.

46. Sankaram, M.B. and T.E. Thompson, *Interaction of cholesterol with various glycerophospholipids and sphingomyelin.* Biochemistry, 1990. **29**(47): p. 10670-5.

47. Lawrence, J.C., et al., *Real-time analysis of the effects of cholesterol on lipid raft behavior using atomic force microscopy.* Biophys. J., 2003. **84**(3): p. 1827-1832.

48. Giocondi, M.-C., et al., *Surface topography of membrane domains.* Biochim. Biophys. Acta, Biomembr., 2010. **1798**(4): p. 703-718.

49. Veatch, S.L. and S.L. Keller, *Separation of liquid phases in giant vesicles of ternary mixtures of phospholipids and cholesterol.* Biophysical Journal, 2003. **85**(5): p. 3074-3083.

50. Karolin, J., et al., *Fluorescence and absorption spectroscopic properties of dipyrromethene boron difluoride (BODIPY) derivatives in liquids, lipid membranes, and proteins.* J. Am. Chem. Soc., 1994. **116**(17): p. 7801-6.

51. Lund-Katz, S., et al., *Influence of molecular packing and phospholipid type on rates of cholesterol exchange.* Biochemistry, 1988. **27**(9): p. 3416-23.

52. Maulik, P.R. and G.G. Shipley, *N-palmitoyl sphingomyelin bilayers: structure and interactions with cholesterol and dipalmitoylphosphatidylcholine.* Biochemistry, 1996. **35**(24): p. 8025-8034.

53. Petrache, H.I., S.W. Dodd, and M.F. Brown, *Area per lipid and acyl length distributions in fluid phosphatidylcholines determined by 2H NMR spectroscopy.* Biophys. J., 2000. **79**(6): p. 3172-3192.

54. Shipley, G.G., L.S. Avecilla, and D.M. Small, *Phase behavior and structure of aqueous dispersions of sphingomyelin.* J. Lipid Res., 1974. **15**(2): p. 124-31.

55. Bittman, R., et al., *Interaction of cholesterol with sphingomyelin in monolayers and vesicles.* Biochemistry, 1994. **33**(39): p. 11776-81.

56. Ramstedt, B. and J.P. Slotte, *Membrane properties of sphingomyelins.* FEBS Lett, 2002. **531**(1): p. 33-7.

57. Veiga, M.P., et al., *Interaction of cholesterol with sphingomyelin in mixed membranes containing phosphatidylcholine, studied by spin-label ESR and IR spectroscopies. A possible stabilization of gel-phase sphingolipid domains by cholesterol.* Biochemistry, 2001. **40**(8): p. 2614-22.

58. Viswanath, P. and K.A. Suresh, *Polar head group interactions in mixed Langmuir monolayers.* Phys Rev E Stat Nonlin Soft Matter Phys, 2003. **67**(6 Pt 1): p. 061604.

59. Gupta, R.K. and K.A. Suresh, *Stabilization of Langmuir monolayer of hydrophobic thiocholesterol molecules.* Colloids Surf., A, 2008. **320**(1-3): p. 233-239.

Chapter 4 — Exploring the Role of POPC in Lipid Domain Formation using Single Molecule Fluorescence

4.1 Introduction

Intriguing evidence suggests that the plasma membrane can segregate lipids and proteins into small functional domains known as lipid rafts, as discussed in Chapter 1 [1-3] . These domains, enriched in cholesterol and saturated lipids, are thought to participate in a host of important processes such as signaling, membrane permeability, protein regulation, and adhesion [4-7] . Their small size and dynamic nature, however, have complicated efforts to characterize these structures in biological tissues. As such, their roles and even existence remain somewhat controversial [8] . This has focused efforts to understand the biophysical factors that affect lipid domain size and stability in model membranes, where the influence of membrane constituents is more easily controlled and measured [9-11] .

Both experiment and theory on simplified models have shown that many factors can influence domain formation in lipid membranes. Langmuir-Blodgett (LB) monolayers composed of lipid mixtures enables highly controlled studies of phase separation and domain structures over a range of lipid ratios and surface pressures. For models of lipid rafts, mixtures of high melting point saturated lipids, such as 1,2-dipalmitoyl-sn-glycero-3-phosphatidylcholine (DPPC), and low melting point unsaturated lipids, such as 1,2-dioleoyl-*sn*-glycero-3-phosphocholine (DOPC), are often employed. These mixtures partition into coexisting liquid-liquid phases with condensed domains rich in DPPC and less ordered domains enriched in DOPC [12-15] . The addition of cholesterol, which is associated with raft formation, can have a condensing effect on the DPPC rich domains as the rigid cholesterol inserts and helps align the surrounding saturated acyl chains [16-21] . These and similar models of lipid raft mixtures generally lead to

the formation of domains on the microns length scale, which are easily visualized with techniques such as fluorescence microscopy.

The raft hypothesis, however, suggests that domains ranging from 10 – 200 nm are formed in biomembranes, which raises interesting questions regarding the mechanisms that stabilize the formation of such small domains. The factors that influence domain size and shape in two-dimensional lipid films were explored in Chapter 1 and are generally understood in terms of a balance between dipolar repulsive interactions and line tension, with the latter being conceptually similar to surface tension in three-dimensions [22, 23] . Like surface tension, the line tension in two-dimensional films is defined as the excess free energy per unit length along the border separating phase domains. High line tension favors large circular domains to minimize phase boundaries while repulsive dipolar forces favor distortions away from circularity. One requirement for the stable formation of small domains like lipid rafts is a reduction in the line tension between domains. How this is accomplished in biological membranes, however, remains poorly understood.

Some studies suggest that hybrid lipids, lipids containing one saturated and one unsaturated tail, may have a preference for the interface between domains in biomembranes and help to lower the line tension between domains [24-28] . In this mechanism, hybrid lipids selectively align along the domain boundary with their saturated tail oriented towards the liquid condensed (LC) domain and unsaturated tail toward the liquid expanded (LE) domain. Lipids thought to have a preference for this interfacial region have been termed lineactants, to highlight their similarity with surface active agents (surfactants) in three-dimensional systems [29] . Lineactant behavior has been inferred from fluorescence microscopy studies using giant unilamellar vesicles (GUVs). GUVs composed of POPC/DSPC(di18:0PC)/Chol found that POPC had a slight preference for domain boundaries [30] .

While conceptually appealing, this mechanism has been questioned. Studies performed in the same group showed that in similarly prepared ternary lipid mixtures of PLPC(16:0-18:2PC)/DSPC/Chol and PAPC(16:0-20:4PC)/DSPC/Chol, the hybrid lipid showed no preference for domain boundaries [30] . This suggests that hybrid lipids may act in other ways to lower line tension and stabilize small domain formation. For example, some hybrid lipids like POPC, PLPC and PAPC are miscible, to some extent, in condensed lipid phases. This miscibility can reduce the compositional differences between two coexisting phases thus lowering line tension.

Here we use both ensemble and single molecule fluorescence measurements to compare LB monolayers composed of equimolar mixtures of DPPC/POPC and DPPC/DOPC to further understand the role of the hybrid lipid POPC in influencing domain size and shape. These two model systems are studied at a range of surface pressures (20 mN/m to 40 mN/m) and in the presence of small amounts of cholesterol to compare changes in domain structure.

Fluorescence measurements of monolayers doped with 0.1 mol % BODIPY-FA, which preferentially partitions into the expanded phase, reveal similar trends in domain size and shape in DPPC/DOPC and DPPC/POPC monolayers with surface pressure. Upon the addition of just 0.1 mol % of cholesterol, however, significant differences emerge. The average LC domain size increases with surface pressure in monolayers containing POPC while domains in monolayers containing DOPC decrease in size. This difference becomes more pronounced in monolayers incorporating 0.1 mol % of the fluorescent cholesterol analog BOIDPY-cholesterol. These trends suggest that POPC is more miscible in DPPC rich domains at higher surface pressures than DOPC. Moreover, it appears that this process is highly influenced by the presence of cholesterol, which is also thought to act as a lineactant in monolayers [31, 32] .

To further probe membrane structure, defocused single molecule fluorescence measurements were conducted [33-36] . Polarized total internal reflection microscopy (PTIRF-M) was used to characterize the emission dipole tilt angle away from the monolayer normal for probe molecules doped into the films at trace levels. We have previously used this method to quantify changes in monolayer structure as a function of surface pressure, environmental factors, and the presence of additives such as sterols and ganglioside [20, 37-41]. Here, the single molecule orientation measurements suggest that lipid packing in the expanded regions of DPPC/DOPC monolayers increases more rapidly with surface pressure than in DPPC/POPC films. This is consistent with POPC reducing packing stress in the expanded region by moving into the condensed domains as surface pressure increases. Additional single molecule studies using the fluorescent lipid analog BOIDPY-cholesterol also support this view. The striking observation that even small amounts of cholesterol can dramatically enhance the miscibility of POPC in the condensed domains at elevated surface pressure is discussed in terms of its role as a lineactant.

4.2 Materials and Methods

DPPC, DOPC, and POPC (Avanti Polar Lipids, Alabaster, AL) were obtained at >99% purity and used without further purification. Lipid stock solutions were prepared of DPPC/DOPC (1:1), DPPC/POPC (1:1), DPPC/DOPC/Chol (49.95:49.95:0.1), and DPPC/POPC/Chol (49.95:49.95:0.1) at a concentration of 1 mg/mL in chloroform (Fisher Scientific, Pittsburgh, PA). The fluorescent cholesterol analog BODIPY-cholesterol (TopFluor Cholesterol, Avanti Polar Lipids, Alabaster, AL) and fluorescent lipid analogs BODIPY-FA (B-3824) and BODIPY-PC (B-3794) (Invitrogen Corporation, Carlsbad, CA) were added to lipid stock solutions at

concentrations of either 0.1 mol % for bulk studies or 10^{-8} mol % for single molecule studies. The chemical structures of the lipids employed in this study are shown in Figure 1.

Approximately 50 µL volumes of lipid solutions were dispersed onto a subphase of ultrapure (18 MΩ) water in a Langmuir-Blodgett trough (Type 611, Nima Technology, Coventry, England). Once lipid stock solutions were dispersed onto the subphase, the chloroform was allowed to evaporate for 15 minutes. Monolayers were compressed at a speed of 100 cm^2/min and expanded at a speed of 80 cm^2/min. The compression and expansion cycles were repeated twice to anneal the monolayer. Each monolayer was then compressed to the target pressure at a rate of 100 cm^2/min and held at that pressure for 10 minutes before transferring onto Piranha-cleaned glass slides. The monolayers were transferred at a dipping velocity of 5 mm/min and all experiments were done in air at a temperature of 22 °C and a relative humidity between 40 and 45 %. Representative isotherms are shown in **Figure 4.1**.

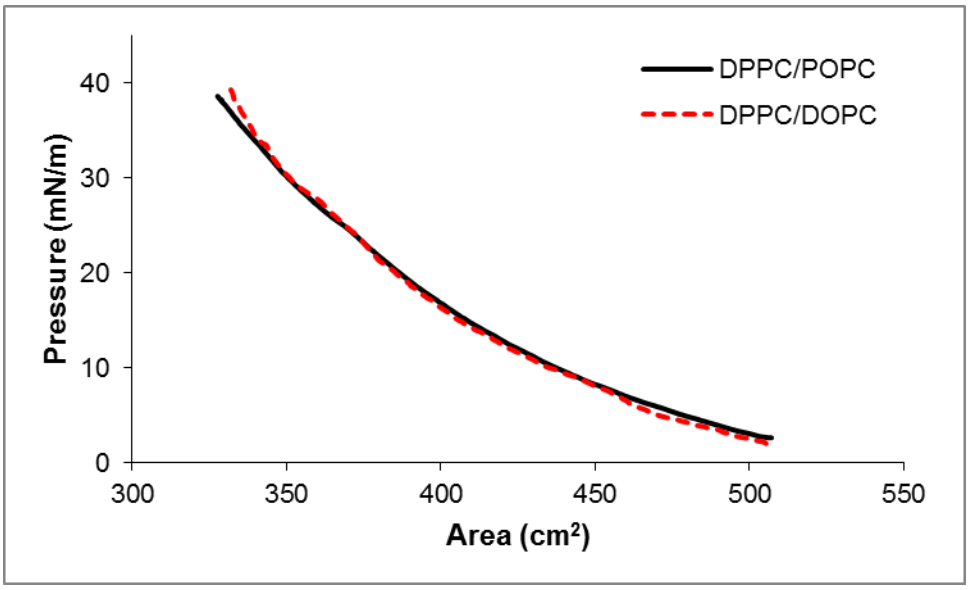

Figure 4.1 – representative isotherms are shown for monolayers prepared using equimolar mixtures of DPPC/POPC and DPPC/DOPC.

Monolayer films were imaged using a total internal reflection microscope (TIRF-M) (Olympus IX71, Olympus, Center Valley, PA) equipped with a 60x, 1.45 NA objective (Achromat, Olympus) for bulk fluorescence imaging and a 100x, 1.45 NA objective for single molecule measurements. The 514 nm line of an argon ion laser (Coherent Innova 90, Coherent, Inc., Santa Clara, CA) was P-polarized using half and quarter wave plates and used as an excitation source. Emission was collected through a ZT514rdc dichroic mirror and HQ522/40m band pass filter (Chroma, Rockingham, VT). A CCD camera (CoolSnap HQ2, Photometrics, Tucson, AZ) was used to collect all images. Image collection was controlled using Micromanager Software (version 1.4.14) with 500 ms integration times and no binning [42] . For single molecule measurements, excitation light was defocused by ~500 nm using a piezo-electric focusing collar (Mad City Laboratories, Inc., Madison, WI). All images were analyzed using ImageJ [43] and MATLAB (Mathworks, Natick, MA).

4.3 Results and Discussion

To investigate the role of the hybrid lipid POPC in lipid phase formation and stabilization, monolayers of DPPC/POPC (1:1) are compared with similarly prepared monolayers of DPPC/DOPC (1:1) both in the presence and absence of small amounts of cholesterol. The mixed monolayers separate into DPPC-rich LC domains and POPC-rich or DOPC-rich LE regions at all surface pressures studied and therefore are well-characterized systems for understanding the role of POPC in influencing domain structure. Several different fluorescent lipid analogs are used to probe domain structure at the bulk and single molecule levels. The structures of the lipids and fluorescent analogs used in this study are shown in **Figure 4.2**.

4.3.1 Fluorescence Microscopy Images

Figure 4.3 compares a series of fluorescence images for the mixed monolayers transferred onto glass substrates at the indicated surface pressures. Two fluorescent lipid analogs were used in **Figure 4.3** to characterize phase structure in the monolayers. The top series of images compares films doped with 0.1 mol % BODIPY-FA while the bottom series shows films incorporating 0.1 mol % BODIPY-cholesterol. The former marker partitions into LE regions of phase separated films while the latter has been shown to mimic natural cholesterol and can be used to stain cholesterol rich regions.

In the top series of images in **Figure 4.3**, the phase structure of DPPC/POPC and DPPC/DOPC monolayers are compared using 0.1 mol % BODIPY-FA. At 20 mN/m, both DPPC/POPC and DPPC/DOPC monolayers exhibit semi-circular dark LC domains surrounded by bright areas incorporating the fluorescent lipid probe, marking LE regions in the film. As the surface pressure is increased to 30 mN/m, the LC domains in both films increase in area and transition to a more branched geometry. At 40 mN/m, the LC areas further increase in size and become more irregular in shape.

The next series of images in **Figure 4.3** show the results from adding a small amount of cholesterol (0.1 mol %) into the films, using the same BODIPY-FA probe. For the DPPC/POPC/Chol mixture, the trends in LC domain size and structure with surface pressure are similar to the films lacking cholesterol. For DPPC/DOPC/Chol, on the other hand, the monolayers exhibit smaller and more numerous LC domains at 30 and 40 mN/m compared with similarly prepared films lacking cholesterol.

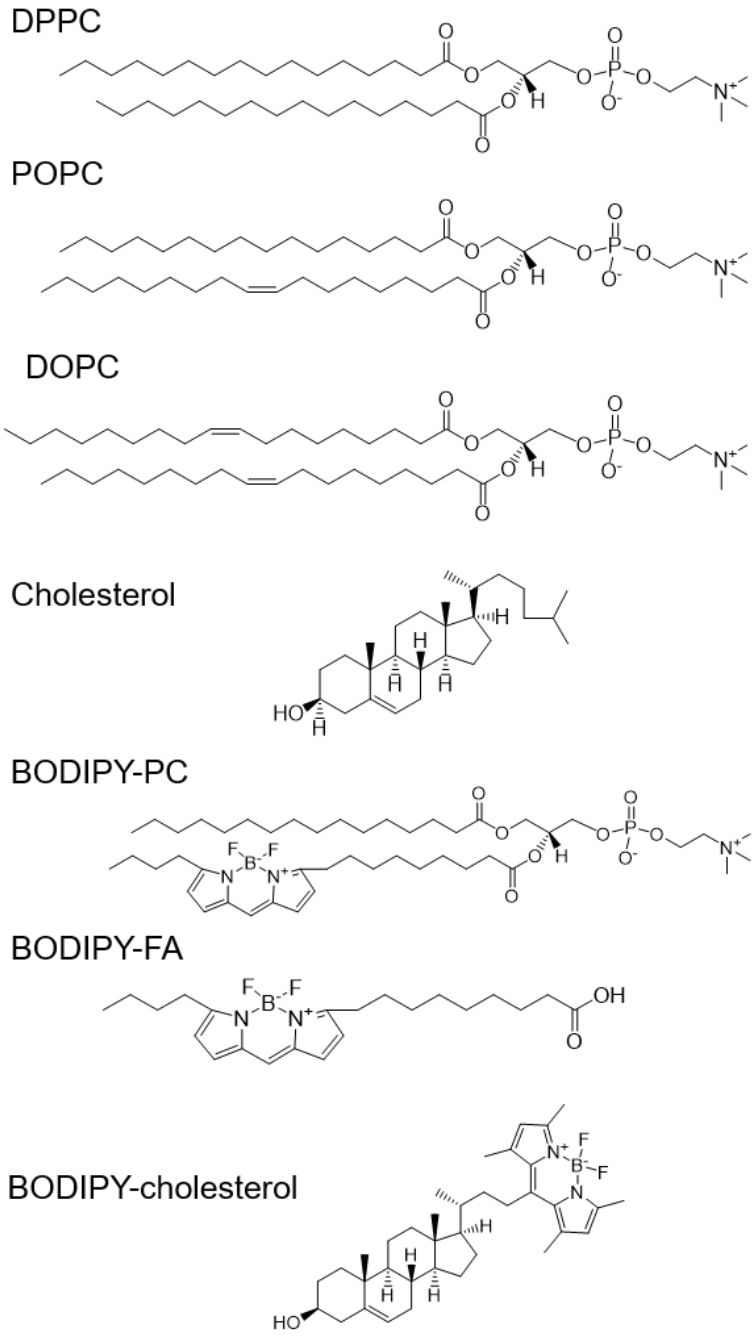

Figure 4.2 – Chemical structures of 1,2-dipalmitoyl-sn-glycero-3-phosphatidylcholine (DPPC), 1-palmitoyl-2-oleoyl-*sn*-glycero-3-phosphocholine (POPC), 1,2-dioleoyl-*sn*-glycero-3-phosphocholine (DOPC), cholesterol, 2-(5-butyl-4,4-difluoro-4-bora-3a,4a-diaza-s-indacene-3-nonanoyl)-1-hexadecanoyl-sn-glycero-3-phosphocholine (BODIPY-PC), 5-butyl-4,4-difluoro-4-bora-3a,4a-diaza-s-indacene-3-nonanoic acid (BODIPY-FA), and 23-(dipyrromethene boron difluoride)-24-norcholesterol (BODIPY-cholesterol).

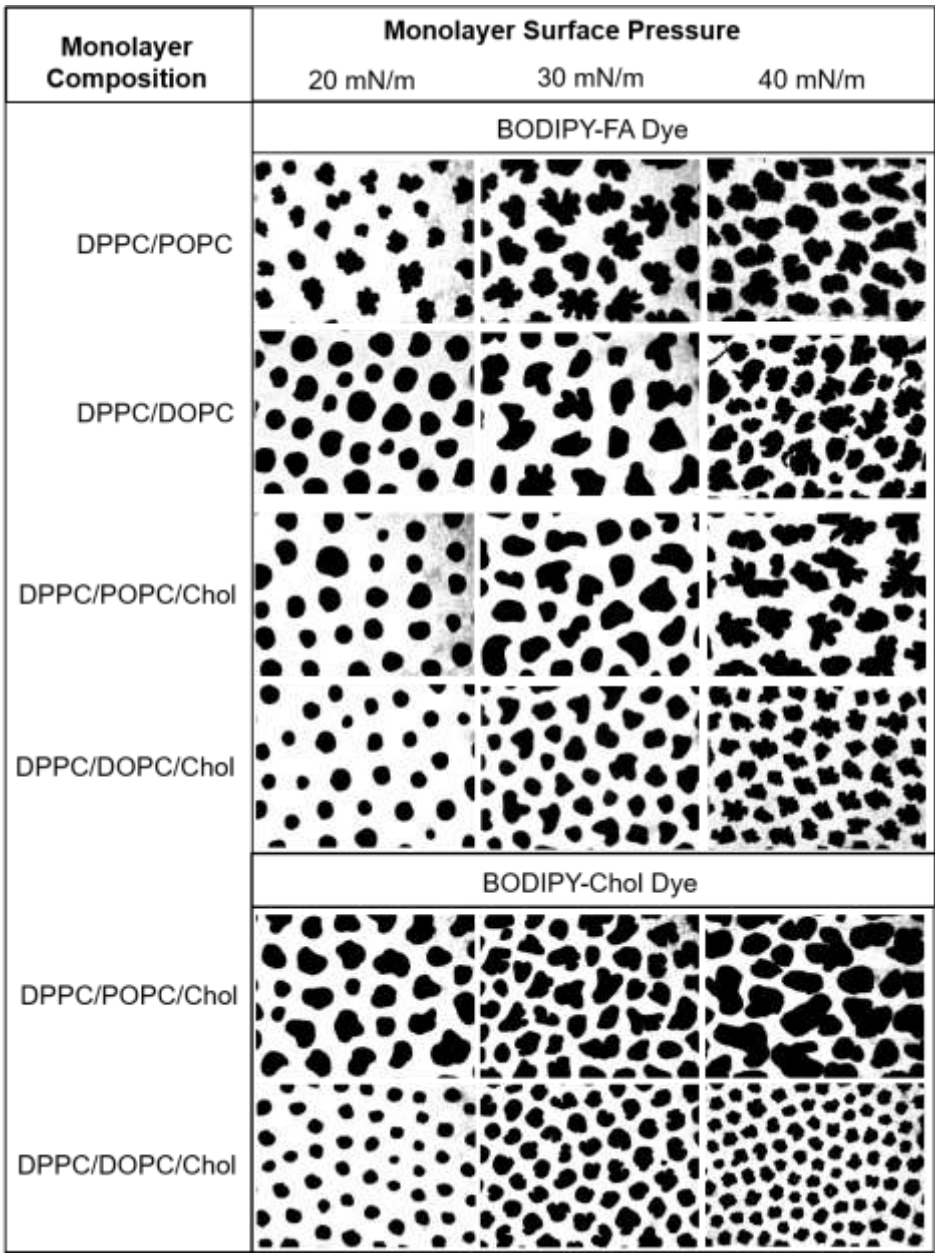

Figure 4.3 – Fluorescence images of DPPC/POPC (1:1) and DPPC/DOPC (1:1) monolayers with and without 0.1 mol % cholesterol in the top series of the figure. These images contain 0.10 mol % of BODIPY-FA. The second series of images shows DPPC/POPC (1:1) and DPPC/DOPC (1:1) with 0.10 mol % of BODIPY-cholesterol dye. All monolayers were transferred at a surface pressure of π=30 mN/m. Each image is 64 μm × 85 μm.

These differences become more pronounced when comparing DPPC/POPC and DPPC/DOPC films doped with 0.1 mol % of the fluorescent cholesterol analog, BODIPY-cholesterol. The bottom series of images in **Figure 4.3** reveal significant differences as surface pressure is increased. The dark, condensed domains in DPPC/POPC monolayers steadily grow in size with surface pressure while those in DPPC/DOPC initially grow as surface pressure increases from 20 to 30 mN/m and then become smaller and more numerous as pressure is increased to 40 mN/m.

4.3.2 Quantitative Analysis of Fluorescence Images

To gain a more quantitative view of how membrane constituents influence domain structure, key parameters were extracted from the images in **Figure 4.3** and are summarized in **Figure 4.4**. Percent LC area (top graphs) and average LC domain size (bottom graphs) were extracted from three separately prepared monolayers at each condition and plotted in **Figure 4.4**. Each plot in **Figure 4.4** compares the results from DPPC/POPC (black circles) monolayers with similarly prepared DPPC/DOPC (red squares) monolayers plotted as a function of surface pressure.

The first column of graphs summarizes the results for mixed monolayers prepared without cholesterol, using the BODIPY-FA fluorescent probe to visualize domains. As seen in the top plot, the average % LC area in both films increases steadily with surface pressure in a similar fashion. The average LC domain size shown in the bottom plot similarly increases in both films up to 30 mN/m, where the plots for the two monolayers diverge somewhat. For DPPC/POPC films, the average LC domain size continues to grow at higher surface pressure while those in DPPC/DOPC films decrease slightly.

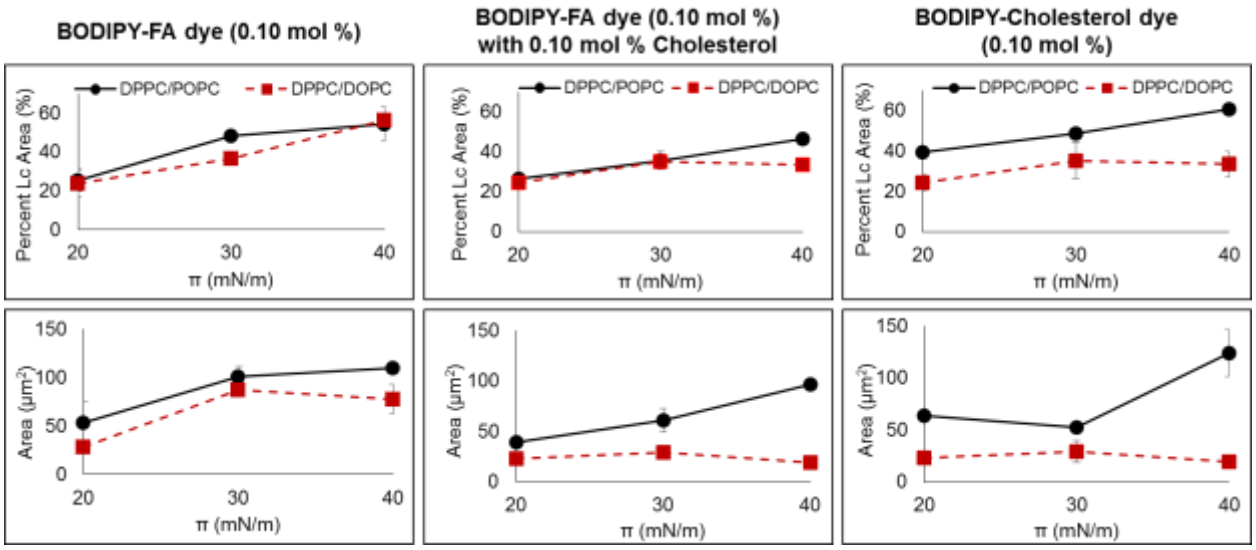

Figure 4.4 – Quantitative data extracted from **Figure 4.2** showing the average percent LC area (top), average LC domain area (middle), and area to perimeter ratio (A/P ratio, bottom) for DPPC/POPC (black circles) and DPPC/DOPC (red squares) monolayers at 20, 30, and 40 mN/m. Each data point represents three separately prepared films.

With the addition of even small amounts of cholesterol, however, significant differences begin to emerge in film structure. The middle column in **Figure 4.4** summarizes the results from films incorporating just 0.1 mol % cholesterol using the same BODIPY-FA fluorescence marker. Both plots, percent LC area and LC domain size, show differences at higher surface pressures. In particular, monolayers of DPPC/POPC/Chol exhibit significantly larger average LC domain size compared with similarly prepared DPPC/DOPC/Chol monolayers at 40 mN/m. Similar trends are observed comparing monolayers prepared with the fluorescent cholesterol analog BODIPY-cholesterol as shown in **Figure 4.4**.

Previous studies have shown that some hybrid lipids are more soluble in condensed phase domains than their di-unsaturated lipid counterparts, thus decreasing the compositional differences between domains. **Figure 4.4** shows that LC domains for monolayers incorporating the hybrid POPC grow in size with surface pressure while those incorporating the di-unsaturated DOPC decrease in size at high surface pressure. This is consistent with a mechanism in which

POPC is able to cross into LC domains at higher surface pressures, thus increasing their size. This process also appears to be facilitated by the presence of cholesterol.

As shown in **Figures 4.3 and 4.4**, the addition of just 0.1 mol % of cholesterol into DPPC/POPC monolayers further increases the average LC domain size at 40 mN/m. At this surface pressure, LC domains are approximately 5 times larger than those in similarly prepared DPPC/DOPC/Chol films. This observation supports the hypothesis that cholesterol exhibits line activity in monolayer systems [31, 32] . If cholesterol is acting as a lineactant, the addition of even a small amount of cholesterol would lower the free energy barrier that POPC would have to overcome to move from the LE to LC phase, allowing more POPC to incorporate into the LC phase at high surface pressure. This is not observed in the monolayers containing DOPC due to the negligible miscibility of di-unsaturated lipids in condensed domains.

4.3.3 Single Molecule Orientation Measurements for Structural Analysis

To gain further insight into these differences, single molecule fluorescence measurements were carried out using a fluorescently labeled lipid (BODIPY-PC) and the fluorescent sterol analog. We have previously shown that the three dimensional orientation of these fluorescent analogs respond to changes in monolayer structure. Changes in surface pressure, relative humidity, and the presence of the additives such as cholesterol and GM1 all lead to orientation changes of these single molecule probes [20, 37-40] .

Previously, we showed that single molecule orientation measurements of the fluorescent lipid analog BODIPY-PC (see **Figure 4.2**) can reveal changes in membrane packing [44]. BODIPY-PC is doped into monolayers at 10^{-8} mol % and partitions into the LE phase. Fluorescence images of the films at the single molecule level are collected using defocused polarized total internal reflection fluorescence microscopy (PTIRF-M). After defocusing ~500

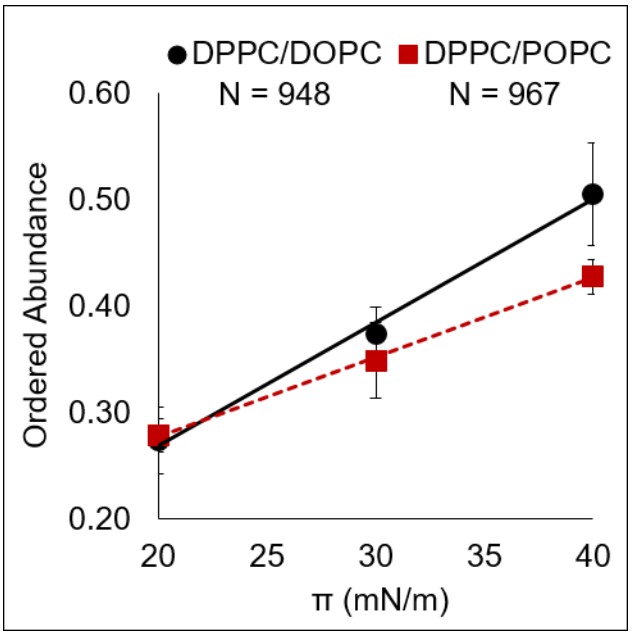

Figure 4.5 – Analysis of monolayers of DPPC/POPC and DPPC/DOPC prepared with 10^{-8} mol % BODIPY-PC. The ordered abundance of each monolayer, equal to the percentage of BODIPY-PC probes that are oriented at $\Phi \leq 10°$, is plotted versus surface pressure. The number of molecules analyzed are indicated by N. This graph shows that DPPC/POPC monolayers are less ordered than DPPC/DOPC monolayers at the same pressures.

nm, distinctive shapes in the single molecule fluorescence features are present and reflect the three-dimensional orientation of the emission dipole in the monolayer [33-36, 45, 46]. The tilt angles of the emission dipole away from the membrane normal are extracted from the images to create tilt angle histograms or plots of ordered abundance. Here ordered abundance is defined as the percentage of emission dipoles that are tilted less than 10° from the membrane normal, as previously described for this fluorescent probe [20] . Past studies have shown that the ordered abundance increases as the surface pressure of the membrane is increased, reflecting the reduced area per lipid in the membrane.

Figure 4.5 compares the ordered abundance of BODIPY-PC in DPPC/POPC and DPPC/DOPC monolayers at 20, 30, and 40 mN/m. As the surface pressure increases, the

ordered abundance of BODIPY-PC in both monolayers increases linearly. The increase, however, rises faster in monolayers incorporating DOPC compared to those with POPC. This difference is consistent with a mechanism in which POPC can move into DPPC rich domains at elevated surface pressures, helping relieve some of the packing stress in the LE phase where the BODIPY-PC marker resides. DOPC, on the other hand, is immiscible in the DPPC domains and thus the ordered abundance rises faster as the surface pressure increases.

Single molecule fluorescence studies were also carried out using the BODIPY-cholesterol shown in **Figure 4.2**. This fluorescently labeled cholesterol analog has been shown to closely mimic natural cholesterol, and we have used it previously to study the role of cholesterol in ternary lipid monolayers [39, 47, 48] . Orientation measurements of BODIPY-cholesterol in DPPC/DOPC monolayers at 20 mN/m illustrate preferred orientations as shown in **Figure 4.6**. The tilt angle histogram shows that most of the BODIPY-cholesterol population orients with their emission dipoles lying in the membrane plane (>72^{o}) with smaller populations oriented at 2-10° and 22-30°. This closely tracks previously measured distributions in similar membranes.

At low surface pressure, the dominant population at >72° was attributed previously to an insertion geometry in which the cholesterol moiety aligns within the monolayer with the BODIPY fluorophore extending out of and bending back towards the surrounding acyl chains. As shown in **Figure 4.6**, very similar BODIPY-cholesterol orientation distributions are observed for both DPPC/DOPC and DPPC/POPC monolayers at low pressure.

As the surface pressure is increased, however, significant differences between the two films emerge. At 30 mN/m, the population oriented at large angles (>72^{o}) disappears in DPPC/DOPC monolayers (red circles) but remains in the DPPC/POPC films (black line). For DPPC/DOPC, the loss of population was previously observed and attributed to a squeeze-out

mechanism at higher surface pressures. Under this hypothesis, the change in distribution of the single molecule orientations occurs because the BODIPY-cholesterol molecule moves from the interior of the lipid monolayer to a position outside of the membrane. The measured change is consistent with a geometry that has the cholesterol moiety lying on top of the acyl chains and the BODIPY moiety inserted in to the chains, with tilt angles favoring 2-10° or 22-30° from the membrane normal. This mechanism is based on other observations showing that headgroup-modified cholesterol molecules can be squeezed out of monolayers at surface pressures lower than the monolayer collapse pressure [49] .

As the surface pressure increases so does packing frustration in the LE regions of the films. In DPPC/DOPC monolayers, the primary mechanism in response is for DOPC molecules in the LE phase to occupy a smaller area per molecule, thus become more ordered. This ordering also occurs in LE regions of DPPC/POPC monolayers, but rises less rapidly with surface pressure as the single molecule data in **Figure 4.5**. This suggests that the monolayers incorporating the hybrid lipid POPC have an additional mechanism for relieving packing frustration by partitioning into the DPPC rich domains at elevated surface pressures. This is further supported by the single molecule BODIPY-cholesterol data shown in **Figure 4.6**. A significantly higher surface pressure is required for the onset of squeeze-out in monolayers incorporating the hybrid lipid POPC compared to those incorporating the doubly unsaturated DOPC. These observations along with the analysis of the ensemble fluorescence data and previous studies suggest that POPC is partially miscible in DPPC rich domains at higher surface pressures. This miscibility reduces the compositional differences between the two phases, thus reducing line tension even in the absence of any lineactant activity. Interestingly, these processes are enhanced in membranes containing small amounts of cholesterol, which itself is thought to act as a lineactant and is a putative component of lipid rafts.

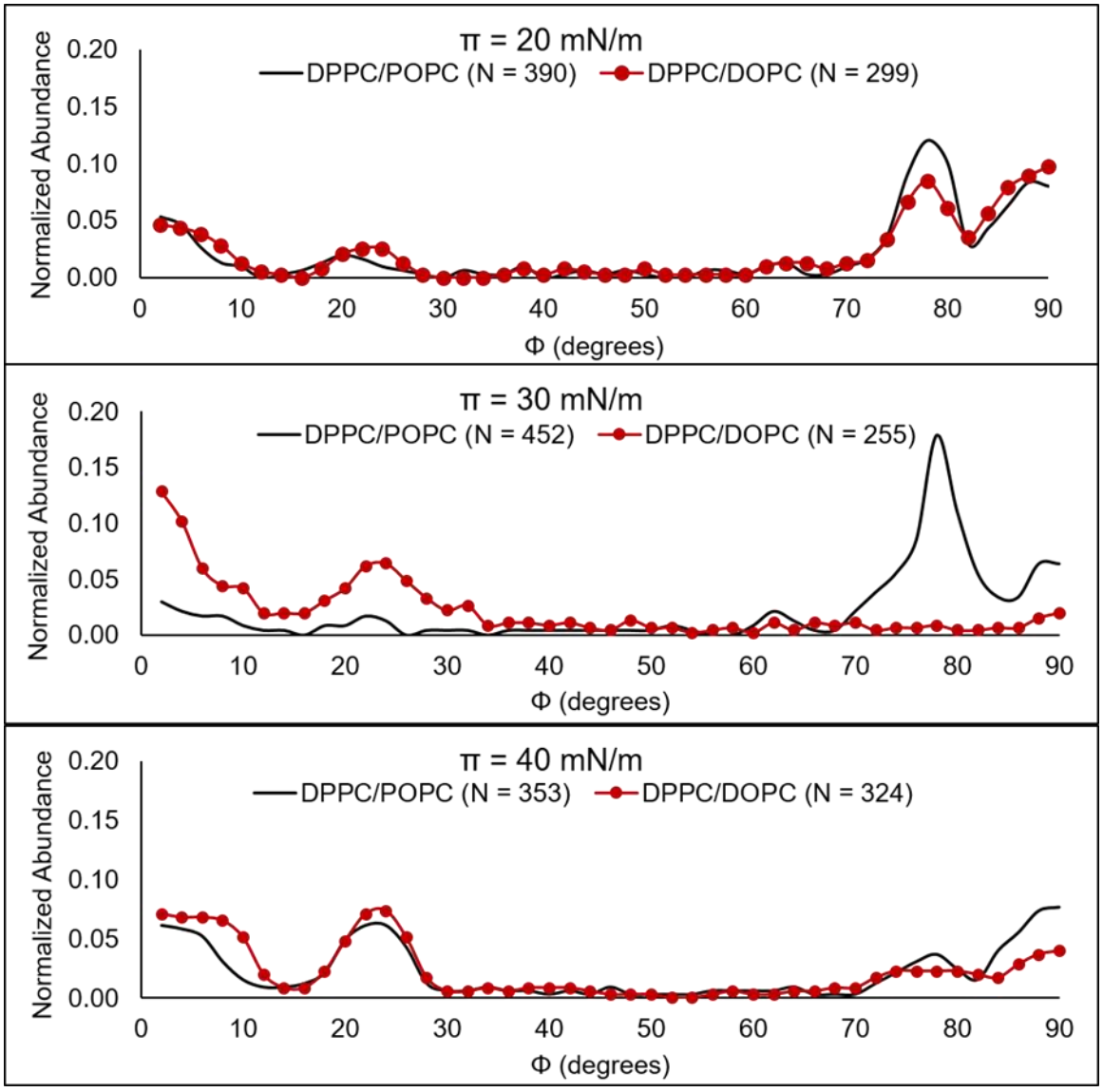

Figure 4.6 – Tilt angle histograms for BODIPY-cholesterol in mixed monolayers of DPPC/POPC and DPPC/DOPC as a function of surface pressure. The number of molecules analyzed are indicated by N, and population histograms are plotted as lines to help guide the eye. At 20 mN/m, the most probably orientation is at >72°. As the pressure is increased, both lipid mixtures undergo a transition where the population at >72° decreases with an increase in the populations at 2-10° and 22-30°.

4.4 Conclusions

Monolayers of DPPC/POPC and DPPC/DOPC are compared as a function of surface pressure and presence of cholesterol to help understand the role of hybrid lipids in domain formation and stabilitzation. Both lipid mixtures separate into DPPC-rich LC domains and unsaturated lipid-rich LE domains at all surface pressures studied. The results from ensemble fluorescence imaging and single molecule orientation measurements suggest that the hybrid lipid POPC can cross into DPPC-rich LC domains to a greater extent than DOPC as surface pressure increases. This process helps relieve packing stress in the LE regions, which is reflected in the single molecule orientation measurements suggest that the hybrid lipid POPC can cross into DPPC/rich LC domains to a greater extent than DOPC as surface pressure increases. This process helps relieve packing stress in the LE regions, which is reflected in the single molecule orientation measurements, and also reduces the compositional differences between coexisting domians, thus lowering the line tension between domains. The role of hybrid lipids in lowering line tension has become important in understanding how small domains, such as lipid rafts, can be formed in biological membranes. While we find no evidence for substantial lineactant activity of POPC, small additions of cholesterol, which is thought to have a lineactant activity, facilitates these processes.

4.5 References

1. Simons, K. and E. Ikonen, *Functional rafts in cell membranes.* Nature, 1997. **387**(6633): p. 569-572.

2. Shaw, A.S., *Lipid rafts: now you see them, now you don't.* Nat. Immunol., 2006. **7**(11): p. 1139-1142.

3. Schmid, F., *Physical mechanisms of micro- and nanodomain formation in multicomponent lipid membranes.* Biochim. Biophys. Acta, Biomembr., 2016: p. Ahead of Print.

4. Nusrat, A., et al., *Tight junctions are membrane microdomains.* J. Cell Sci., 2000. **113**(10): p. 1771-1781.

5. Rawicz, W., et al., *Elasticity, strength, and water permeability of bilayers that contain raft microdomain-forming lipids.* Biophys J, 2008. **94**(12): p. 4725-36.

6. Hakomori, S.-I., *Cell adhesion/recognition and signal transduction through glycosphingolipid microdomain.* Glycoconjugate J., 2001. **17**(3/4): p. 143-151.

7. Ikonen, E., *Roles of lipid rafts in membrane transport.* Curr. Opin. Cell Biol., 2001. **13**(4): p. 470-477.

8. Levental, I. and S.L. Veatch, *The continuing mystery of lipid rafts.* J. Mol. Biol., 2016. **428**(24_Part_A): p. 4749-4764.

9. Miersch, S. and B. Mutus, *Membrane lipid domains: techniques for visualization and characterization.* Curr. Anal. Chem., 2007. **3**(1): p. 81-92.

10. Johnston, L.J., *Nanoscale Imaging of Domains in Supported Lipid Membranes.* Langmuir, 2007. **23**(11): p. 5886-5895.

11. Veatch, S.L. and S.L. Keller, *Seeing spots: Complex phase behavior in simple membranes.* Biochim. Biophys. Acta, Mol. Cell Res., 2005. **1746**(3): p. 172-185.

12. Stottrup, B.L., S.L. Veatch, and S.L. Keller, *Nonequilibrium behavior in supported lipid membranes containing cholesterol.* Biophys. J., 2004. **86**(5): p. 2942-2950.

13. Davis, J.H., J.J. Clair, and J. Juhasz, *Phase equilibria in DOPC/DPPC-d62/cholesterol mixtures.* Biophys. J., 2009. **96**(2): p. 521-539.

14. Fritzsching, K.J., J. Kim, and G.P. Holland, *Probing lipid-cholesterol interactions in DOPC/eSM/Chol and DOPC/DPPC/Chol model lipid rafts with DSC and 13C solid-state NMR.* Biochim. Biophys. Acta, Biomembr., 2013. **1828**(8): p. 1889-1898.

15. Veatch, S.L. and S.L. Keller, *Separation of liquid phases in giant vesicles of ternary mixtures of phospholipids and cholesterol.* Biophys. J., 2003. **85**(5): p. 3074-3083.

16. Weis, R.M. and H.M. McConnell, *Cholesterol stabilizes the crystal-liquid interface in phospholipid monolayers.* J. Phys. Chem., 1985. **89**(21): p. 4453-9.

17. Hung, W.-C., et al., *The condensing effect of cholesterol in lipid bilayers.* Biophys. J., 2007. **92**(11): p. 3960-3967.

18. Kim, K.H., et al., *Effect of cholesterol nanodomains on monolayer morphology and dynamics.* Proc. Natl. Acad. Sci. U. S. A., 2013. **110**(33): p. E3054-E3060,SE3054/1-SE3054/6.

19. de Meyer, F. and B. Smit, *Effect of cholesterol on the structure of a phospholipid bilayer.* Proc. Natl. Acad. Sci. U. S. A., 2009. **106**(10): p. 3654-3658.

20. Livanec, P.W., H.A. Huckabay, and R.C. Dunn, *Exploring the Effects of Sterols in Model Lipid Membranes Using Single-Molecule Orientations.* J. Phys. Chem. B, 2009. **113**(30): p. 10240-10248.

21. Lawrence, J.C., et al., *Real-time analysis of the effects of cholesterol on lipid raft behavior using atomic force microscopy.* Biophys. J., 2003. **84**(3): p. 1827-1832.

22. Heinrich, M.C., et al., *Critical Exponents for Line Tension and Dipole Density Difference from Lipid Monolayer Domain Boundary Fluctuations.* J. Phys. Chem. B, 2008. **112**(27): p. 8063-8068.

23. Benvegnu, D.J. and H.M. McConnell, *Line tension between liquid domains in lipid monolayers.* J. Phys. Chem., 1992. **96**(16): p. 6820-4.

24. Hassan-Zadeh, E., et al., *Complex Roles of Hybrid Lipids in the Composition, Order, and Size of Lipid Membrane Domains.* Langmuir, 2014. **30**(5): p. 1361-1369.

25. Muller, P. and F. Gallet, *First measurement of the liquid-solid line energy in a Langmuir monolayer.* Phys. Rev. Lett., 1991. **67**(9): p. 1106-9.

26. Benvegnu, D.J. and H.M. McConnell, *Surface dipole densities in lipid monolayers.* J. Phys. Chem., 1993. **97**(25): p. 6686-91.

27. Palmieri, B., et al., *Line active molecules promote inhomogeneous structures in membranes: Theory, simulations and experiments.* Adv. Colloid Interface Sci., 2014. **208**: p. 58-65.

28. Shimokawa, N., M. Nagata, and M. Takagi, *Physical properties of the hybrid lipid POPC on micrometer-sized domains in mixed lipid membranes.* Phys. Chem. Chem. Phys., 2015. **17**(32): p. 20882-20888.

29. Trabelsi, S., et al., *Linactants: Surfactant Analogues in Two Dimensions.* Phys. Rev. Lett., 2008. **100**(3): p. 037802/1-037802/4.

30. Heberle, F.A., et al., *Hybrid and nonhybrid Lipids exert common effects on membrane raft size and morphology.* J. Am. Chem. Soc., 2013. **135**(40): p. 14932-14935.

31. Veatch, S.L., K. Gawrisch, and S.L. Keller, *Closed-Loop Miscibility Gap and Quantitative Tie-Lines in Ternary Membranes Containing Diphytanoyl PC.* Biophysical Journal, 2006. **90**(12): p. 4428-4436.

32. Veatch, S.L. and S.L. Keller, *Organization in Lipid Membranes Containing Cholesterol.* Physical Review Letters, 2002. **89**(26): p. 268101.

33. Bartko, A.P. and R.M. Dickson, *Imaging Three-Dimensional Single Molecule Orientations.* J. Phys. Chem. B, 1999. **103**(51): p. 11237-11241.

34. Bohmer, M. and J. Enderlein, *Orientation imaging of single molecules by wide-field epifluorescence microscopy.* J. Opt. Soc. Am. B, 2003. **20**(3): p. 554-559.

35. Forkey, J.N., M.E. Quinlan, and Y.E. Goldman, *Measurement of single macromolecule orientation by total internal reflection fluorescence polarization microscopy.* Biophys. J., 2005. **89**(2): p. 1261-1271.

36. Patra, D., I. Gregor, and J. Enderlein, *Image Analysis of Defocused Single-Molecule Images for Three-Dimensional Molecule Orientation Studies.* J. Phys. Chem. A, 2004. **108**(33): p. 6836-6841.

37. Armendariz, K.P. and R.C. Dunn, *Ganglioside Influence on Phospholipid Films Investigated with Single Molecule Fluorescence Measurements.* J. Phys. Chem. B, 2013. **117**(26): p. 7959-7966.

38. Armendariz, K.P., et al., *Single molecule probes of membrane structure: Orientation of BODIPY probes in DPPC as a function of probe structure.* Analyst (Cambridge, U. K.), 2012. **137**(6): p. 1402-1408.

39. DeWitt, B.N. and R.C. Dunn, *Interaction of Cholesterol in Ternary Lipid Mixtures Investigated Using Single-Molecule Fluorescence.* Langmuir, 2015. **31**(3): p. 995-1004.

40. Huckabay, H.A. and R.C. Dunn, *Hydration Effects on Membrane Structure Probed by Single Molecule Orientations.* Langmuir, 2011. **27**(6): p. 2658-2666.

41. Song, K.C., et al., *Orientation of Fluorescent Lipid Analogue BODIPY-PC to Probe Lipid Membrane Properties: Insights from Molecular Dynamics Simulations.* J. Phys. Chem. B, 2011. **115**(19): p. 6157-6165.

42. Amodaj, N., R. Vale, and N. Stuurman, *Micro-Manager: Open Source software for light microscope imaging.* Microscopy Today, 2007. **15**(3): p. 42-43.

43. Schneider, C.A., W.S. Rasband, and K.W. Eliceriri, *NIH Image to ImageJ: 25 years of image analysis.* Nature Methods, 2012. **9**: p. 671-675.

44. Livanec, P.W. and R.C. Dunn, *Single-Molecule Probes of Lipid Membrane Structure.* Langmuir, 2008. **24**(24): p. 14066-14073.

45. Bartko, A.P. and R.M. Dickson, *Three-Dimensional Orientations of Polymer-Bound Single Molecules.* J. Phys. Chem. B, 1999. **103**(16): p. 3053-3056.

46. Toprak, E., et al., *Defocused orientation and position imaging (DOPI) of myosin V.* Proc. Natl. Acad. Sci. U. S. A., 2006. **103**(17): p. 6495-6499.

47. Li, Z., E. Mintzer, and R. Bittman, *First synthesis of free cholesterol-BODIPY conjugates.* J. Org. Chem., 2006. **71**(4): p. 1718-1721.

48. Robalo, J.R., et al., *Behavior of Fluorescent Cholesterol Analogues Dehydroergosterol and Cholestatrienol in Lipid Bilayers: A Molecular Dynamics Study.* J. Phys. Chem. B, 2013. **117**(19): p. 5806-5819.

49. Gupta, R.K. and K.A. Suresh, *Stabilization of Langmuir monolayer of hydrophobic thiocholesterol molecules.* Colloids Surf., A, 2008. **320**(1-3): p. 233-239.

Chapter 5—Alternative Model Membrane Systems: Spin-Coated Supported Lipid Bilayers

5.1 Introduction

Several model membrane types were introduced in Chapter 1, including Langmuir-Blodgett (LB) monolayers, Langmuir-Blodgett/Langmuir-Schaefer (LB/LS) bilayers, and unilamellar vesicles. These and other model membranes have been used extensively to investigate membrane properties and offer the ability to minimize the complexity of natural membranes for analytical investigation. However, each model type has certain advantages and limitations. For example, supported lipid bilayers (SLBs) preserve fundamental properties of biological bilayers, like thickness and lateral fluidity, and can be prepared using vesicle fusion of unilamellar vesicles [1]. In this method, a small volume of unilamellar vesicle solution in warm buffer is incubated with a hydrophilic substrate. When individual vesicles interact with the substrate, they rupture and self-assemble to form a fluid, planar bilayer. However, this technique has a few limitations. Vesicle fusion requires the use of a hydrophilic substrate for vesicles to rupture and self-assemble, excluding analysis techniques that require gold, titanium dioxide, aluminum oxide, or nanostructured substrates [2]. Additionally, SLBs formed using this technique are hydrated and cannot easily be dried without causing irreversible damage to their structure [3, 4].

Despite a great deal of investigation into SLBs, very little is currently known about their properties under dry conditions. Dry bilayers can be analyzed using techniques that are not appropriate for hydrated bilayers, including conductive Atomic Force Microscopy (c-AFM), Scanning Tunneling Microscopy (STM), Scanning Electron Microscopy (SEM), and Secondary Ion Mass Spectrometry (nano-SIMS), to name a few examples [5]. In addition, certain techniques, like polarized total internal reflection florescence microscopy (PTIRF-M) for single molecule orientation analysis, introduced in Chapter 2, are more robust under dry conditions

where individual molecule reorientation dynamics are limited [6]. Instrumental limitations have prevented these techniques from being used to investigate hydrated bilayers, but the information that they provide on dry bilayers could be of interest in helping to understand hydrated bilayers. Much effort has been put forth, therefore, to prepare and investigate air-stable, dry bilayers.

A variety of techniques have been explored to prepare dry SLBs. These efforts have seen limited success, though. An obvious technique would utilize a vacuum to evaporate away the buffer solution; however this disrupts the substrate – bilayer interactions and produces irreversible damage to the bilayer structure and morphology. Additives like lyoprotectants and proteins have been included with vesicles to preserve the bilayer during drying but have a tendency to precipitate out of the membrane when dry and can alter membrane properties [7-9]. Freeze-drying has been used to prepare high-quality, dry bilayers but is challenging to reproduce successfully [10, 11]. Recently, dry lipid bilayers have been prepared using the spin-coating technique, where lipids are dissolved into a high vapor pressure solvent and spin-coated onto a substrate. The solvent is subsequently evaporated away to leave an air-stable bilayer or multilayer that can be used to model biological membrane problems and has even been applied as a model of the human epidermis [10-12].

Early analysis of spin-coated SLBs has shown that they can have structure similar to SLBs prepared using vesicle fusion. Dry, spin-coated SLBs of DOPC (18:1 Δ9-cis PC) were analyzed using atomic force microscopy (AFM) and exhibited uniform structure and thickness comparable to hydrated DOPC bilayers [13]. Bilayers of POPC (16:0-18:1 PC) were hydrated to 20 – 30 % relative humidity (RH) and showed domain formation with areas of high and low order. Analysis of the height differences between these domains was, on average, 5 nm and comparable to hydrated POPC bilayers with fluid and solid phase domains [14]. Liquid ordered and liquid disordered domains naturally formed in dry bilayers prepared using POPC and DPPC (16:0

PC), comparable to vesicle fusion and LB/LS deposition results [14]. Additionally, researchers have shown that both bilayers and multilayers can be formed using spin-coating, depending on the concentration of lipid solution used [13]. X-ray reflectivity measurements on DMPC (14:0 PC) demonstrated that uniform, homogeneous multilayers of as many as 22 membrane bilayers thick have been prepared [15]. Dry spin-coated SLBs have many of the advantages of hydrated SLBs, as the resulting bilayer has a planar geometry for simplified imaging and analysis and the composition of the bilayer can be carefully controlled.

Here, hydrated SLBs of DPPC/DOPC (1:1) and SM/DOPC (1:1) are prepared using vesicle fusion and compared to dry bilayers of the same lipid compositions prepared using spin-coating. SLBs of DPPC/DOPC (1:1) are prepared with a variety of cholesterol concentrations to demonstrate that dry SLBs respond to the presence of biological additives. Lastly, single molecule analysis is performed on spin-coated bilayers to investigate their molecular level structure. The data will be compared to previous work using comparable Langmuir-Blodgett monolayers and discussed in terms of a goal of preparing and characterizing dry lipid bilayers for biological analysis.

5.2 Materials and Methods

5.2.1 Spin-Coated Supported Lipid Bilayers

DPPC (16:0 PC), DOPC (18:1 Δ9-Cis PC), chicken egg SM (fatty acid distribution 86% 16:0, 6% 18:0, 3% 22:0, 3% 24:1, 2% unknown), BODIPY-cholesterol (Avanti Polar Lipids, Alabaster, AL), cholesterol, hexadecane, and methanol (Sigma Aldrich, St. Louis, MO) were obtained at >99% purity. Texas Red 1,2-dihexadecanoyl-*sn*-glycero-3-phosphoethanolamine triethylammonium salt (Texas Red DHPE) (Life Technologies, Carlsbad, CA) was obtained at >98% purity. All lipids were used without further purification. Lipid stock solutions of DPPC,

DOPC, SM and cholesterol solutions were each prepared in chloroform at 25 mg/mL and diluted to appropriate ratios at a final concentration of 1 mM in 98% hexane with 2 % (w/w) methanol. BODIPY-cholesterol and Texas Red DHPE solutions were prepared and diluted in methanol to obtain appropriate working concentrations. The structures of all relevant lipids are shown in **Figure 5.1**.

Piranha-cleaned glass slides were rinsed, dried, and affixed to a spin-coater. Using a pipet, 250 µL of 1 mM lipid solution were added to the center of the slide. The spin-coater was

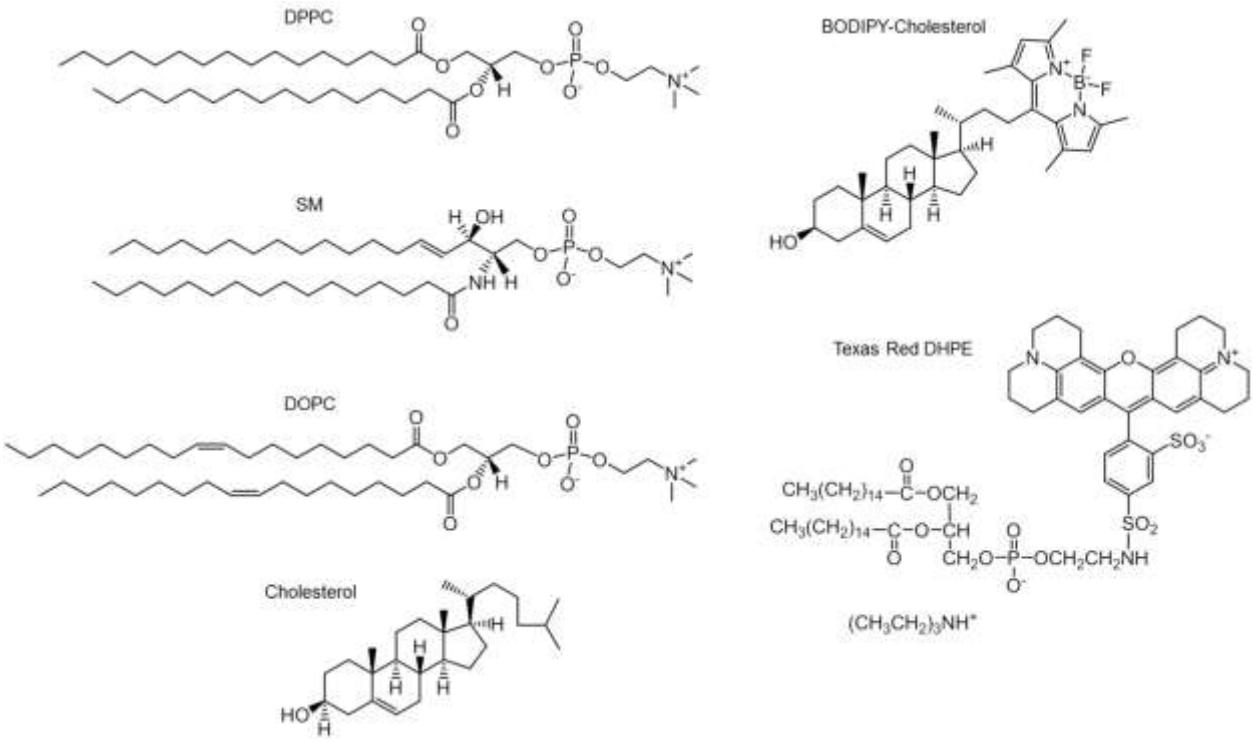

Figure 5.1- Structures of 1,2-Dipalmitoyl-*sn*-glycero-3-phosphatidylcholine (DPPC), 1,2-dioleoyl-sn-glycero-3-phosphocholine (DOPC), chicken egg sphingomyelin (SM), cholesterol, 23-(dipyrromethene boron difluoride)-24-norcholesterol (BODIPY-cholesterol), and Texas Red 1,2-dihexadecanoyl-*sn*-glycero-3-phosphoethanolamine triethylammonium salt (Texas Red DHPE) are shown.

allowed to rotate at 2000 RPM for 20 seconds and 3000 RPM for another 40 seconds, for a total spin time of 60 seconds. Finally, the slides were transferred and stored in a vacuum chamber for at least 1 hour to remove any excess solvent before imaging.

5.2.2 Preparing Small Unilamellar Vesicle (SUVs) Solution

To prepare a vesicle solution, lipid stock solutions were diluted in chloroform to a concentration of 5 mg/mL in 4 mL glass vials, and the chloroform was evaporated away under a gentle stream of nitrogen gas. The vials were stored under vacuum for at least 12 hours to remove residual solvent. A buffer of 20 mM HEPES with 100 mM NaCl and 0.02 % NaN_3 at a pH of 7 was prepared. The buffer solution was heated to 45 - 55 °C and the lipids were resuspended in warm buffer to a final concentration of 1 mM. The solutions were immediately vortexed for 60 seconds and transferred to a 60 °C water bath. The vesicles were allowed to swell under these conditions for 1 hour and were vortexed every 15 minutes. Next, the vials were suspended in a 60 °C bath sonicator and allowed to sonicate until the lipid solutions changed from opaque to clear, indicating that small (<100 nm) unilamellar vesicles had formed. Vesicle solutions were kept at 60 °C and used the same day as prepared.

5.2.3 Vesicle Fusion Method for Supported Lipid Bilayers

Glass cover slips were cleaned using Piranha solution. Before use the slides were rinsed thoroughly with deionized water and dried under a gentle stream of nitrogen gas. PDMS wells of 1 cm^2 were affixed to the clean, dry slides. Approximately 50 µL of warm (60 °C) vesicle solution was transferred to the PDMS well and allowed to incubate for 30 minutes while a bilayer formed. The slides were rinsed with 3 – 5 mL of 60 °C deionized water, allowed to cool

naturally to room temperature, and imaged immediately under excess water to prevent bilayer drying.

5.2.4 Model Membrane Imaging

Monolayers were imaged using a total internal reflection microscope (TIRF-M) (Olympus IX71, Olympus, Center Valley, PA) equipped with a 60x, 1.45 NA objective (Achromat, Olympus) for bulk fluorescence imaging and a 100x, 1.45 NA objective for imaging single molecules. Excitation light from the 514 nm line of an argon-ion laser (Coherent Innova 90, Coherent, Inc., Santa Clara, CA) was P-polarized using half and quarter wave plates. Emission was collected through a ZT514rdc dichroic mirror and HQ522/40m band pass filter (Chroma, Rockingham, VT). All images were collected using a cooled CCD camera (CoolSnap HQ2, Photometrics, Tucson, AZ). Image collection was controlled using Micromanager software (version 1.4.14) with 500 ms integration times and no binning [16]. For single molecule measurements, excitation light was defocused by ~500 nm. All images were analyzed using ImageJ (U.S. National Institutes of Health, Bethesda, MD) and MATLAB (Mathworks, Natick, MA).

5.3 Results and Discussion

A technique for preparing dry, air-stable lipid bilayers is of interest for a number of surface analysis techniques that cannot be applied to hydrated bilayers. Additionally, certain analysis techniques require the use of specialized substrates that are unsuitable for vesicle fusion, like gold or titanium dioxide. Here, we are investigating spin-coating to prepare dry SLBs. They are

compared to SLBs prepared using vesicle fusion, which is a popular technique for investigating lipid phase separation in bilayers.

In order to evaluate spin-coated SLBs for suitability, SLBs were prepared using both the spin-coating method and a vesicle fusion method for comparison. For spin-coating, 1 mM lipid solutions were prepared in hexane with 2 % (w/w) methanol. Solution was transferred to a hydrophilic glass substrate and spin-coated onto the substrate for 60 seconds, as described in section 5.2. The bilayer was stored under vacuum for 1 hour after preparation to ensure that all solvent had been removed. SLBs were also prepared using vesicle fusion. Here, wells were affixed to hydrophilic substrates and vesicle solution added. The solution was allowed to incubate for 30 minutes while a bilayer self-assembled and was rinsed with 60 °C water to remove excess lipid. A surplus of warm water was left on the hydrated bilayer to prevent it from drying during analysis. The bilayer was allowed to cool naturally to room temperature (20 – 22 °C) before any images were taken.

In **Figure 5.2**, a series of images of SLBs prepared by vesicle fusion are shown. In this figure, two fluorescent lipid analogs are used to determine the lipid phases present in the films. Images A and C are prepared using BODIPY-cholesterol and images B and D are prepared using Texas Red DHPE. In **Figure 5.2**, Image A shows DPPC/DOPC (1:1) with BODIPY-cholesterol and has irregular dark domains surrounded by a continuous bright phase. In Image B, when Texas Red DHPE is used, the same irregular domains are seen but include the fluorophore. As Texas Red DHPE is well known to partition into disordered domains in bilayers, this indicates that the irregularly shaped domains are disordered and the continuous phase is ordered in this set of images [17, 18]. A similar partitioning behavior was seen in SM/DOPC (1:1), where in Image C, BODIPY-cholesterol is used and stains the continuous, ordered phase. In Image D, Texas Red DHPE stains the irregularly shaped, disordered domains.

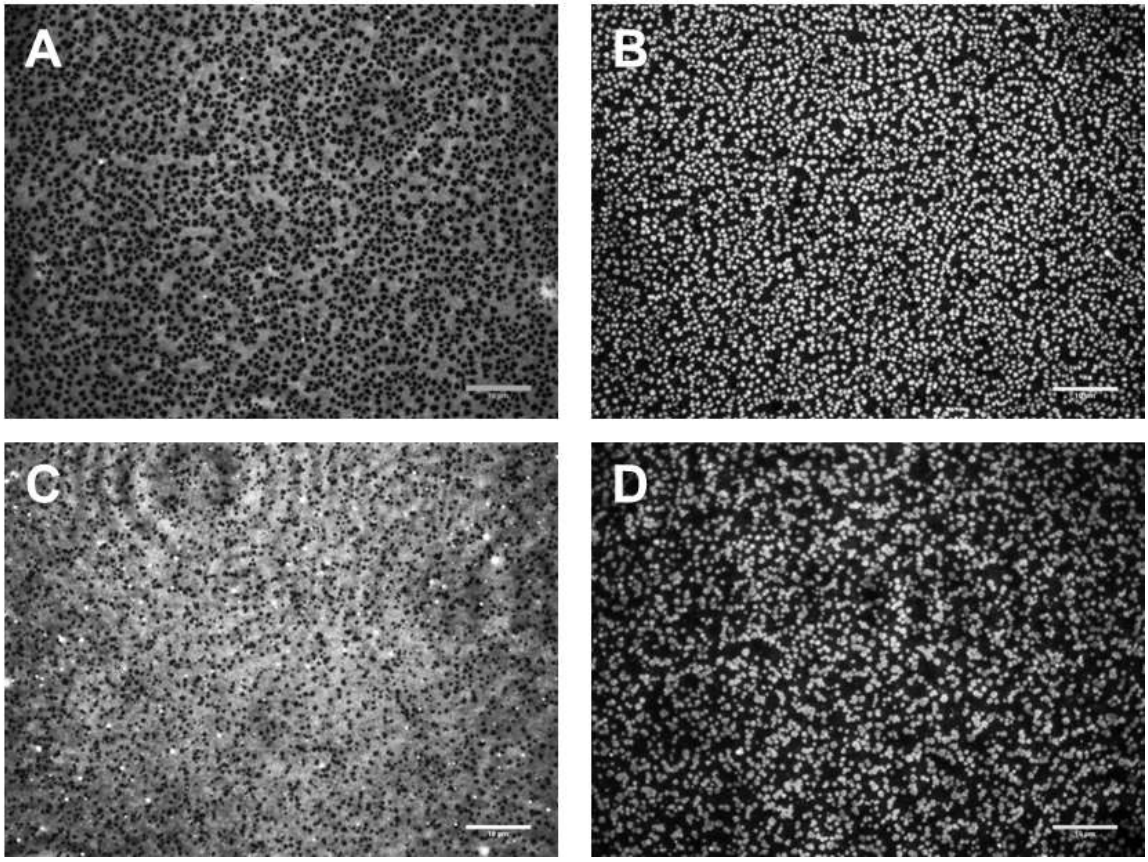

Figure 5.2 shows several supported lipid bilayers (SLBs) prepared using 0.10 mol % BODIPY-cholesterol (A, C) and Texas Red DHPE (B, D). Bilayers A and B were prepared using (1:1) DPPC/DOPC and bilayers C and D were prepared using (1:1) SM/DOPC. The scale bar is 10 μm.

Next, SLBs were prepared using spin-coating to create dry bilayers. These are compared to SLBs prepared using vesicle fusion to form hydrated bilayers. Three lipid mixtures were chosen for an initial comparison of bilayer structure. All six films are shown in **Figure 5.3**, starting with an equimolar mixture of DPPC (saturated lipid) and DOPC (unsaturated lipid) in the top row (A – B). In both films, the fluorescent dye used is BODIPY-cholesterol which stains the more ordered phase. The hydrated bilayers (A) exhibit phase separation into areas of high and low order, with irregularly shaped disordered domains that exclude the BOIDPY-cholesterol. Additionally, differences in domain size are observed. The average domain area of the

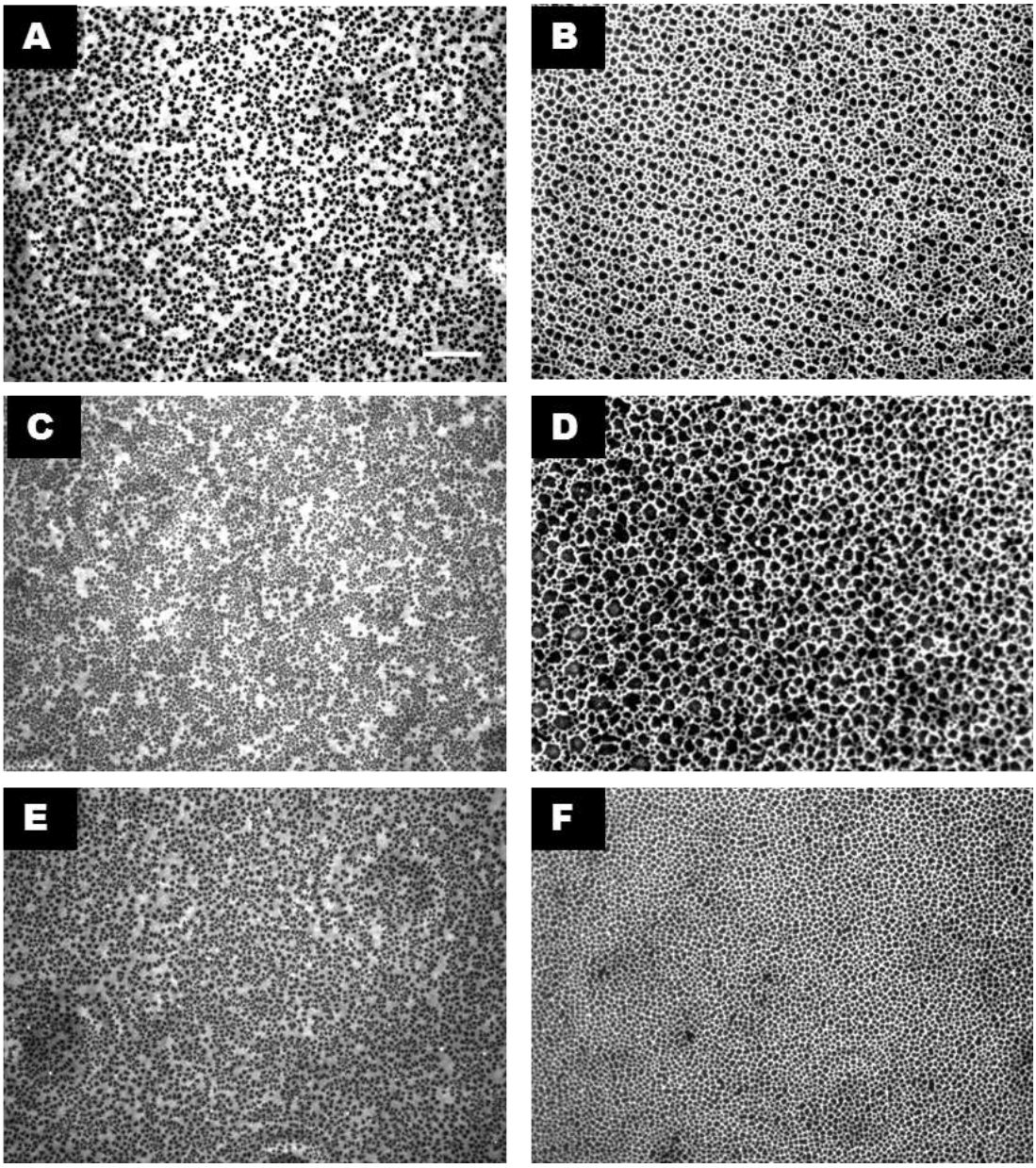

Figure 5.3 compares SLBs prepared using vesicle fusion (A, C, E) to SLBs prepared using spin-coating (B, D, F). Images A and B are of (1:1) DPPC/DOPC, images C and D are of 0.2 mol % cholesterol in DPPC/DOPC, and images E and F are of 20 mol % cholesterol in DPPC/DOPC. Each image is 64 µm x 85 µm.

disordered domains in the hydrated bilayer is 4.10 ± 0.03 μm^2 and in the dry bilayer is 6.9 ± 0.5 μm^2, a 69 % increase in domain size.

In the next two images (C – D), 0.2 mol % cholesterol has been included in the DPPC/DOPC lipid matrix to determine if the spin-coated films are sensitive to small concentrations of additives. Both bilayers respond to the addition of cholesterol with decreasing domain size. Again, the domains in the spin-coated bilayers are larger by an average of 89%. Finally, the bottom row of images shows films prepared with DPPC/DOPC/Chol (2:2:1). Under these conditions, the average area of the disordered domains in the hydrated bilayers is 0.6 ± 0.1 μm^2 and in dry bilayers is 0.65 ± 0.05 μm^2. This data collectively demonstrates that spin-coated, dry bilayers are structurally similar to hydrated bilayers under certain conditions and respond to the presences of biologically relevant additives. Additionally, the domains present in dry and hydrated bilayers undergo similar trends in changing size as a function of cholesterol. Once it had been demonstrated that dry bilayers respond to the addition of additives, a series of spin-coated SLBs were prepared using DPPC/DOPC (1:1) with varying concentrations of cholesterol to compare to the monolayer data presented in Chapter 3. This data is presented in **Figure 5.4**.

Figure 5.4 shows a series of dry spin-coated bilayers prepared with increasing amounts of cholesterol. The first bilayer (A) contains 0.0 mol % cholesterol and shows dark domains surrounded by a continuous, bright domain. Based upon the trends observed in **Figure 5.2**, it seems reasonable to conclude that the dark domains are disordered and the continuous fluorescent domain is the ordered phase. From 0.0 mol % cholesterol to 6.0 mol % cholesterol (Image G), the area of the films occupied by the dark, disordered domains increases. At 8.0 mol %, the more ordered domains become predominant and increase in size through 40 mol %. This trend, summarized in **Figure 5.5**, is somewhat different than what was observed for Langmuir-Blodgett monolayers in Chapter 3, where a cholesterol-rich domain became apparent at higher cholesterol concentrations. This raises the question of if this cholesterol-rich phase is able to form in dry bilayers or if it has formed but is not readily apparent under these conditions.

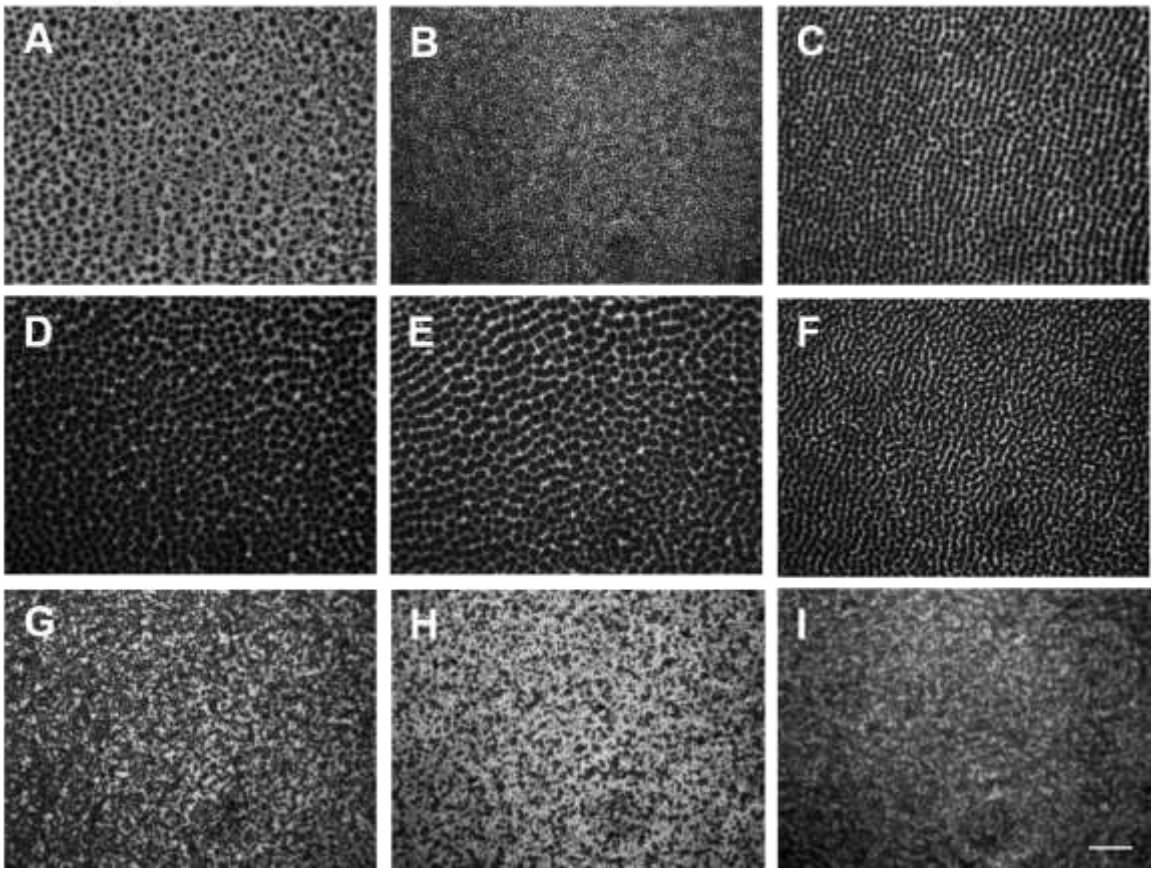

Figure 5.4 – This series of images shows bilayers prepared by spin-coating. All nine bilayers are of (1:1) DPPC/DOPC with increasing cholesterol concentration. Image A contains 0 mol % cholesterol, image B has 0.2 mol %, image C has 1.0 mol %, image D has 2.0 mol %, image E has 3.0 mol %, image F has 6.0 mol %, image G has 8.0 mol %, H has 20 mol %, and image I has 40 mol % cholesterol. The scale bar is 10 μm.

Finally, having determined how BODIPY-cholesterol partitions into the bilayers and that they respond to the addition of cholesterol, single molecule imaging and analysis was perfomred using defocused polarized total internal reflection fluorescence microscopy (PTIRF-M). We have previously used single molecule orientation measurements to evaluate the role that cholesterol plays in monolayer domain formation [19, 20]. Those studies are extended here to compare the tilt angle histograms of BODIPY-cholesterol doped into dry SLBs of DPPC/DOPC/Chol and SM/DOPC/Chol and compared with the monolayer results presented in Chapter 3.

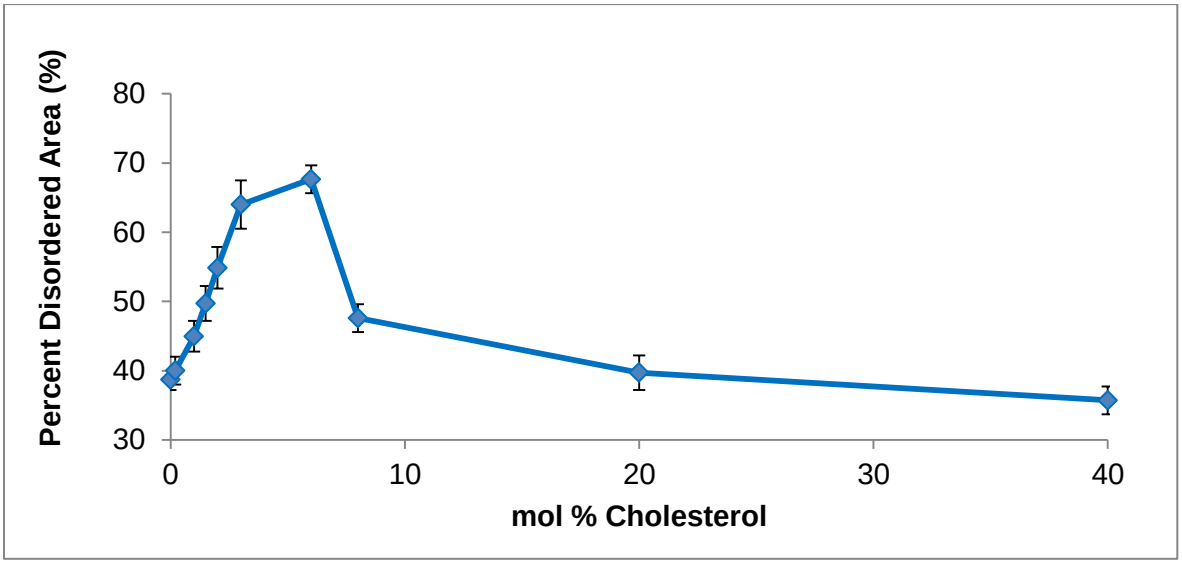

Figure 5.5 shows a plot of the average area of the film occupied by the dark disordered domains in Figure 5.4. Three bilayers at each concentration of cholesterol were analyzed to generate this plot.

Figure 5.6 compares tilt angle histograms of the single molecule orientations of BODIPY-cholesterol in DPPC/DOPC/Chol and SM/DOPC/Chol. The single molecule data was collected with three cholesterol concentrations at 0 %, 3%, and 40% cholesterol. **Figure 5.6** shows that the tilt angle histograms of the DPPC/DOPC/Chol bilayers at the top of the figure. At all three cholesterol concentrations, the BODIPY-cholesterol favors two orientations, with large populations at 0-10° or 70-90°. The molecules seem to reorient from 70-90° to 0-10° as cholesterol is increased, which is most apparent when comparing 0% and 40% cholesterol.

Single molecule analysis was also performed on SM/DOPC/Chol, and here the trends are somewhat more apparent. Again, the BOIDPY-Cholesterol orients at either 0-10° or 70-90°, with the latter being favored. As cholesterol is added, a transition is seen where the BODIPY-

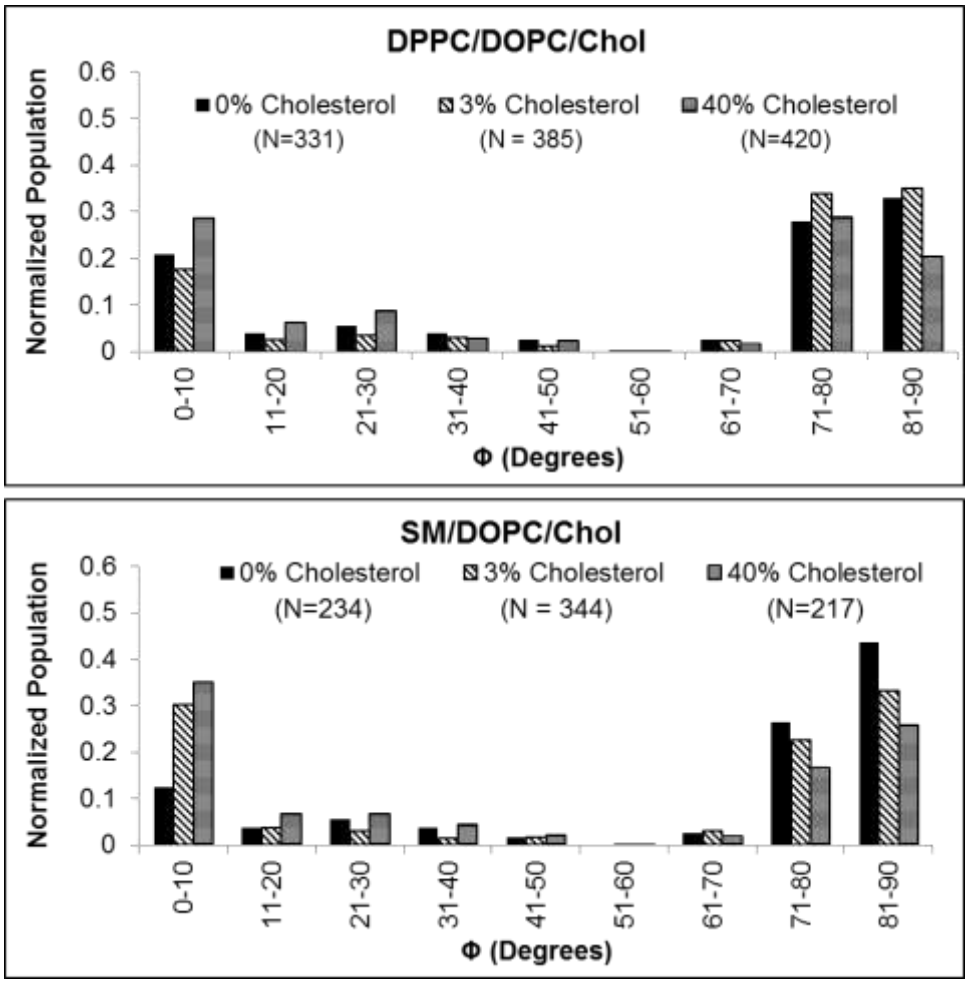

Figure 5.6 shows the single molecule orientation histograms for BODIPY-cholesterol in DPPC/DOPC (1:1) and SM/DOPC (1:1) at 0%, 3% and 40 mol % cholesterol. The single molecule data was binned every 10° to aid in data interpretation and the total number of fluorophores analyzed at each condition are indicated on the graphs by N.

cholesterol molecules reorient to favor insertion geometry of less than 10°. The pattern of reorientation seen here is similar to what was observed in Chapter 3, where the insertion geometry of BODIPY-cholesterol was investigated in Langmuir-Blodgett monolayers. In monolayers, a large population of fluorophores was observed with tilt angles greater than 70° at low cholesterol concentrations and transitioned to favor a tilt angle of less than 24° at higher cholesterol concentrations. A similar trend is observed here, however the changes in the tilt angle histograms seem to be somewhat less dramatic in dry bilayers than in monolayers as

cholesterol is increased. Overall, this data demonstrates that dry spin-coated SLBs can be used to investigate bilayer properties and undergo similar trends as a function of additives like cholesterol.

5.4 Conclusions

SLBs were prepared using a spin-coating technique to create dry, air-stable lipid bilayers. Dry bilayers are challenging to prepare using other techniques, yet necessary for many analytical measurements. Thus, new methods for preparing dry bilayers are of interest. Spin-coated bilayers of DPPC/DOPC (1:1) were prepared and compared to hydrated bilayers of the same composition prepared using vesicle fusion. Similar trends in domain size and morphology were observed using bulk fluorescence techniques. A series of spin-coated bilayers were prepared using DPPC/DOPC (1:1) with varying concentrations of cholesterol to demonstrate that the resulting bilayers respond to biologically interesting additives. Finally, single molecule analysis was performed using polarized total internal reflection microscopy to track changes in BODIPY-cholesterol orientation, and while some variation in single molecule distribution was observed, this model membrane system proved to undergo a less dramatic structural reorientation due to cholesterol than dry monolayers.

5.5 References

1. Tamm, L.K. and H.M. McConnell, *Supported phospholipid bilayers.* Biophys. J., 1985. **47**(1): p. 105-13.

2. Gillissen, J.J.J., S.R. Tabaei, and N.-J. Cho, *A phenomenological model of the solvent-assisted lipid bilayer formation method.* Phys. Chem. Chem. Phys., 2016. **18**(35): p. 24157-24163.

3. Cremer, P.S. and S.G. Boxer, *Formation and Spreading of Lipid Bilayers on Planar Glass Supports.* J. Phys. Chem. B, 1999. **103**(13): p. 2554-2559.

4. Raedler, J., H. Strey, and E. Sackmann, *Phenomenology and Kinetics of Lipid Bilayer Spreading on Hydrophilic Surfaces.* Langmuir, 1995. **11**(11): p. 4539-48.

5. Dols-Perez, A., L. Fumagalli, and G. Gomila, *Structural and nanomechanical effects of cholesterol in binary and ternary spin-coated single lipid bilayers in dry conditions.* Colloids Surf., B, 2014. **116**: p. 295-302.

6. Huckabay, H.A. and R.C. Dunn, *Hydration Effects on Membrane Structure Probed by Single Molecule Orientations.* Langmuir, 2011. **27**(6): p. 2658-2666.

7. Chiantia, S., N. Kahya, and P. Schwille, *Dehydration Damage of Domain-Exhibiting Supported Bilayers: An AFM Study on the Protective Effects of Disaccharides and Other Stabilizing Substances.* Langmuir, 2005. **21**(14): p. 6317-6323.

8. Holden, M.A., et al., *Creating Fluid and Air-Stable Solid Supported Lipid Bilayers.* J. Am. Chem. Soc., 2004. **126**(21): p. 6512-6513.

9. Bennun, S.V., R. Faller, and M.L. Longo, *Drying and Rehydration of DLPC/DSPC Symmetric and Asymmetric Supported Lipid Bilayers: a Combined AFM and Fluorescence Microscopy Study.* Langmuir, 2008. **24**(18): p. 10371-10381.

10. Kraft, M.L., et al., *Quantitative analysis of supported membrane composition using the NanoSIMS.* Appl. Surf. Sci., 2006. **252**(19): p. 6950-6956.

11. Kraft, M.L., et al., *Phase Separation of Lipid Membranes Analyzed with High-Resolution Secondary Ion Mass Spectrometry.* Science (Washington, DC, U. S.), 2006. **313**(5795): p. 1948-1951.

12. Mueller, J., et al., *Preparation of a New Oligolamellar Stratum Corneum Lipid Model.* Langmuir, 2016. **32**(18): p. 4673-4680.

13. Dols-Perez, A., et al., *Ultrathin Spin-Coated Dioleoylphosphatidylcholine Lipid Layers in Dry Conditions: A Combined Atomic Force Microscopy and Nanomechanical Study.* Langmuir, 2011. **27**(21): p. 13165-13172.

14. Simonsen, A.C. and L.A. Bagatolli, *Structure of Spin-Coated Lipid Films and Domain Formation in Supported Membranes Formed by Hydration.* Langmuir, 2004. **20**(22): p. 9720-9728.

15. Mennicke, U. and T. Salditt, *Preparation of Solid-Supported Lipid Bilayers by Spin-Coating.* Langmuir, 2002. **18**(21): p. 8172-8177.

16. Edelstein, A., et al., *Computer control of microscopes using μManager.* Curr Protoc Mol Biol, 2010. **Chapter 14**: p. Unit14.20.

17. Stottrup, B.L., S.L. Veatch, and S.L. Keller, *Nonequilibrium behavior in supported lipid membranes containing cholesterol.* Biophys. J., 2004. **86**(5): p. 2942-2950.

18. Stottrup, B.L., D.S. Stevens, and S.L. Keller, *Miscibility of ternary mixtures of phospholipids and cholesterol in monolayers, and application to bilayer systems.* Biophys. J., 2005. **88**(1): p. 269-276.

19. DeWitt, B.N. and R.C. Dunn, *Interaction of Cholesterol in Ternary Lipid Mixtures Investigated Using Single-Molecule Fluorescence.* Langmuir, 2015. **31**(3): p. 995-1004.

20. Livanec, P.W., H.A. Huckabay, and R.C. Dunn, *Exploring the Effects of Sterols in Model Lipid Membranes Using Single-Molecule Orientations.* J. Phys. Chem. B, 2009. **113**(30): p. 10240-10248.

Chapter 6—Alternative Model Membrane Systems: Droplet Interface Bilayers

6.1 Introduction

Another recent model membrane system that will be discussed is the droplet interface bilayer (DIB). The idea for a DIB was first articulated in 2005 with the goal of miniaturizing planar bilayer systems for application in microfluidics or arrays [1]. A conceptually simple experimental design was proposed where two aqueous droplets are placed in a solution of lipids in oil. A lipid monolayer forms around each droplet, with the lipid headgroups at the aqueous surface and the tail groups oriented out into the oil solution. When the droplets are brought together, the authors predicted that a bilayer would be created at the interface between the two droplets. The most common experimental design involves a low melting temperature lipid dissolved in hexadecane, with two small water droplets, usually 100 to 500 nL in volume, added. This experimental design offers a few unique advantages to planar model membranes, as the resulting bilayer is spherical and the angle of curvature can be controlled by changing the volume. This configuration is ideal for studying membrane transport, dynamics and heterogeneity [2].

DIBs were used initially to study ion channels [3, 4] and pore-forming toxins [5-7] under biologically similar conditions. Using the DIB format, proteins or peptides that form a membrane pore are included in an aqueous droplet and the activity of the pore is be monitored using an analytical technique like fluorescence or electrochemistry. Additionally, asymmetric DIBs can be fabricated by preparing aqueous vesicle solutions and placing small volumes of those solutions in oil to study bilayer asymmetry [8]. DIBs have been incorporated into a variety of platforms, including microfluidics for rapid screening or multiplexed analysis [9-11].

The DIB platform was further modified to create planar bilayer interfaces for imaging studies. Planar droplet bilayers are prepared using an aqueous surface, like a hydrogel, and a single aqueous droplet into a solution of lipids in oil [12]. When the aqueous droplet comes into contact with the hydrophilic substrate, a bilayer is created between the two. DIBs have many advantages for investigating biological problems, as they can be prepared rapidly and are versatile. Concerns when using this technique include that the oil is not a mimic of biological conditions and can become dissolved into the lipid bilayer, altering its properties [13].

A unique application for DIBs will be presented here, where an LB monolayer is deposited onto a solid substrate, immersed in hexadecane oil, and a droplet of vesicle solution is added onto the monolayer. The interface between these two surfaces is particularly interesting, as when the vesicle solution is added to the monolayer, small attoliter volumes of hexadecane oil become trapped between the monolayer and the vesicle solution. This creates an array of oil in water droplets, similar to an emulsion. The lipids act as a surfactant in this system, stabilizing the small oil droplets. This design will be investigated using fluorescence microscopy to image and characterize the trapped oil droplets. We believe that this platform is ideal for modeling surfactants in emulsions as it is planar for imaging and offers a high degree of control over the organic component and surfactant identity.

6.2 Materials and Methods

6.2.1 Langmuir-Blodgett Monolayers

Langmur-Blodgett (LB) monolayers were prepared using an LB trough on piranha cleaned glass slides as described in Chapter 3. Briefly, DPPC/DOPC (1:1) solutions were prepared at 1 mg/mL in chloroform by diluting from stock solutions. Texas Red DHPE was included at a concentration of 0.10 mol % in the stock solutions to stain the more expanded phase of the

monolayer. Approximately 50 µL of lipid solution was dispersed onto the subphase of ultrapure water (18 MΩ). The solvent was allowed to evaporate for 15 minutes before the monolayers were annealed using two expansion and compression cycles. Monolayers were compressed at a speed of 100 cm^2/min and expanded at 80 cm^2/min. The monolayers were then compressed at a speed of 100 cm^2/min to the target pressure and held for 10 minutes before transferring onto the substrate at a rate of 5 mm/min.

6.2.2 Small Unilamellar Vesicle (SUV) Solution

Vesicle solutions were prepared as described in Chapter 5. Lipid stock solutions of DPPC and DOPC were diluted in chloroform to prepare a final lipid mixture of DPPC/DOPC (1:1) at 5 mg/mL in 4 mL glass vials. The chloroform was evaporated away using a gentle stream of nitrogen gas and stored under vacuum for at least 12 hours to remove all solvent. Next, the lipids were rehydrated in a buffer of 20 mM HEPES with 100 mM and 0.02 % NaN_3 at 45 – 55 °C to a concentration of 1 mM. The solutions were vortexed to resuspended the lipids into vesicles. The vesicles were allowed to swell at 60 °C for 1 hour, vortexing approximately every 15 minutes. Finally, the vials containing the vesicle solutions were placed in a sonicator at 60 °C and allowed to sonicate until the solutions changed from cloudy to clear in appearance, signaling that vesicles of less than 100 nm in diameter had been formed.

6.2.3 Preparing Droplet Interface Bilayers using LB Monolayers and Vesicle Droplets

A unique platform for preparing DIBs was used, where an LB monolayer of DPPC/DOPC (1:1) with 0.10 mol % Texas Red DHPE formed one leaflet of the bilayer and a droplet of aqueous vesicle solution formed the other droplet. To prepare these bilayers, first an LB

monolayer was prepared as described above. A plastic well was affixed to the monolayer and filled with approximately 500 µL of hexadecane. Next, a 0.5 µL droplet of DPPC/DOPC (1:1) vesicle solution was gently pipetted into the hexadecane and allowed to settle at the bottom of the well. At the interface between the LB monolayer and vesicle droplet, a bilayer was present.

6.2.4 Imaging

The DIBs were imaged using a total internal reflection microscope (TIRF-M) (Olympus IX71, Olympus, Center Valley, PA) equipped with a 60x, 1.45 NA objective (Achromat, Olympus) for bulk fluorescence imaging. The excitation source used was the 514 nm line of an argon-ion laser (Coherent Innova 90, Coherent, Inc., Santa Clara, CA), and emission was collected through a ZT514rdc dichroic mirror and HQ522/40m band pass filter (Chroma, Rockingham, VT) . Images were collected using a cooled CCD camera (Coolsnap HQ2, Photometrics, Tucson, AZ) and controlled using Micromanager software with 100 ms integration time and no binning [14]. All images were analyzed using ImageJ software (U.S. National Institutes of Health, Bethesda, MD).

6.3 Results and Discussion

Droplet interface bilayers are formed by dissolving amphiphilic lipid molecules in oil and bringing two aqueous droplets together in the oil solution. When the aqueous droplets are brought into contact with one another, lipid molecules act as surfactants that prevent two droplets from coalescing. An alternative design is tested here, where a DIB is formed between a planar LB monolayer and a droplet of vesicle solution. In order to characterize the behavior of lipids at water—oil interface, a series of DIB studies were performed. First, an LB monolayer of

DPPC/DOPC (1:1) with 0.10 mol % Texas Red DHPE to stain the expanded phase was deposited onto a glass substrate. Next, the monolayer was immersed in hexadecane, which served as the oil phase in this experiment. Lastly, 0.5 µL of aqueous unilamellar vesicle solution was added to the oil. At the interface between the monolayer and the droplet, a bilayer was formed and investigated using fluorescence microscopy.

Before preparing a DIB using the format proposed, an initial test was carried out to determine if an LB monolayer is stable over time in hexadecane. For this study, an LB monolayer of DPPC/DOPC (1:1) was prepared with Texas Red DHPE included to stain the expanded phase. This monolayer was transferred at an equivalent surface pressure of 30 mN/m onto a glass slide where expanded and condensed domains were apparent. In this monolayer, shown in image A of **Figure 6.1**, Texas Red DHPE stains the more expanded, DOPC rich phase and the DPPC rich phase is dark [15, 16]. A plastic well was affixed to the monolayer-coated slide, filled with hexadecane, and allowed to sit for 4 hours. The monolayer was imaged before adding oil, shown in **Figure 6.1 A**, and after 4 hours, shown in **Figure 6.1 B**, to determine if the phase structure was altered by the oil. The monolayer does not appear to become delaminated from the substrate or change in structure after 4 hours in hexadecane, suggesting that it is stable.

A 0.5 µL droplet of aqueous vesicle solution of (1:1) DPPC/DOPC was next added to the oil. **Figure 6.2** shows the result of adding vesicle solution to the oil immersed monolayer. Small spherical structures are seen at the surface of the dark, DPPC rich domains of the monolayer. These are thought to be oil that is trapped between the top and bottom leaflet of the bilayer as it forms. This experiment was repeated many times, and the oil droplets become trapped every time that a bilayer is prepared using this method. Additionally, the oil droplets are always trapped on the DPPC rich domains, indicating that the composition of the monolayer plays some role in this phenomenon. Analysis of the trapped oil droplets was performed using ImageJ

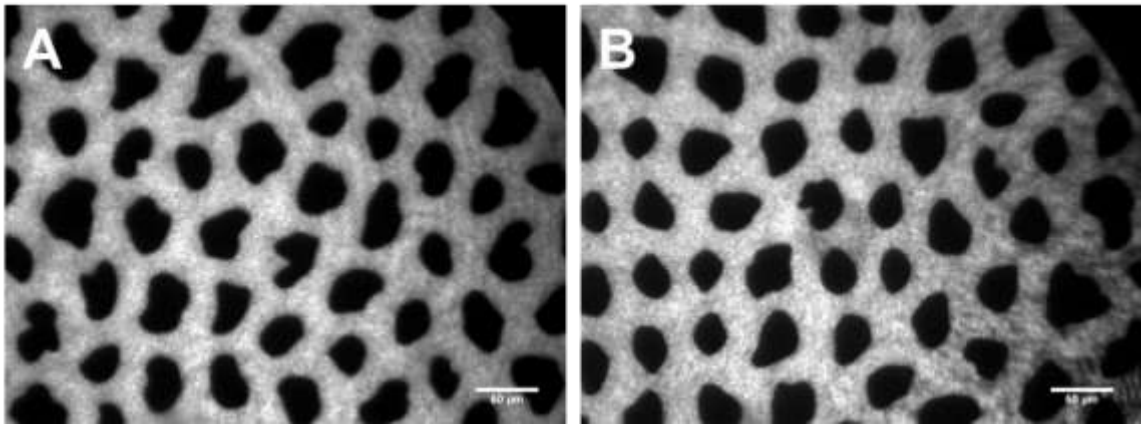

Figure 6.1 – Monolayers of (1:1) DPPC/DOPC at 30 mN/m. Image A was taken of the monolayer dry, in air. Image B was taken after the monolayer was immersed in hexadecane oil for 4 hours. The scale bar is 50 μm.

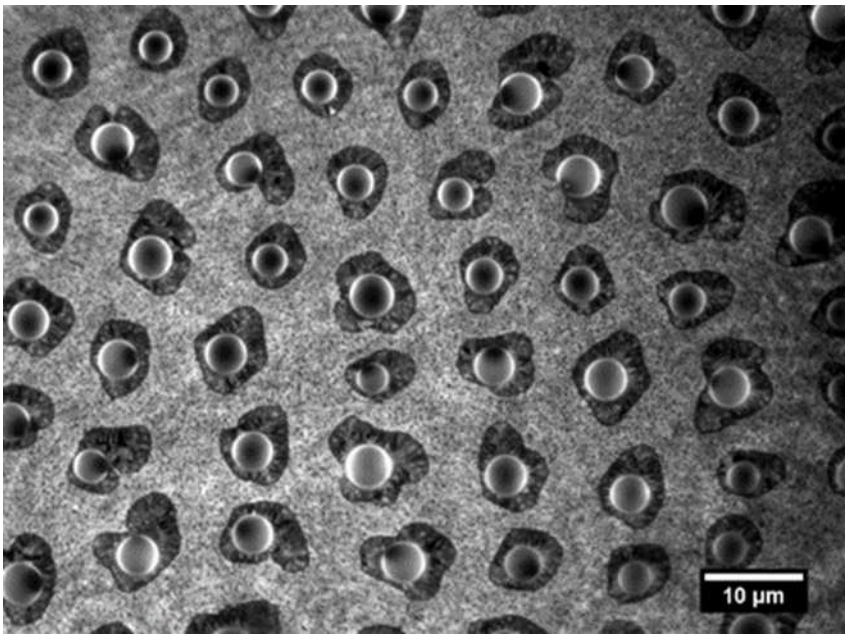

Figure 6.2 – Small volume oil droplets are trapped at the interface between an LB monolayer and aqueous vesicle solution. The oil droplets preferentially locate themselves on the saturated DPPC domains of the LB monolayer. The scale bar is 10 μm.

software to determine the size of the trapped oil droplets, and they were found to be approximately 2.2 μm in radius with a calculated volume of approximately 45 aL.

Monolayers were next prepared at a range of surface pressures with the goal of changing the DPPC domain size to investigate if the oil droplets would respond. Monolayers were prepared at 5 mN/m increments from 10 mN/m to 40 mN/m for analysis. At 10 mN/m and 15 mN/m, no oil droplets formed when aqueous vesicle solution was added to the lipid monolayer. At 20 mN/m, however, droplets did form and were smaller in diameter than those previously observed with an average droplet radius of 1.7 μm and volume of approximately 20 aL. At 25 mN/m, the droplet radius increased to 2.3 μm with a volume of approximately 50 aL. At 30 mN/m and 35 mN/m, the oil droplets decreased in radius and volume. By 40 mN/m, the oil droplets would not form. This data is summarized in **Figure 6.3**, along with representative monolayer images at each surface pressure. The average condensed domain area for each LB monolayer was also determined using ImageJ software and the oil droplet radius tracks the condensed domain area, with larger domains yielding larger trapped oil droplets. This trend suggests that the composition of the LB monolayer could be used to tune the size of the trapped oil droplets.

Further investigation of the oil droplets revealed that they are coated in a layer of lipids, which helps to stabilize the oil domains within the aqueous droplet above. Furthermore, lipid phase structure was observed on the surface of the oil phase. Phase separation is shown in more detail in **Figure 6.4,** where dark domains are seen within a continuous, bright domain at the surface of the oil droplets. Time lapsed data collection shows that the domains are freely diffusing around the surface of the droplets. Frames from the time lapsed data are shown in **Figure 6.5**, where movement of the dark domains can be seen. In this image, frames were collected every 100 msec. If the trends from previous data are consistent in this system, the dark domains are enriched in DPPC and the bright areas are enriched in DOPC.

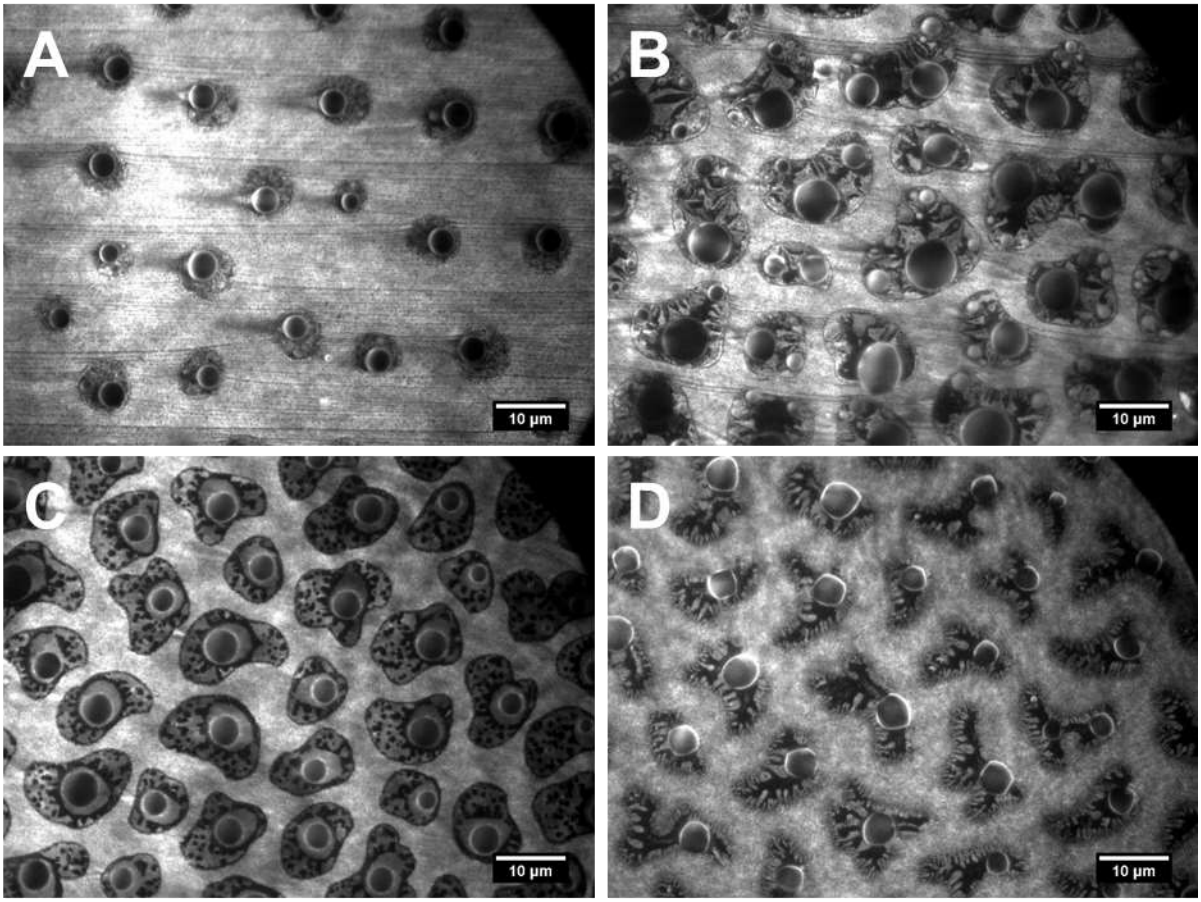

	20 mN/m (A)	25 mN/m (B)	30 mN/m (C)	35 mN/m (D)
Average Domain Area (μm^2)	9 ± 2	17 ± 5	15 ± 4	11 ± 3
Droplet Radius	1.7	2.3	2.2	1.9
Calculated Droplet Volume (aL)	21	53	46	28

Figure 6.3 – Representative data is shown for (1:1) DPPC/DOPC monolayers with aqueous droplets at four different surface pressures. The oil droplets that form between the monolayer and aqueous phase were analyzed using ImageJ and the average condensed domain area is shown in the top row, the average droplet radius in the center row, and the calculated droplet volume in the bottom row. The scale bar on all images is 10 µm.

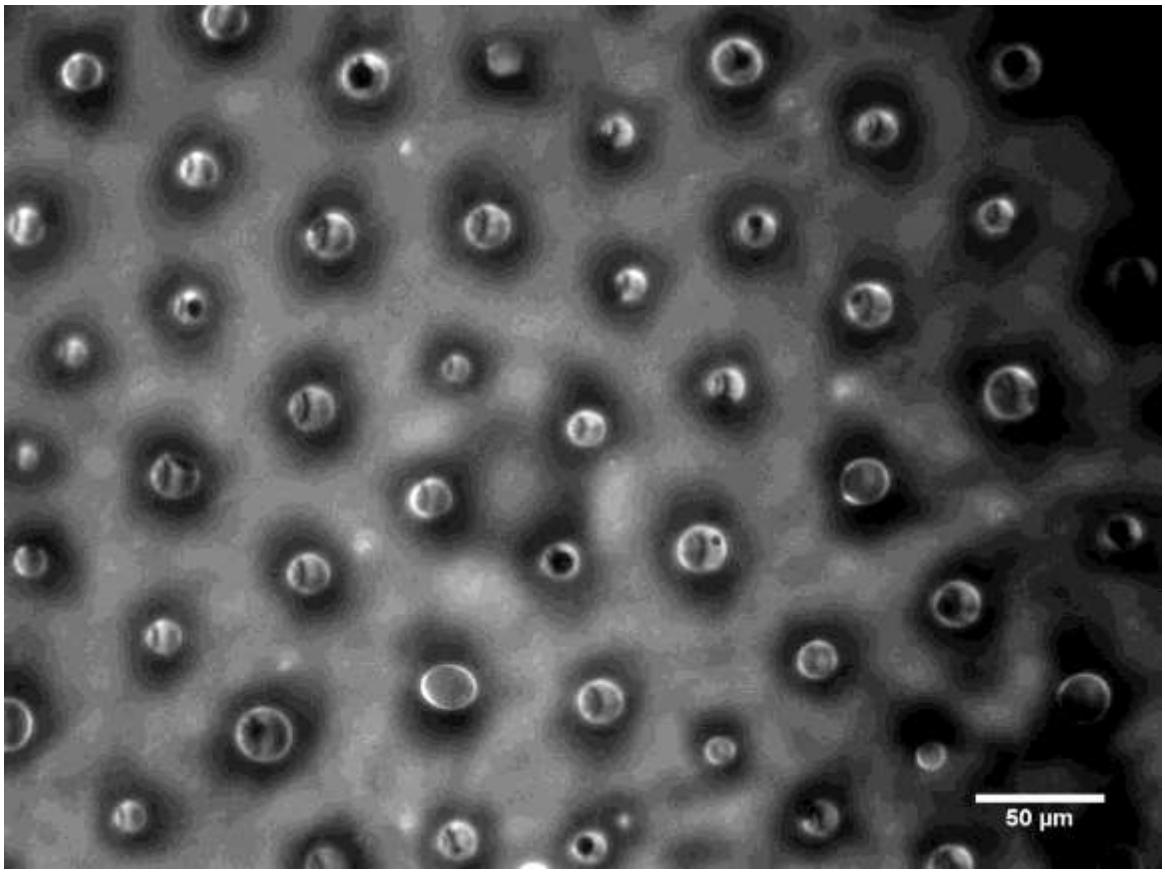

Figure 6.4 – Shows lipid domains forming on the surface of trapped oil droplets. This image was taken of DPPC/DOPC monolayers at 25 mN/m with DPPC/DOPC vesicle solution on top. Texas Red DHPE dye was included in the monolayer and in the vesicle solution. The scale bar is 50 µm.

This experimental method provides a unique and controlled way to prepare emulsions on a planar surface in order to investigate its properties. There are a number of interesting potential applications for this type of surfactant – emulsion model system. For example, many drugs exhibit low solubility in water and high solubility in oil. In order to administer drugs of this type, lipophilic derivatives are prepared and dispensed as oil-in-water emulsions. The format shown above could be used to investigate relevant characteristics of drug emulsions like biocompatibility, physical stability, and cytotoxic activity [17, 18]. Phosphocholine (PC) emulsions are specifically of interest because of their application to membrane biology, however this technique could be used to investigate a variety of surfactant—emulsion systems.

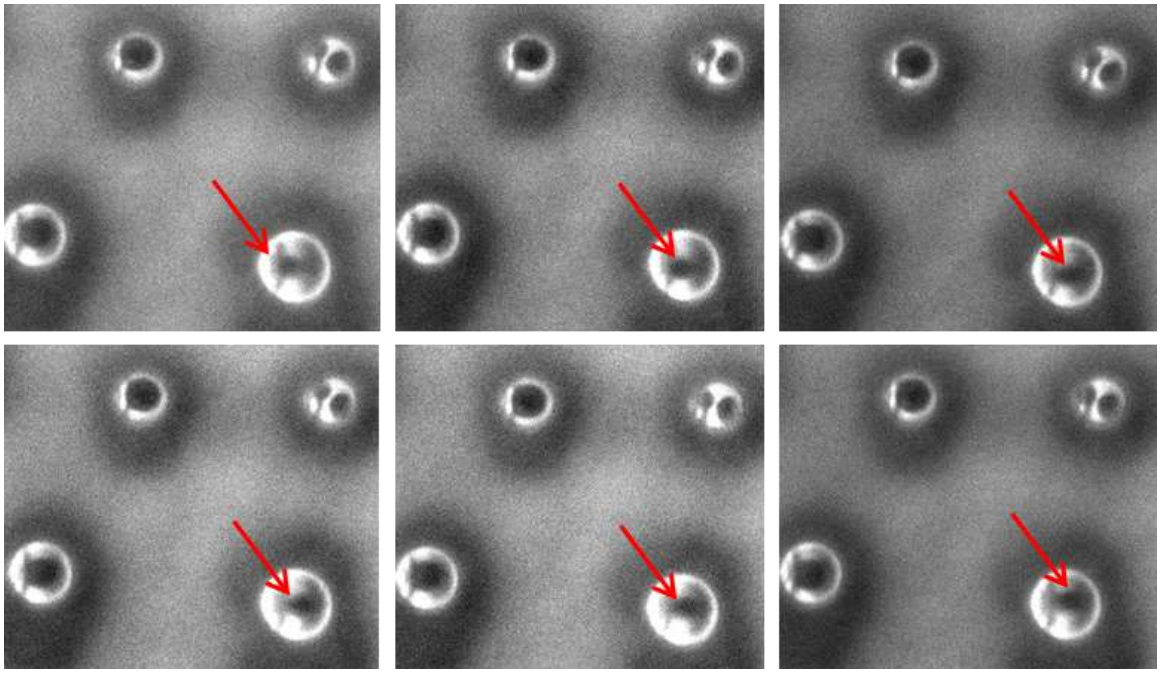

Figure 6.5 shows the dynamics of lipid domains on oil droplets. The red arrow indicates one such domain that is able to freely diffuse around on the surface of the droplet. Each frame was collected over 100 msec and is 19.1 μm × 21.1 μm.

6.4 Conclusions

A novel technique for preparing a planar monolayer was shown, where an LB monolayer was deposited onto a glass substrate and immersed in hexadecane oil. An aqueous droplet of vesicle solution was added, and a bilayer created between the LB monolayer and the lipids in the vesicle solution. Interestingly, small oil droplets were formed between the condensed domains of the LB monolayer and the aqueous phase. These droplets were evaluated using epifluorescence to show that they respond to changes in condensed domain area and are coated in a layer of PC molecules. This technique is ideal for investigating surfactants in an emulsion in a controlled manner.

6.5 References

1. Bayley, H., et al., *Droplet interface bilayers.* Mol. BioSyst., 2008. **4**(12): p. 1191-1208.

2. Bayley, H., et al., *Droplet interface bilayers.* Molecular bioSystems, 2008. **4**(12): p. 1191-1208.

3. Leptihn, S., et al., *In Vitro Reconstitution of Eukaryotic Ion Channels Using Droplet Interface Bilayers.* J. Am. Chem. Soc., 2011. **133**(24): p. 9370-9375.

4. Syeda, R., et al., *Screening Blockers Against a Potassium Channel with a Droplet Interface Bilayer Array.* J. Am. Chem. Soc., 2008. **130**(46): p. 15543-15548.

5. Fischer, A., et al., *Ultrasensitive detection of protein translocated through toxin pores in droplet-interface bilayers.* Proc. Natl. Acad. Sci. U. S. A., 2011. **108**(40): p. 16577-16581, S16577/1-S16577/5.

6. Huang, J., et al., *Direct Quantitation of Peptide-Mediated Protein Transport across a Droplet-Interface Bilayer.* J. Am. Chem. Soc., 2011. **133**(40): p. 15818-15821.

7. Rojko, N., et al., *Imaging the Lipid-Phase-Dependent Pore Formation of Equinatoxin II in Droplet Interface Bilayers.* Biophys. J., 2014. **106**(8): p. 1630-1637.

8. Hwang, W.L., et al., *Asymmetric Droplet Interface Bilayers.* J. Am. Chem. Soc., 2008. **130**(18): p. 5878-5879.

9. Fischer, A., et al., *Ultrasensitive detection of protein translocated through toxin pores in droplet-interface bilayers.* Proc Natl Acad Sci U S A, 2011. **108**(40): p. 16577-81.

10. Harriss, L.M., et al., *Imaging Multiple Conductance States in an Alamethicin Pore.* J. Am. Chem. Soc., 2011. **133**(37): p. 14507-14509.

11. Holden, M.A., D. Needham, and H. Bayley, *Functional Bionetworks from Nanoliter Water Droplets.* J. Am. Chem. Soc., 2007. **129**(27): p. 8650-8655.

12. Leptihn, S., et al., *Constructing droplet interface bilayers from the contact of aqueous droplets in oil.* Nat. Protoc., 2013. **8**(6): p. 1048-1057.

13. Taylor, G.J., et al., *Direct in situ measurement of specific capacitance, monolayer tension, and bilayer tension in a droplet interface bilayer.* Soft Matter, 2015. **11**(38): p. 7592-7605.

14. Edelstein, A., et al., *Computer control of microscopes using μManager.* Curr Protoc Mol Biol, 2010. **Chapter 14**: p. Unit14.20.

15. Stottrup, B.L., D.S. Stevens, and S.L. Keller, *Miscibility of ternary mixtures of phospholipids and cholesterol in monolayers, and application to bilayer systems.* Biophys. J., 2005. **88**(1): p. 269-276.

16. Stottrup, B.L., S.L. Veatch, and S.L. Keller, *Nonequilibrium behavior in supported lipid membranes containing cholesterol.* Biophys. J., 2004. **86**(5): p. 2942-2950.

17. Lundberg, B.B., et al., *A lipophilic paclitaxel derivative incorporated in a lipid emulsion for parenteral administration.* J. Controlled Release, 2003. **86**(1): p. 93-100.

18. Rub, M.A., et al., *Surface, micellar, and thermodynamic properties of antidepressant drug nortriptyline hydrochloride with TX-114 in aqueous/urea solutions.* J. Phys. Org. Chem., 2016: p. Ahead of Print.

Chapter 7—Summary and Future Directions

7.1 Summary

Our goals in this work were to apply a technique that had been developed and characterized by previous students, using defocused imaging to characterize the three dimensional orientations of fluorophores in model membrane systems, to investigate relevant biological problems in the field of membrane biophysics. The lipid raft hypothesis was selected for investigation, as despite decades of investigation the mechanisms at play in rafts and even their very existence is still debated.

Two interesting questions regarding lipid rafts were investigated in this work. In Chapter 3, the unique role that cholesterol plays in lipid rafts was probed. A fluorescent cholesterol analog with properties similar to native cholesterol, BODIPY-cholesterol, was chosen for this study. BODIPY-cholesterol was shown to behave similarly to natural cholesterol in Langmuir-Blodgett monolayers. Additionally, this work showed that BODIPY-cholesterol, and by extension natural cholesterol, undergoes unique interactions with sphingomyelin, another important raft component. This work was used to support the hypothesis that intermolecular interactions, including hydrogen bonding between the cholesterol headgroup and sphingomyelin headgroup and favorable van der Waals interactions between the cholesterol backbone and surrounding acyl tail groups, stabilize raft domains. These intermolecular interactions help to create the highly ordered, fluid structure that lipid raft domains exhibit.

In Chapter 4, another open question from the lipid raft literature was probed using single molecule analysis. Lipid raft domains are known to have a small diameter, 10 – 200 nm on average, and the mechanisms that stabilize small domains in a complex biological matrix are not clearly understood. One hypothesis is that hybrid lipids, lipids with one saturated tail group and one unsaturated tail group that have properties intermediate between ordered and

disordered domains, play an important role in stabilizing raft domains. Hybrid lipids are thought to either prefer the interfacial region between domains in order to minimize line tension or partition into ordered domains, making the two coexisting domains more compositionally similar and reducing line tension in that way. This was investigated using LB monolayers of DOPC, which has two saturated tail groups, and comparing to the hybrid lipid POPC, which has one unsaturated tail group. Bulk and single molecule data showed that POPC reduced ordering in condensed domains, supporting the latter hypothesis mentioned above.

In Chapters 5 and 6, alternative model membrane systems were evaluated. First, in chapter 5, a method for preparing dry supported lipid bilayers (SLBs) was discussed. Dry bilayers are challenging to prepare yet can be analyzed using a variety of techniques that are not appropriate for hydrated bilayers. Thus, a spin-coating method was used to prepare dry bilayers at a range of lipid compositions and evaluated using bulk and single molecule fluorescence. This technique was shown to be promising for investigating the properties of dry bilayers to understand biological problems.

In Chapter 6, another alternative model membrane system, the droplet interface bilayer (DIB) was used. This model is ideal for evaluating complex membrane transport and dynamics problems using a variety of analysis techniques. Here, a platform was evaluated where a planar bilayer was prepared using an LB monolayer and a droplet of vesicle solution. We observed that small volumes of oil become trapped between the two bilayer leaflets in this arrangement, and can be used as a model for surfactant – emulsion analysis. This technique provides a planar format for imaging oil droplets in an aqueous medium, and the lipids used acted as surfactants to stabilize the mixture. The identity of the oil and lipids can easily be modified, providing a versatile method for studying the complex interactions in emulsions.

7.2 Future Directions

In the previous two chapters, alternative model membrane systems were introduced that offer unique properties. In particular, droplet interface bilayers (DIBs) were explored as a means of creating planar bilayers and were shown to be useful in investigating the role of surfactants, like phosphocholine (PC) molecules, in emulsions. However, DIBs are an ideal format to study membrane transport and could be used to investigate a number of questions in this field. With this goal in mind, a next obvious step in this line of research would be to utilize the DIB format to investigate a biologically relevant membrane question. Additionally, as several model membrane systems have been employed in this work, it would be advantageous to collect complementary information using other model membranes like dry and hydrated supported lipid bilayers to aid in characterizing the relatively new DIB format.

To achieve these goals, two future studies are proposed here. First, it would be useful to further characterize the DIB platform using defocused single molecule analysis to determine if the lipid structure of this model membrane is comparable to the structure seen using other model systems. Next, the DIB platform is suggested as a format to investigate a newly proposed mechanism of drug resistance.

Recently, lipid biosynthesis has been hypothesized to play a significant role in drug resistance, as drug resistant cell lines have been observed to have highly ordered cell membranes that are rich in cholesterol and sphingomyelin. The composition of DIBs can be controlled by adjusting the composition of the lipid vesicle solution that is used to prepare the DIBs. Thus, it would be useful to prepare DIBs of a variety of lipid mixtures and monitor their permeability using a drug that is known to be affected by drug resistance. Further, LB monolayers and hydrated SLBs could be prepared using DIB lipid mixture to quantitatively evaluate changes in their structural order.

7.2.1 Lipid Biosynthesis and Drug Resistance

Drug resistance is one of many challenging that arises when treating cancer. A theory of to explain the development of drug resistance is that the dosage administered to a patient is limited by what the patient can tolerate. This dosage may not be high enough to cause the cancer cells to die, subjecting cancer cells to subtherapeutic dosages. When the cells are subjected to low concentrations of drug, they adapt to the changing microenvironment and over time become resistant to that drug [1, 2]. This broad theory does not address the specific mechanisms of drug resistance, though. Many possible mechanisms have been investigated and lead to two possible groups of mechanisms, with drug resistance being caused either by low intracellular drug accumulation or by alterations in the apoptotic pathways to prevent cell death [3-6]. However, recently a new possible mechanism has been demonstrated that suggests that drug resistance is caused by altered lipid biosynthesis, limiting drug transport across the cell membrane [7].

This work was done using two different breast cancer cell lines, the drug resistant MCF-7/ADR cells and drug sensitive MCF-7 cells. Investigation has shown that the drug resistant cell line has a very different lipid composition than the drug sensitive parent line, and that doxorubicin, a common cancer drug, interacts more strongly with lipids isolated from the resistant line than the sensitive line. Analysis of the specific lipids present in each lipid extract showed that the drug resistant cell lines are enriched in rigid, saturated lipids, specifically cholesterol and sphingomyelin [8, 9]. This observation can be explained by the higher than average methylation of DNA and lower than average sphingomyelinase activity in cell resistant lines, which leads to a buildup of sphingomyelin and cholesterol in the membrane [10, 11]. Cell membranes with large amounts of cholesterol and sphingomyelin have altered biophysical properties, including high structural order and increased lipid packing density which decreases the ability of a drug to permeate the membrane.

Initial work investigating this hypothesis was performed using a Langmuir-Blodgett (LB) trough to prepare model bilayers from lipid extracts and test how doxorubicin partitions into the bilayer [12]. Later studies were carried out by treating live cells with drugs to track changes in lipid composition [13]. Investigation of doxorubicin transport across DIBs of various lipid compositions would add to this field of study by providing a method to systematically alter lipid bilayer composition and track the movement of doxorubicin from one droplet of the DIB to another. This format is particularly interesting because many conditions that could otherwise alter drug transport can be controlled. For example, one alternative hypothesis for drug resistance is that the acidic environment around a tumor ionizes drugs, reducing their membrane permeability [14]. As this study will be performed in buffer at physiological pH, this mechanism for reduced permeability is prevented. Additionally, using DIBs, pH can be altered to investigate how altering the drug's microenvironment changes its membrane permeability.

7.2.3 Single Molecule Investigation using DIBs

DIBs are a relatively new model membrane system and their properties are still being investigated. It would be useful to understand how lipid monolayers, like LB monolayers, are structured when immersed in hexadecane oil in order to compare the structure and properties of DIBs to other model systems. In order to accomplish this goal, defocused single molecule analysis, as described in Chapter 2, could be performed on LB monolayers that have been immersed in hexadecane. To further understand the structure of DIBs, a planar DIB could be prepared using a hydrogel as a substrate and lipids dissolved in oil, along with a small concentration of fluorescent lipid analog. If imaged in TIR for single molecule analysis, as described again in Chapter 2, only the fluorophores at the interface should be excited by the evanescent field, so single molecule measurements could be taken under these conditions.

7.2.4 DIB investigation of Doxorubicin Transport

As high sphingomyelin (SM) concentration has been observed in drug resistant cell lines, it is important to understand how changes in SM concentration alter the permeability of bilayers to drugs like doxorubicin. To investigate this, DIBs of four different SM concentrations would be prepared. The bilayers would all contain SM, DOPC (18:1 Δ9-Cis PC), and cholesterol. The cholesterol concentration would remain constant at 30 mol %, while the ratio of SM to DOPC is varied. The actual concentrations used would be (2:5:3) SM/DOPC/Chol, (3:4:3) SM/DOPC/Chol, (4:3:3) SM/DOPC/Chol, and (5:2:3) SM/DOPC/Chol. These are listed in increasing lipid order, with the bilayer containing 50 mol % sphingomyelin expected to be most ordered and least permeable. The structure of these compounds is shown in **Figure 1**.

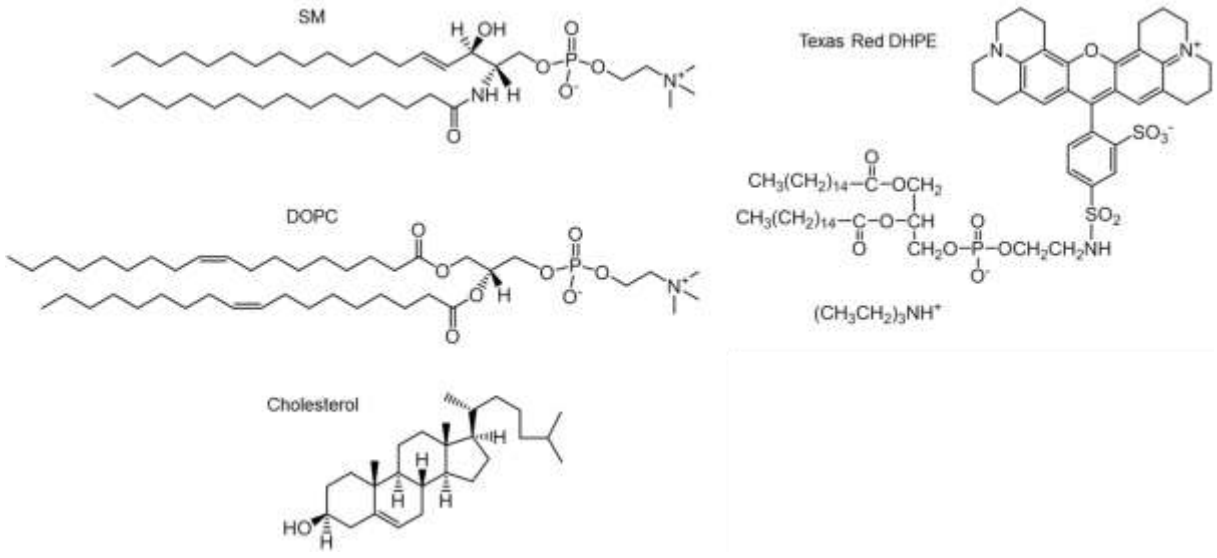

Figure 7.1 – Shows the chemical structure of compounds that will be employed in this study. Sphingomyelin will be extracted from chicken eggs and is a mixture of compounds. The most predominant form is shown here.

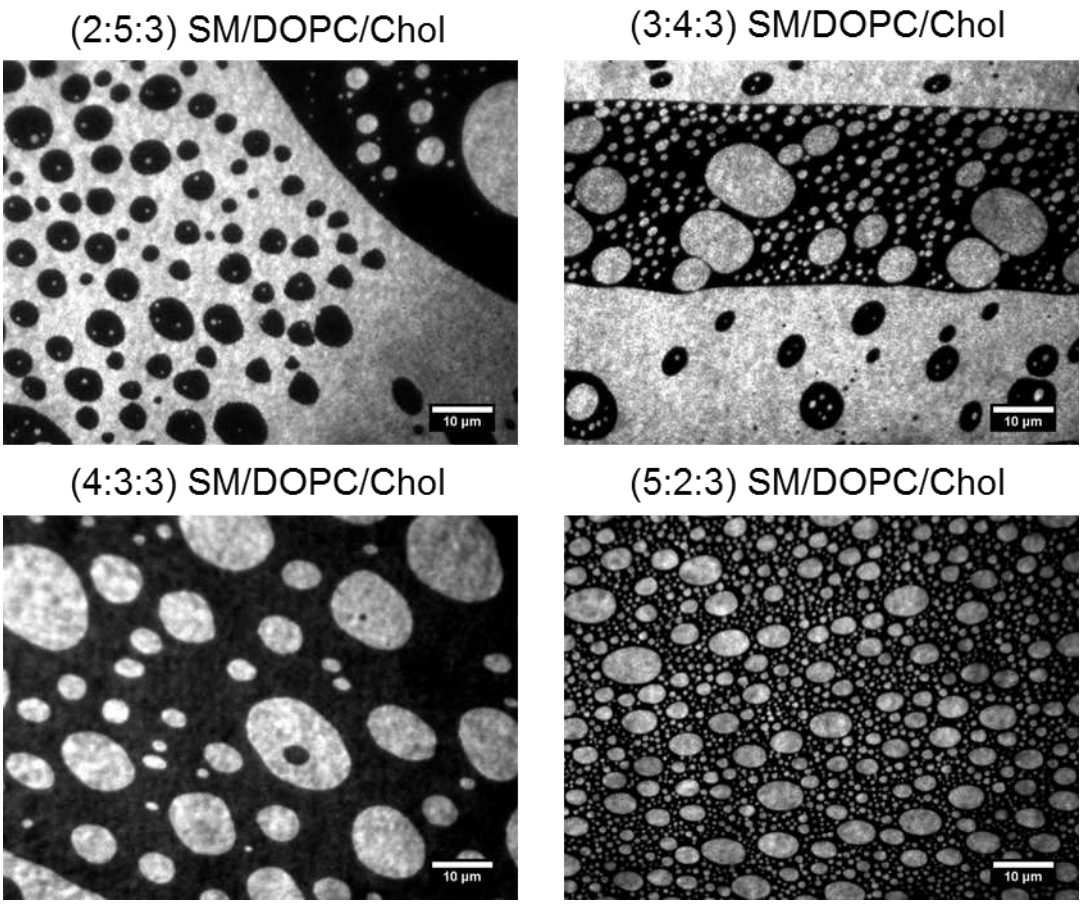

Figure 7.2 – Langmuir-Blodgett (LB) monolayers of SM/DOPC/Chol in varying ratios. The monolayer shown in the top-left image has the smallest concentration of SM and is the least ordered. The monolayers increase in order as the concentration of SM increases. All four monolayers were all prepared using Texas Red DHPE to stain the more expanded phase and transferred at 30 mN/m. The scale bar is 10 µm.

Initial work towards this goal was performed using the LB trough to prepare monolayers of the four lipid mixtures, and images of the monolayers are shown in **Figure 7.2**. The monolayers were prepared using Texas Red DHPE to stain the disordered area of the membrane. **Figure 7.2** shows that the monolayers being with a large fluorescent area and dark, circular condensed domains. As the SM concentration is increased, the disordered domains become circular and surrounded by condensed domain, until finally at 50 mol % SM there are small, circular disordered domains and much of the film is condensed. This trend is expected based on SM's

ordered structure. This work could be expanded by preparing hydrated SLBs using vesicle fusion to determine how the order and structure of these bilayers change as a function of increasing sphingomyelin.

Next, unilamellar vesicle solutions of the four lipid compositions would be prepared and added to hexadecane to create DIBs [15, 16]. One droplet of the DIB will contain doxorubicin HCL, which is water soluble and naturally fluorescent. By tracking the changes in fluorescence over time, the permeability of each lipid mixture can be characterized. This study will provide specific information on how the changing ratio of SM to unsaturated lipid (DOPC) impacts the drugs ability to move across the membrane and provide more data on the theory that lipid composition influenced drug resistance.

7.3 Conclusions

Drug resistance remains a major clinical issue. Understanding the exact mechanisms that lead to drug resistance is, therefore, vitally important. Recent evidence suggests that the biophysical properties of drug resistant cancer cells are different from drug sensitive cells. This is thought to be caused by a buildup of SM and cholesterol in drug resistant cells. Initial investigation of this hypothesis has shown that certain drugs, like doxorubicin, interact more strongly with the lipids in drug resistant cells and that the lipid composition of drug resistant cells favors lipids that cause higher order and more dense lipid packing. The experiment described in this chapter aid in investigating this hypothesis with a systematic investigation of membrane structure and its relationship to drug permeability, while furthering the fields understanding of DIB structure through single molecule analysis and comparisons to other more widely utilized model membrane systems.

7.4 References

1. Lyman, G.H., *Weight-based chemotherapy dosing in obese patients with cancer: back to the future.* J Oncol Pract, 2012. **8**(4): p. e62-4.

2. Goldie, J.H. and A.J. Coldman, *The genetic origin of drug resistance in neoplasms: implications for systemic therapy.* Cancer Res, 1984. **44**(9): p. 3643-53.

3. Larsen, A.K. and A. Skladanowski, *Cellular resistance to topoisomerase-targeted drugs: from drug uptake to cell death.* Biochim. Biophys. Acta, Gene Struct. Expression, 1998. **1400**(1-3): p. 257-274.

4. Gottesman, M.M., *Mechanisms of cancer drug resistance.* Annu. Rev. Med., 2002. **53**: p. 615-627.

5. Qiao, L. and B.C.Y. Wong, *Targeting apoptosis as an approach for gastrointestinal cancer therapy.* Drug Resist. Updates, 2009. **12**(3): p. 55-64.

6. Knappskog, S. and P.E. Lonning, *P53 and its molecular basis to chemoresistance in breast cancer.* Expert Opin. Ther. Targets, 2012. **16**(S1): p. S23-S30.

7. Peetla, C., S. Vijayaraghavalu, and V. Labhasetwar, *Biophysics of cell membrane lipids in cancer drug resistance: Implications for drug transport and drug delivery with nanoparticles.* Adv. Drug Delivery Rev., 2013. **65**(13-14): p. 1686-1698.

8. Hendrich, A.B. and K. Michalak, *Lipids as a target for drugs modulating multidrug resistance of cancer cells.* Curr. Drug Targets, 2003. **4**(1): p. 23-30.

9. Pallares-Trujillo, J., F.J. Lopez-Soriano, and J.M. Argiles, *Lipids. A key role in multidrug resistance? (review).* Int. J. Oncol., 2000. **16**(4): p. 783-798.

10. Vijayaraghavalu, S., et al., *Epigenetic Modulation of the Biophysical Properties of Drug-Resistant Cell Lipids to Restore Drug Transport and Endocytic Functions.* Molecular pharmaceutics, 2012. **9**(9): p. 2730-2742.

11. Gouaze, V., et al., *Glutathione peroxidase-1 overexpression prevents ceramide production and partially inhibits apoptosis in doxorubicin-treated human breast carcinoma cells.* Mol. Pharmacol., 2001. **60**(3): p. 488-496.

12. Peetla, C., et al., *Drug Resistance in Breast Cancer Cells: Biophysical Characterization of and Doxorubicin Interactions with Membrane Lipids.* Mol. Pharmaceutics, 2010. **7**(6): p. 2334-2348.

13. Vijayaraghavalu, S., et al., *Epigenetic Modulation of the Biophysical Properties of Drug-Resistant Cell Lipids to Restore Drug Transport and Endocytic Functions.* Mol. Pharmaceutics, 2012. **9**(9): p. 2730-2742.

14. De Milito, A. and S. Fais, *Tumor acidity, chemoresistance and proton pump inhibitors.* Future Oncol., 2005. **1**(6): p. 779-786.

15. Leptihn, S., et al., *Constructing droplet interface bilayers from the contact of aqueous droplets in oil.* Nat. Protoc., 2013. **8**(6): p. 1048-1057.

16. Hwang, W.L., et al., *Asymmetric Droplet Interface Bilayers.* J. Am. Chem. Soc., 2008. **130**(18): p. 5878-5879.